Evaluation of natural aerosols in CRESCENDO-ESMs: Mineral Dust

Ramiro Checa-Garcia[1], Yves Balkanski[1], Samuel Albani[8], Tommi Bergman[5], Ken Carslaw[2], Anne Cozic[1], Chris Dearden[10], Beatrice Marticorena[3], Martine Michou[4], Twan van Noije[5], Pierre Nabat[4], Fiona M. O'Connor[7], Dirk Olivié[6], Joseph M. Prospero[9], Philippe Le Sager[5], Michael Schulz[6], and Catherine Scott[2]

[1]Laboratoire des Sciences du Climat et de l'Environnement, CEA-CNRS-UVSQ, IPSL, Gif-sur-Yvette, France
[2]Institute for Climate & Atmospheric Science, School of Earth & Environment, University of Leeds, United Kingdom
[3]LISA, Universités Est-Paris & Diderot-Paris, France
[4]CNRM, Université de Toulouse, Météo-France, CNRS, Toulouse, France
[5]Royal Netherlands Meteorological Institute, De Bilt, Netherlands
[6]Norwegian Meteorological Institute, Oslo, Norway
[7]Met Office Hadley Centre, Exeter, United Kingdom
[8]Department of Environmental & Earth Sciences, University of Milano-Bicocca, Italy
[9]Department of Atmospheric Sciences, University of Miami, USA
[10]Centre for Environmental Modelling & Computation (CEMAC), School of Earth & Environment, University of Leeds, UK

Correspondence: Ramiro Checa-Garcia (ramiro.checa-garcia@lsce.ipsl.fr)

Abstract.

This paper presents an analysis of the mineral dust aerosol modelled by five Earth System Models (~~ESM~~ESMs) within the Coordinated Research in Earth Systems and Climate: Experiments, kNowledge, Dissemination and Outreach (CRESCENDO) project. We quantify the global dust cycle described by each model in terms of global emissions~~together with~~, together with, dry and wet ~~depositions~~deposition, reporting large differences in ratio of dry over wet deposition across the models not directly correlated with the range of particle sizes emitted. The multi-model mean dust emissions ~~was 2954~~ with 5 ESMs is 2836 $\mathrm{Tg\,yr^{-1}}$ but with a large uncertainty due mainly to the difference in the maximum dust particle size emitted. ~~For~~ The multi-model mean of the subset of ~~ESMs without particles~~ four ESMs without particle diameters larger than 10 $\mu\mathrm{m}$ ~~we obtained~~ is 1664 (σ=~~650~~651) $\mathrm{Tg\,yr^{-1}}$. Total dust emissions in the simulations with identical nudged winds from reanalysis give us better consistency between models~~with 1530~~, i.e. this multi-model mean global emissions with 3 ESMs is 1613 (σ=~~282~~278) $\mathrm{Tg\,yr^{-1}}$, but 1834 (σ=666) $\mathrm{Tg\,yr^{-1}}$ without nudged winds and same the models. Significant discrepancies in the globally averaged dust mass extinction efficiency explain why even models with relatively similar ~~dust load global~~ global dust load budgets can display strong differences in dust optical ~~depths~~depth. The comparison against observations has been done in terms of dust optical depths based on MODIS (Moderate Resolution Imaging Spectroradiometer) satellite products, showing a global consistency in terms of preferential dust sources and transport across the Atlantic. ~~However,~~ The global localisation of source regions is consistent with MODIS, but we found regional and seasonal differences between models and observations when we quantified the cross-correlation of time-series over dust emitting regions. To faithfully compare local emissions between models we introduce a re-gridded ~~normalization~~ normalisation method, that also can be compared with

satellite products derived from dust events frequencies. Dust total ~~depositions are compared with~~ deposition is compared with an instrumental network to assess global and regional differences. We ~~found~~ find that models agree with observations ~~distant from dust sources~~ within a factor of 10 for data stations distant from dust sources, but the approximations of dust particle size distribution at emission contributed to a misrepresentation of the actual range of deposition values when instruments are close to dust emitting regions. The ~~observational~~ observed dust surface concentrations also are reproduced to within a factor of 10. The comparison of total aerosol optical ~~depths with AERONETv3~~ depth with AERONET (AErosol RObotic NETwork) stations where dust is dominant shows large differences between models, ~~however~~ although with an increase of the inter-model consistency when the simulations are conducted with nudged-winds. The increase ~~of~~ in the model ensemble consistency also means a better agreement with observations, which we have ascertained for dust total deposition, surface concentrations and optical depths (against both ~~AERONETv3 and MODIS-DOD~~ AERONET and MODIS retrievals). We ~~estimated~~ introduce a method to ascertain the contributions per mode consistent with the multi-modal direct radiative effects, that we apply to study the direct radiative effects of a multi-modal representation of the dust particle size distribution that includes the largest particles~~measured at FENNEC experiment. We introduced a method to ascertain the contributions per mode consistent with the multimodal direct radiative effects.~~ .

1 Introduction

Mineral dust is a key element of the Earth system. It plays an important role in our planet's energy budget, in both the long-wave (LW) and the short-wave (SW) spectrum, by direct radiative effects and feedbacks on the climate system (Knippertz and Stuut, 2014). It also contributes significantly to the global aerosol burden. Kok et al. (2017), based on models and observations, estimated that global emissions are 1700 $\mathrm{Tg\,yr^{-1}}$ (with a range between 1000-2700 $\mathrm{Tg\,yr^{-1}}$ and particle diameters up to 20 $\mu\mathrm{m}$) which indicates that mineral dust, together with sea spray, have the largest mass emission fluxes of primary aerosols. ~~It~~ Furthermore, it is transported by the atmospheric flow from emission source regions to distant remote regions up to thousands of kilometres (Kaufman et al., 2005; Li et al., 2008). When it is deposited over the ocean (Schulz et al., 2012) dust constitutes a source of minerals, in particular iron ~~(Wang et al., 2015; Mahowald et al., 2005; Mahowald, 2011)~~ (Wang et al., 2015; Mahowald et al., 20 phosphorus (Wang Rong et al., 2014), therefore it indirectly participates in the carbon cycle and the ocean removal of carbon dioxide from the atmosphere (Gruber et al., 2009; Shaffer et al., 2009). When dust is deposited over land it impacts on ecosystems (Prospero et al., 2020) and snow albedo (Painter et al., 2007). In the troposphere dust contributes to heterogeneous chemical reactions (Tang et al., 2017; Dentener et al., 1996; Perlwitz et al., 2015; Bauer, 2004) and ice nucleation (Tang et al., 2016; Atkinson et al., 2013; Hoose and Möhler, 2012; Prenni et al., 2009) but also behaves as cloud condensation nuclei (Bègue et al., 2015), presenting additional interactions with precipitation (Solomos et al., 2011). Air quality studies link dust concentrations with health effects (Monks et al., 2009) but also with visibility (Mahowald et al., 2007). Additionally, transport and deposition

Table 1. Main characteristics of the CRESCENDO models used in this study and the simulation experiments analyzed: PD (Present Day), PDN (Present Day with nudged winds), PI (Pre-Industrial aerosol and chemistry forcings). Resolution is given in degrees (longitude x latitude), and all dust emissions are interactively driven by wind speed. DPSD stands for Dust Particle Size Distribution, detailed information for each model is given in Supplement, Tables S.MD.8 and S.MD.9. To describe the modelling of largest particles we defined two classifiers: (D10) to differenciate those schemes that explicity aim to model diameters larger than $> 10\mu m$. (BM20), if a specific bin or mode for particles larger than $20\mu m$ is defined (Yes), is not included (Not) or is joint into a single mode/bin with smaller particles than $20\mu m$ particles (Mix). κ^{DUST} means the refractive index used for mineral dust aerosols. For additional information of the dust schemes and their implementation in the Earth System Models key References are given.

Model Full-Name	Short-Name	Resolution	Levels	Experiments	DPSD	Large-Particles		κ^{DUST}	References
						D10	BM20	Dust Refraction Index	
IPSL-CM6-INCA5	IPSL	2.50x1.25	79	PD, PDN, PI	modes: 1	No	No	$1.520 - i1.47 \cdot 10^{-3}$	(1)
CNRM-ESM2-1	CNRM-3DU	1.40x1.40	91	PD, PDN, PI	bins: 3	Yes	No	$1.51 - i8.0 \cdot 10^{-3}$	(2)
CNRM-ESM2-1-CRESC	CNRM-6DU	1.40x1.40	91	PD, PDN, PI	bins: 6	Yes	Mix	$1.51 - i8.0 \cdot 10^{-3}$	(2)
NorESM1.2	NorESM	1.25x0.94	30	PD, PDN, PI	modes: 2	No	No	$1.530 - i2.40 \cdot 10^{-3}$	(3)
EC-Earth3-AerChem	EC-Earth	3.00x2.00	34	PD, PI	modes: 2	No	No	$1.517 - i1.09 \cdot 10^{-3}$	(4)
UKESM1	UKESM	1.87x1.25	85	PD, PI	bins: 6	Yes	Yes	$1.520 - i1.48 \cdot 10^{-3}$	(5)
IPSL-CM6-INCA5-4DU	IPSL-4DU	2.50x1.25	79	Special PDN	modes: 4	Yes	Yes	$1.520 - i1.47 \cdot 10^{-3}$	(6)

Dust Schemes description: (1) Schulz et al. (1998), (2) Michou et al. (2020), (3) Zender et al. (2003), (4) Tegen et al. (2002), (5) Woodward (2001b), (6) Albani et al., 2020; in prep.
Earth System Model description: (1 & 6) Boucher et al. (2020), (2) Séférian et al. (2019), (3) Kirkevåg et al. (2018), (4) van Noije et al. (2020), (5) Sellar et al. (2019); Mulcahy et al. (2020).

of dust plays a role in the design and maintenance of solar energy stations in semi-desert areas (Piedra et al., 2018), whereas at the Earth's surface fine dust particles (diameter smaller than 2.5 µm) can cause long-term respiratory problems (Pu and Ginoux, 2018a; Longueville et al., 2010). At regional scales dust has been reported to influence the West African (Strong et al., 2015; Biasutti, 2019) and Indian monsoons ~~(Sharma and Miller, 2017)~~(Sharma and Miller, 2017; Jin et al., 2021).

As a consequence, the dust cycle is actively analysed on regional (Pérez et al., 2006; Konare et al., 2008) and global scales, based on observations and models, covering aspects related to optical properties, mineral composition, emission processes, transport and deposition (Tegen and Fung, 1994). Current global models represent reasonably well the atmospheric lifetime of dust particles with a diameter of less than 20 µm (Kok et al., 2017), supporting a consistent ~~modeling~~ modelling of the dust atmospheric cycle: emission, transport and deposition. Very large dust particles with diameters of several tens of micrometers are, however, seldomly represented in these models, and have become an active area of research (van der Does et al., 2018; Di Biagio et al., 2020).

Detailed comparisons between observations and models ~~indicates~~ indicate that the latter are not yet capturing the full dust spatial and temporal distribution in terms of its various properties. This is due to the fact that current Earth system models are limited to approximate phenomenological descriptions of the dust ~~mobilization~~ mobilisation (Zender et al., 2003). These dust emissions schemes are based on either a saltation process (Marticorena and Bergametti, 1995) or a brittle fragmentation model (Kok, 2011), but in both cases the momentum transfer between the wind in the boundary layer and the soil particles

Table 2. CRESCENDO-ESM experiments analysed: PD (Present Day), PDN (Present Day with nudged winds), PI (Pre-Industrial aerosol and chemistry forcings). The sea-surface temperatures (SSTs) and ice cover are prescribed based on CMIP6-DECK-AMIP (Durack and Taylor, 2018). The solar forcing is using the input4MIPs dataset (Matthes et al., 2017) but NorESM uses the previous dataset. The gas and aerosol emissions are consistent with CMIP6 but depending on the complexity of the gas-phase species, ozone can be prescribed with either ozone concentrations from a previous full chemistry simulation or the input4MIPs ozone forcing dataset (Checa-Garcia et al., 2018; Hegglin et al., 2016). Wind fields used for the specified dynamics are obtained from re-analysis of ERA-Interim (Dee et al., 2011).

	PD	PDN	PI
Time Period	2000-2014	2000-2014	2000-2014
SSTs and ice cover	prescribed	prescribed	prescribed
Aerosol Precursors	Present-Day	Present-Day	1850
Anthropogenic Emissions	Present-Day	Present-Day	1850
Solar Forcing	Present-Day	Present-Day	Present-Day
Wind Fields	modelled	prescribed	modelled

is conditioned by erodibility or ~~roughness surface~~ surface roughness parameters, which sometimes are simply scaled to be in agreement with observations of aerosol index and/or aerosol optical depth. These ~~constrains allow for~~ constraints allow the models to reproduce reasonably well the dust optical depth (Ridley et al., 2016) but cannot fully constrain the whole range of the dust particle size distribution. This explains the considerable differences in ~~terms of~~ surface concentrations and vertical deposition fluxes when global models are evaluated against dust observations at regional and local scales. These challenges increase in regions with strong seasonal cycles and sparse vegetation cover, that require a description of the evolving vegetation, like the Sahel or semi-arid regions. ~~Others~~ Other difficulties emerge when the anthropogenic component of ~~the~~ atmospheric dust has to be ascertained, as it requires ~~to account for~~ land use change and agricultural activities to be considered. Optical properties of mineral dust aerosols are another field of research as both the refractive index and the particle shape introduce uncertainties on the estimation of scattering and absorption properties (Nousiainen, 2009). Finally, the total mass of mineral dust emitted to the atmosphere is mostly conditioned by a few events with intense surface winds, as the dust emission flux has a non-linear dependence on the wind speed, which the models pursue to capture. Actually, the meteorological phenomena conditioning these events exhibit regional dependencies, e.g. in West Africa deep convection (Knippertz and Todd, 2012) and nocturnal low-level jets (Heinold et al., 2013; Washington and Todd, 2005) have been found to be key drivers~~, while recently, (Yu et al., 2019)~~. Recently, Yu et al. (2019) reported differences in the frequency of dust events between the Gobi ~~and Taklamaklan deserts~~(very high frequency of dust events in March and April) and Taklamaklan (more than half of events from May to September) deserts, which can be interpreted by a larger role in dust activation of the nocturnal low-level jet in Taklamaklan (Ge et al., 2016).

The relevance of dust on the Earth system implies that most climate models have introduced parametrization schemes to describe properly the dust cycle in the last two decades. Woodward (2001b) describes the parametrization implemented in the Hadley Centre climate model, Miller et al. (2006) introduces the NASA Goddard dust model, Schulz et al. (1998) and

Table 3. Observations used for the comparison of the CRESCENDO models against observations indicating the spatial and temporal scales considered. Loadings and Mass Extinction Efficiency (MEE) were derived from model results only and are compared between them. L=local, N=Network, G=Global, R=Regional, A=Annual, M=Monthly, CM=Monthly-Climatology, CA=Annual-Climatology, TS=Time-Series-Avaliable.

Diagnostic	Dataset	Spatial	Temporal	Reference	Comments
Aerosol Optical Depth	AERONET	(L, N)	(A, M, TS)	(Giles et al., 2019)	Aeronet v3
	MODIS	(G, R)	(A, M)	(Sayer et al., 2014)	DeepBlue-v6
	MISR	(G, R)	(A, M)	(Diner et al., 2002)	
Ångström Exponent	AERONET	(L, N)	(A, M, TS)	(Giles et al., 2019)	Aeronet v3
	MISR	(G)	(A, M)	(Diner et al., 2002)	
Dust optical depth	AERONET dusty	(L, N)	(A, M, TS)	(Giles et al., 2019)	Subset of AERONET
	MODIS DOD	(G, R)	(A, M)	(Pu and Ginoux, 2018b)	See Supplementary
	IASI dust	(G, R)	(A, M)	(Peyridieu et al., 2013)	Near-Infrared
Surface concentration	UMOAC	(L, N)	(CA, CM)	(Prospero and Nees, 1986)	Filter Collectors
	Mahowald-2009	(L, N)	(CA)	(Mahowald et al., 2009)	
	INDAAF-PM10	(L)	(TS, CA)	(Marticorena et al., 2017)	INDAAF dataset
Dust deposition flux	Network-H2011	(N)	(CA)	(Huneeus et al., 2011)	Compilation dataset
	Network-SET-M	(N)	(CA)	(O'Hara et al., 2006; Vincent et al., 2016)	Compilation dataset
Wet/dry deposition flux	INDAAF-dep	(L)	(TS,CM)	(Marticorena et al., 2017)	INDAAF dataset

later Schulz et al. (2009) show the implementation of dust emissions in the INteraction of Chemistry and Aerosols (INCA) module of the IPSL model. Pérez et al. (2011) for the BSC-DUST model, and more recently other models either incorporate new dust schemes or ~~improved~~ improve on previous ones, e.g. Albani et al. (2014) and Scanza et al. (2015) in the CAM climate model, LeGrand et al. (2019) for the GOCART (Goddard Chemistry Aerosol Radiation and Transport) aerosol model, ~~(Klingmüller et al., 2018)~~ Klingmüller et al. (2018) in the EMAC atmospheric-chemistry climate model, Colarco et al. (2014) in the NASA GEOS-5 climate model, Astitha et al. (2012) and Gläser et al. (2012) in the ECHAM climate model. Therefore comparisons to ascertain how the models are improving the description of dust related processes are needed to make progress in the above challenges. A broad comparison of 15 AeroCom models (including both climate models and chemistry transport models) in terms of dust has been conducted by Huneeus et al. (2011) and more recently a comparison of ~~7 CMIP5 models regarding~~ dust optical depth in 7 CMIP5 (Coupled Model Intercomparison Project phase 5) climate models (Pu and Ginoux, 2018b). Albani et al. (2014) ~~shows~~ show a detailed comparison of several dust schemes of the CAM climate model. However, as the evolution of ESMs and dust schemes continues, in parallel with the availability of longer and new/refined observations, ~~an~~ exhaustive comparisons of dust cycles modelling, covering scales from ~~global to local, is~~ the global to the local, are still needed.

This study aims ~~for~~ to carry out an extensive comparison between observations and five Earth system models from the Coordinated Research in Earth Systems and Climate: Experiments, kNowledge, Dissemination and Outreach (CRESCENDO) project which aims to develop the current European ESMs through targeted improvements to a range of key processes, in

particular natural aerosols and trace gases. We compare the ESMs against observations in terms of optical properties (dust optical depth, Ångström exponent), surface concentration, wet and dry deposition, and dust ~~emission~~emissions, and how these aspects evolve in time and space. The paper is structured as follows: ~~section~~ Sect. 2 describes the models analysed, which is followed by ~~section~~ Sect. 3 describing the observational datasets used, and the methods (~~section~~ Sect. 4). The results of the comparison are presented first at the global scale (~~Section~~ Sect. 5.1), showing also its climatological spatial patterns (~~Section 5.2). Followed~~ Sect. 5.2), followed by sections describing: dust emission (~~Section~~ Sect. 5.3), dust deposition (~~Section~~ Sect. 5.4), dust optical depths (~~Section~~ Sect. 5.5) and surface concentrations (~~Section~~ Sect. 5.6). These results are then discussed in ~~section 6 and the main conclusion are summarised.~~ Sect.6 where the main conclusions are also summarised. Our final summary of future research recommendations is in Sect. 7. The supplementary information is a single document but organised according with the several sections of the main paper: Supplement MD has additional information ~~of~~ in sections 2 (models) and 3 (datasets). Supplement GL ~~complement section~~ complements Sect. 5.1. The other supplement parts refer to each of the diagnostics analysed.

2 Models description

Five different Earth System Models ~~, see table 1,~~ (Table 1) constitute the CRESCENDO-ESM ensemble: CNRM-ESM2-1, NorESM1.2, EC-Earth3-AerChem, IPSL-CM6-INCA5 and ~~UKESM~~UKESM1 with 2 different dust schemes for CNRM-ESM2-1 and IPLS-CM6-INCA5 (hereafter we refer to each model with the short-names in Table 1). This ensemble covers the two main methods to describe the dust particle size distribution: binned/sectional and multi-modal log-normal.

In the sectional methodology the full size distribution is divided ~~on~~ into a fixed number of bins, while inside each bin the size distribution is considered invariant. For CNRM-ESM2-1 two different ~~sectional descriptions~~ dust schemes based on two different sets of bins have been evaluated, see Table S.MD.8 for further details, named here CNRM-6DU (with 6 bins) and CNRM-3DU (with 3 bins). The UKESM model includes 6 bins, with both UKESM and CNRM-6DU covering also particles with diameters larger than 20μm, with two bins in the case of the UKESM model and one bin in the case of the CNRM-6DU model.

In the case of modal description the evolution of the size distribution is controlled by balance equations of mass and number concentrations of each mode, as they effectively constrain a log-normal distribution with fixed width. In CRESCENDO there are two main approaches: EC-Earth and NorESM are considering bi-modal size distributions (~~one fine or~~ with one fine/accumulation mode and one coarse mode) ~~but~~ mixed with other aerosols, whereas IPSL is considering ~~a non-mixed~~ an externally mixed single dust coarse mode (see Table S.MD.9). The limit between coarse and fine particles is located at about 1 μm (while accumulation refers to fine particles from 0.1 μm to 1 μm). ~~Several experiments~~ Denjean et al. (2016) aimed to estimate the typical parameters of a multi-modal description of the dust size distribution ~~: first~~ but confined to the range of sizes typical of accumulation and coarse modes~~(Denjean et al., 2016) but~~ . Recent experiments are also including larger particles ~~(Ryder et al., 2018). Several studies (Adebiyi and Kok, 2020) propose~~ (Ryder et al., 2018, 2019). A new analysis by Adebiyi and Kok (2020) proposes that the coarse mode, and more specifically those particles with diameter larger than 20 μm

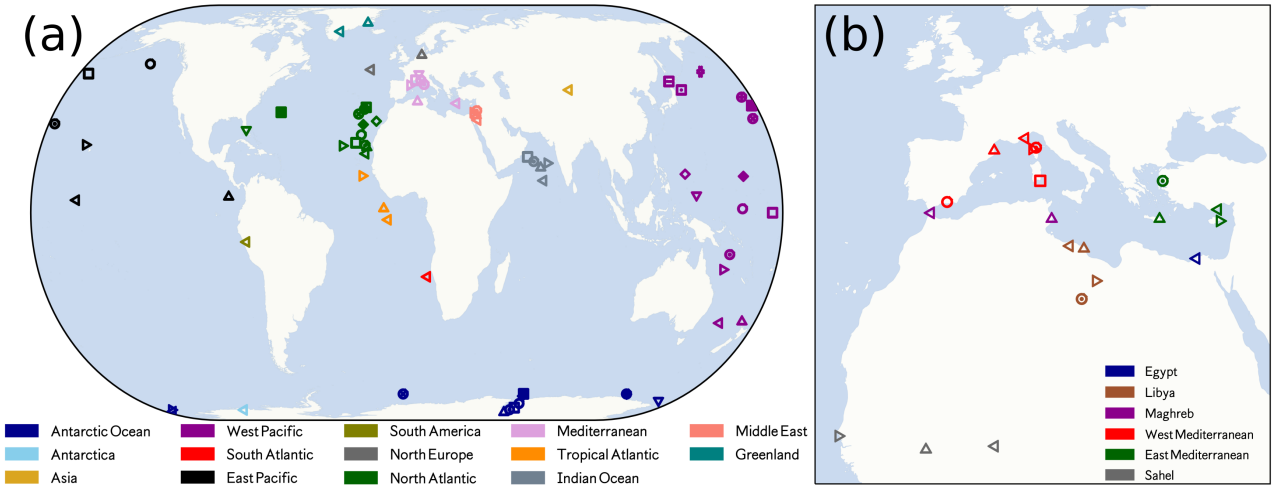

Figure 1. Panel (a): Map with the stations of the dataset named Network-H2011 which collects annual dust deposition fluxes for multiple years (Huneeus et al., 2011). Panel (b): Map with the stations of the dataset named Network-SET-M which collects additional station data in the Mediterranean region where observations have been reported by O'Hara et al. (2006) and Vincent et al. (2016), and station data over the Sahel (Marticorena et al., 2017). The different colours represent the region where each station belongs to.

are important to better understand the global dust cycle (often referred to as super-coarse and giant dust particles). Therefore, we also compared the ~~CRESCENDO ESMs~~ CRESCENDO-ESMs modal dust schemes, with a new dust scheme of the IPSL model with 4 insoluble dust modes ~~(Albani and et al, 2021; Di Biagio et al., 2020)~~ (Albani and et al, 2021) whose properties
140 are based ~~in FENNEC campaign (Rocha-Lima et al., 2018). Table~~ on the FENNEC campaign (Rocha-Lima et al., 2018; Di Biagio et al., 20 Table S.MD.9 shows the modal approaches in CRESCENDO, and how they compare with the IPSL-4DU.

To better describe the CRESCENDO ensemble diversity in the modelling of the coarse mode (large particles), two classifiers are introduced in Table 1: one to differentiate those dust schemes that aim to include particles with diameters larger than $10\mu m$, and the other one to indicate whether the model explicitly has a bin/mode for particles with diameters larger than $20\mu m$.

145 All the models provide standard approaches that estimate dust ~~mobilization~~ mobilisation based on a velocity threshold, information on soil texture (clay/~~silk)and~~ silt), erodibility factors (including soil moisture or accumulated precipitation) and prescribed vegetation cover. Conceptually, a fraction of the horizontal flux of dust particles, dominated by sandblasting, is actually transformed into a vertical flux with a mass efficiency factor and then effectively transported by the atmosphere. EC-Earth emissions are calculated following the scheme described by Tegen et al. (2002) based on the horizontal dust flux proposed by
150 Marticorena and Bergametti (1995), which is also used in the UKESM dust scheme ~~(Woodward, 2001a)~~(Woodward, 2001b). The NorESM emissions are estimated with the ~~DEAD~~ Dust Entrainment And Deposition (DEAD) model (Zender et al., 2003). The IPSL dust emission has been described by Schulz et al. (2009, 1998), and the ~~CNRM~~ CNRM-3DU model (Nabat et al., 2012) used also ~~(Marticorena and Bergametti, 1995)~~ Marticorena and Bergametti (1995) with an emitted size distribution based on ~~(Kok, 2011).~~ Kok (2011), while the CNRM-6DU is a revised version of the CNRM-3DU dust scheme.

Although none of the models ~~implements~~ have implemented an explicit mineralogical description of dust particles, the optical refractive index effectively accounts for global average of the mixture of minerals present in the mineral dust aerosol. Therefore, those optical properties are representative for the global mineralogical composition rather than a description of the soil-type dependence of the mineralogy that would imply local differences on emitted optical properties. This approximation is considered to drive specific ~~bias on those regions with~~ biases in those regions where the fraction of hematite or goethite minerals induce larger values of optical absorption, as shown by (Balkanski et al., 2007, 2021). The refractive index, expressed as $\kappa^{DUST} = n - ki$, of each model is shown in Table 1. They have similar values for the real component, but the imaginary component, although small, can be different by a factor of 2 which implies discrepancies in mass absorbing efficiency. Beyond the refractive index, the optical model used to estimate the key optical properties is another factor of diversity.

In all the models the particle size is described by the geometric diameter, where the dust particles with irregular shapes are modelled by spherical particles with the same effective volume. Regarding optical properties they are calculated based on Mie scattering, this approximation is reasonable as far as the orientation of the particles is randomly distributed, but any physical process that breaks this hypothesis, like preferential transport of specific geometries or physical processes that promote a specific orientation of the particles, will imply a bias in the methodology. The geometry of the particles also affects the gravitational settling, and therefore the transport of particles with specific geometries (Li and Osada, 2007) and their lifetime in the atmosphere. Recently, Huang et al. (2020) have estimated that the asphericity increases gravitational settling lifetime by 20% for both fine and coarse modes. Additionally, the spherical approximation is considered to underestimate the optical extinction of mineral dust (Kok et al., 2017). This hypothesis also affects the actual area of the global mineral dust surface which is important in heterogeneous chemistry (Bauer, 2004) and influences tropospheric chemistry. ~~The geometry of the particles also affects the gravitational settling, and therefore the transport of particles with specific geometries (Li and Osada, 2007) and their lifetime in the atmosphere.~~

~~Panel (a): Stations of the dataset named H2011 which collects annual dust deposition fluxes for multiple years (Huneeus et al., 2011). Panel (b): Dataset named SET-M which collects additional stations in the Mediterranean region were observations have been reported by (O'Hara et al., 2006; Vincent et al., 2016), and stations over Sahel (Marticorena et al., 2017). The different colors represent the region where each station belongs to.~~

2.1 Model experiments

Because the models have interactive dust emissions, wind fields play a prominent role ~~on~~ in dust emission and transport (Timmreck and Schulz, 2004). Therefore, this study contrasts two different present-day forcing experiments: one with winds generated by the dynamical part of the climate model (named PD), and the other nudged to re-analysed winds ~~from ERA-Interim~~ (named PDN) from ERA-Interim (Dee et al., 2011). The historical greenhouse gases concentrations are consistent with (Meinshausen et al., 2017). The models IPSL and IPSL-4DU were run without explicit gas-phase interactive chemistry activated, therefore they use the CMIP6 ozone forcing database ~~(Checa-Garcia et al., 2018; Checa-Garcia, 2018)~~(Checa-Garcia et al., 2018). The CNRM-ESM2-1 has explicit chemistry ~~at~~ in the stratosphere and upper-atmosphere (Michou et al., 2020). A last simulation where aerosols and chemistry emissions are prescribed for 1850 (named PI) is presented as well, see Table ~~1~~2. All

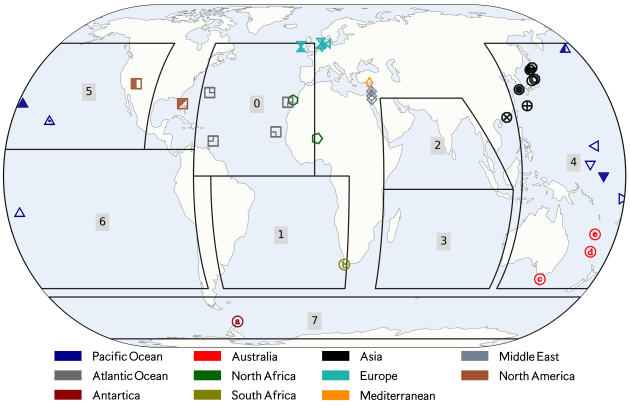

Figure 2. Map with 36 stations where surface concentrations were monitored by UMOAC (University of Miami Oceanic Aerosols Network) and also those described by Mahowald et al. (2009). Colours represent the region where each station belongs to. The regions correspond to those used for the regional analysis of dust deposition over the ocean: North Atlantic (0), South Atlantic (1), North-Indian Ocean (2), South-Indian Ocean (3), Pacific West (4), Pacific North-East (5), Pacific South-East (6) and Antarctic Ocean (7). For each of the oceanic regions a land-mask is also applied to filter inland grid-cells.

the simulations are from 2000 to 2014 plus at least 1 year of spin-up (except NorESM-PDN that covers 2001 to 2014). All the simulations implement prescribed ~~SSTs~~ sea surface temperatures (SSTs) of present-day conditions ~~. The additional CRESCENDO simulation named PI-PIsst with pre-industrial SST is not analysed in this study~~according to input4MIPs dataset (Durack and Taylor, 2018). The solar forcing implemented by all the models is derived from the dataset of Matthes et al. (2017). The comparison between the PD and PDN experiments inform about the role of wind fields to explain model diversity. The difference between PD and PI dust emissions allow us to evaluate whether the effects in the climate system due to non-dust emissions have a discernible impact on the global dust cycle (as both PD and PI have been prescribed with the same SSTs). A summary of the properties of the model experiments is given in Table 2.

3 Observational datasets

The observational ~~datasets used to ascertain~~ data-sets used to assess the performance of the CRESCENDO ESMs in their representation of mineral dust are based on a compilation of ground-site and satellite measurements. Table 3 ~~summarizes~~ summarises the different available datasets used, and the spatial and temporal scales applied in the analysis. Additionally, this table includes datasets representative of either a monthly or a yearly climatology (respectively referred to as CM and CA in Table 3). In this section these datasets are briefly described, but we refer to the original publications for further details. For those datasets with specific pre-processing the additional details are given in the supplementary material.

3.1 Surface Deposition flux

This dataset comprises ~~the~~ deposition flux observations described in Huneeus et al. (2011), composed from several ~~measurements~~ measurement campaigns over land and ocean (Figure 1 panel a), and named hereafter *Network-H2011*, plus an additional set of measurements at stations in the Mediterranean and Sahel regions (Figure 1 panel b), named hereafter *Network-SET-M* for which data values are shown ~~on~~ in the Table S.MD.5.

The set *Network-H2011* gives deposition fluxes estimated from sedimentation corresponding to ~~DIRTMAP~~ the DIRTMAP (Dust Indicators and Records of Terrestrial and MArine Palaeo-environments) database (Kohfeld and Harrison, 2001), while direct measurements of deposition fluxes were acquired during the SEAREX campaign (Ginoux et al., 2001) mostly in the Northern Hemisphere. Mahowald et al. (2009) describes 28 sites where dust deposition is inferred assuming a 3.5% fraction of iron. The compilation also includes observations of deposition fluxes deduced from ice core data according to Huneeus et al. (2011). The dataset covers a range of total dust flux ~~depositions~~ deposition from 10^{-3} to $0.5\cdot\ 10^{3}\,\mathrm{g\,m^{-2}yr^{-1}}$ but without a homogeneous distribution of values over this range. Only two stations have observational values larger than $100\,\mathrm{g\,m^{-2}yr^{-1}}$ and the bulk set of stations comprised values of between 0.1 and 75 $\mathrm{g\,m^{-2}yr^{-1}}$.

The dataset *Network-SET-M* includes field measurements for 20 additional stations located in the Mediterranean and Sahel regions to represent both deposition near to dust sources (O'Hara et al., 2006), as well as at intermediate distances from them (Vincent et al., 2016). The values in this dataset ranges ~~values~~ from 4.2 to 270 $\mathrm{g\,m^{-2}yr^{-1}}$ and allow us to ~~visualize~~ visualise regional differences in the dust deposition flux. The INDAAF (International Network to study Deposition and Atmospheric composition in Africa) stations (Marticorena et al., 2017) provide us with an estimation of the inter-annual variability which is large ~~on~~ in the Sahel region (see the Table S.MD.7)

~~Maps with 36 stations where surface concentration was monitored by UMOAC (University of Miami Oceanic Aerosols Network) and also those described by Mahowald et al. (2009). Colors represent the region where each station belongs to. The regions correspond to those used for the regional analysis of dust deposition over the ocean: North Atlantic (0), South Atlantic (1), North-Indian Ocean (2), South-Indian Ocean (3), Pacific East (4), Pacific North-West (5), Pacific South-West (6) and Antarctic Ocean (7).~~

3.2 Surface concentrations

~~A~~ The first part of the climatological dataset for dust concentrations (see Table S.MD.4) at the surface has been adopted from estimations done by the University of Miami Oceanic Aerosols Network (UMOAN) whose instruments are filter collectors deployed in the North Atlantic and Pacific Oceans (Prospero and Nees, 1986; Prospero and Savoie, 1989). This dataset provides climatological monthly averages with a standard deviation that represents inter-annual variability. The second part of the climatological dataset is based on yearly values from the ~~stations~~ station data shown in ~~(Mahowald et al., 2009)~~Mahowald et al. (2009). The dataset comprises of 36 stations with values from $5\cdot10^{-2}$ to 100 $\mu\mathrm{g\,m^{-3}}$ distributed within the full range of values but grouped in clusters correlated with the geographical regions they belong to.

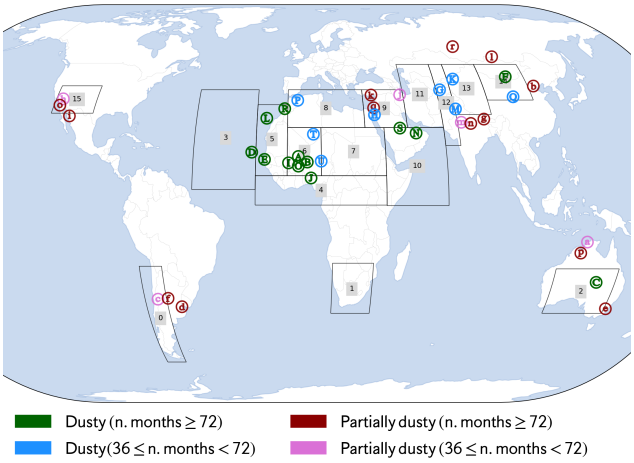

Figure 3. ~~Maps of~~ Map showing the 39 dusty stations from AERONET, classified in two groups: 21 dust-dominated stations (uppercase letters), and 18 stations where dust is important but not necessarily dominant (lower-case letters). The ~~colors~~ colour allows ~~to differentiate~~ differentiating also the number of months in the observed time-series. The regions for the preferential dust emission sources (plus Mid-Atlantic region) are indicated with numbered boxes. The region number correspond to the names of the regions to which they belong: South-America (0), South-Africa (1), Australia (2), Mid-Atlantic (3), ~~Sahel/~~Gulf of Guinea (4), Western Sahara (5), Mali/Niger (6), ~~Bodele~~Bodélé/Sudan (7), North Sahara (8), North ~~MiddleEast~~ Middle-East (9), ~~South-MiddleEast~~ South Middle=East (10), Kyzyl Kum (11), Thar (12), Taklamakan (13), Gobi Desert (14), North-America (15).

Table 4. Given the mass mixing rations X_s, airmass a_{mass}, optical depths τ_s per species s and air density ρ_{air}. We indicate here the method used to estimate other diagnostics. (i,j) are the coordinates/index of each cell grid, l represents the level/layer. $A(i,j)$ is the area of (i,j) grid cell, l_0 represents the surface layer. The units refer to those of original CRESCENDO diagnostics.

Diagnostic	Symbol	Equation	Units
Grid cell area	$A(i,j)$	Diagnostic provided by models	m^2
Mass mixing ratio	$X_s(i,j,l)$	Diagnostic provided by models	$\mathrm{kg\,kg}^{-1}$
Airmass	$a_{mass}(i,j,l)$	Diagnostic provided by models	kg
Optical depth at 550nm	$\tau_s(i,j)$	Diagnostic provided by models	-
Grid cell loadings	$L_s(i,j)$	$\sum_l \left[X_s(i,j,l) \cdot a_{mass}(i,j,l) A(i,j)^{-1}\right]$	$\mathrm{kg\,m}^{-2}$
Total column load	TL_s	$\sum_{i,j} L_s(i,j)A(i,j) = \sum_{i,j,l} X_s(i,j,l) \cdot a_{mass}(i,j,l)$	kg
Surface concentrations	$\widetilde{x_s}(i,j)$	$X_s(i,j,l_0) \cdot \rho_{air}(i,j,l_0)$	$\mathrm{kg\,m}^{-3}$
MEE at 550nm (†)	$m_s^{ee}(i,j)$	$\tau_s(i,j) L_s(i,j)^{-1}$	$\mathrm{kg}^{-1}\,\mathrm{m}^2$ (‡)

† MEE: Mass Extinction Efficiency. ‡ The MEE shown in the analysis has units $\mathrm{g}^{-1}\,\mathrm{m}^2 = 10^{-3}\mathrm{kg}^{-1}\,\mathrm{m}^2$.

3.3 INDAAF stations of data

The multi-instrument network was deployed in the ~~frame~~ framework of the African Monsoon Multidisciplinary Analysis, and belongs to the INDAAF set of data-stations. Marticorena et al. (2010) described the collocated measurements of wet and dry deposition, as well as, surface concentrations (of particulate matter smaller than 10 μm) at three stations in the Sahel region, see Tables S.MD.6 and S.MD.7 and Figure 1 panel (b). The stations also measured precipitation, wind velocity and surface temperature. Additionally, in the same ~~location~~ locations there are AERONET sun-photometers to measure aerosol optical depths.

3.4 AERONET optical properties

The AERONET (Aerosol Robotic Network) database implemented in our comparisons ~~rely~~ relies on the Version 3 (Level 2.0) algorithm. Based on this new algorithm the entire database of observations ~~has been~~ was reprocessed in 2018 (Giles et al., 2019). The database comprises aerosol optical depths and Ångström exponents, as well as, fine and coarse optical properties obtained with a new cloud-screening quality control scheme. The actual division threshold between fine and coarse particles is ascertained by the inversion algorithm that aims to differentiate aerosol particles from ice crystals and it lies between 0.44 and 0.99 μm.

The network database provides daily data, allowing for events analysis, and there is also a monthly time resolution dataset, used here to examine decadal, yearly and seasonal properties. We processed ~~the~~ data from 300 stations ~~from~~ of the full network to explore general properties~~and~~. For the dust analysis we selected those stations where ~~it is considered that mineral dust is an important part of~~ all the models together considered dust to be an important contributor to the aerosol composition ~~based on the presence of dust~~ (at the geographical ~~position by all the models~~location of the AERONET station). This subset is named here dusty set of stations, which are shown in Figure 3. It comprises 39 stations divided ~~on~~ into two subsets: those stations where the dust has a *dominant* role in terms of ~~optical depths~~ the optical depth ($\tau_{440}^{dust} > 0.5\tau_{440}^{all-aer}$ for all models ~~along the seasonal cycle~~and all the months of the year, where $\tau_{440}^{all-aer}$ refers to optical depth at 440 nm of all aerosols and τ_{440}^{dust} is the optical depth of mineral dust aerosols at 440 nm), and those where the dust is *important* although not ~~necessary~~ necessarily dominant for all the models (even if ~~for a specific model but not all~~ the dust optical depth ~~contributes with~~ from a single model contributes more than 50% of the total aerosol optical depth). The first subset comprises of 21 stations, and it is ~~noted~~ denoted with upper-case letters in Figure 3. The second ~~has~~ comprises 19 stations, ~~noted~~ and it is denoted with lower-case letters. The dusty stations set over Africa is consistent with the stations analysed by Huneeus et al. (2011) based on Bellouin et al. (2005) criteria, but it has been extended with stations in Australia, South-America, North-America and Asia ~~consitent on (Klingmüller et al., 2018)~~consistent with Klingmüller et al. (2018). Figures with the seasonal cycle of aerosol optical ~~depths~~ depth of the dusty dominant and important stations ~~seasonal cycle~~ that highlight the classification criteria are shown in the supplement material (Figures S.DOD.10 and S.DOD.11).

Table 5. Statistics used to inter-compare models and observations and perform model inter-comparisons. N indicates the number of observations or sample size. When the analysis refers to a global performance of the model over a set of instruments, N represents the number of stations. When the statistical analysis is done over a time series of values, N represents the number of time samples usually corresponding to a specific location. Pearson Correlation Coefficient (ρ), bias (δ), normalised bias (δ_N), Ratio of standard deviations (Σ), Normalised mean absolute error (θ_N) and Root mean square error (RMSE=η).

Statistic Estimator
$\rho = Cov(log_{10}X, log_{10}Y)/(\sigma(log_{10}X)\sigma(log_{10}X))$
$\delta = N^{-1}\sum_{i=1}^{N}(x_i^{(mod)} - x_i^{(obs)})$
$\delta_N = \sum_{i=1}^{N}(x_i^{(mod)} - x_i^{(obs)})/(\sum_{i=1}^{N} x_i^{(obs)})$
$\Sigma = \sigma_{mod}/\sigma_{obs}$
$\theta_N = \sum_{i=1}^{N}\left\|x_i^{(mod)} - x_i^{(obs)}\right\|/(\sum_{i=1}^{N} x_i^{(obs)})$
$\eta = N^{-1}\sqrt{\sum_{i=1}^{N}(x_i^{(mod)} - x_i^{(obs)})^2} = RMSE$

3.5 MODIS dust related products

Interactions between dust and radiation are defined through three optical properties: dust optical depth (DOD), single scattering albedo (ω) and the asymmetry parameter which defines the ratio of the radiation scattered forward over the radiation scattered backward. For the dust coarse mode, the dust optical depth can be estimated using the Moderate Resolution Imaging Spectroradiometer (MODIS) enhanced deep-blue (DB) aerosol optical depth (Sayer et al., 2014) as done by Pu and Ginoux (2018b) with the additional support of the MODIS product of single-scattering albedo (ω) and Ångström exponent (α). The rationale of the method relies on the properties of these three optical parameters applied to ~~aerosols~~ aerosol particles. First, α is very sensitive to particle size, so there are ~~parametrizations~~ parametrisations of aerosol optical ~~depths~~ depth that use it to separate each mode contribution. Second, aerosols with low absorption and large scattering like sea-salt have $\omega \simeq 1$, whereas mineral dust is considered an absorbing aerosol. Third, the dependency of $\alpha(\lambda)$ ~~in~~ on wavelength contains a signature of the aerosol composition. Given this information, we have considered 2 different MODIS dust optical depth related datasets. One of them is a pure filter of aerosol optical depth to differentiate those pixels where dust is expected to be the dominant contribution to aerosol optical depth, but without ~~the~~ an attempt to estimate the actual fraction of mineral dust, so it is considered here as an upper threshold of the actual DOD of the coarse mode (because particles of dust with diameters below 1 µm are thought to contribute less ~~and~~ than 10% to the total dust optical depth). The other method aims to explicitly separate sea-salt, and ~~proceed to re-scale~~ proceeds to rescale the aerosol optical depth to ascertain an actual value of DOD, and according to Pu and Ginoux (2018b) it may be considered a lower-bound of the DOD. Additional information and a comparison of these created products are given in the supplementary information, see Figures S.MD.2 and S.MD.3.

Table 6. Global dust mass balance, dust loading, dust optical depth (DOD), mass extinction efficiency (MEE) and lifetime for each model and each experiment available. CNRM has two configurations one specific for CRESCENDO referred as CNRM-6DU and another for CMIP6 denoted as CNRM-3DU. The UKESM is not diagnosing the dust sedimentation separately and dry deposition flux diagnostics accounts for all removal of dust except for wet deposition. The units are Tgyr^{-1} for emissions and depositions tendencies, Tg for Load, $\mathrm{m}^2\,\mathrm{g}^{-1}$ for MEE and days for lifetime. MEE is calculated as the mean of the MEE(x,y) field, while $\widehat{MEE}$ is the ratio of DOD and Load mean fields. Δ represents the ratio of the Net (Emission-Total Deposition) relative to emission in %. $\mathcal{R}_{dep}$ is the ratio of total dry (including gravitational settling) over total wet deposition. MM-mean shows the multi-model mean for each experiment (and each variable) and MM-σ the estimated multi-model standard deviation. Note that some statistical estimations (indicated with ‡) related to the deposition are not including the UKESM model as we cannot separate gravitational settling from other dry deposition processes. Due to the larger values of the Δ parameter, CNRM-6DU is not included in the statistics noted with $^{\parallel}$ and ‡.

Model	Exp.	Emi. [Tg yr^{-1}]	Dep. [Tg yr^{-1}]	Net [Tg yr^{-1}]	Δ %	Dry Dep. [Tg yr^{-1}]	Wet Dep. [Tg yr^{-1}]	Sedim. [Tg yr^{-1}]	$\mathcal{R}_{dep}$	DOD -	Load [Tg]	MEE [m^2g^{-1}]	$\widehat{MEE}$ [m^2g^{-1}]	Lifetime [day]
CNRM-3DU	PD	2605.2	2679.6	-74.5	-2.86	1708.1	753.8	217.8	2.55	0.011	13.3	0.63	0.44	1.9
EC-Earth	PD	1126.6	1126.7	-0.12	-0.01	367.8	493.2	265.7	1.28	0.029	11.7	1.86	1.27	3.8
IPSL	PD	1557.5	1558.9	-1.44	-0.1	329.3	968.3	261.3	0.61	0.026	16.4	0.82	0.82	3.8
NorESM	PD	1368.2	1368.3	-0.09	-0.01	84.0	275.7	1008.6	3.96	0.023	7.2	2.86	1.63	1.9
UKESM	PD	7524.4	7527.6	-3.21	-0.04	*6566.3*†	949.8	-	6.91	0.011	18.1	0.5	0.31	0.9
MM-mean	PD	2836.4$^{\parallel}$	2852.2$^{\parallel}$	-	-	622.3‡	622.8‡	438.5‡	-	0.02$^{\parallel}$	13.32$^{\parallel}$	1.33$^{\parallel}$	0.89$^{\parallel}$	2.5$^{\parallel}$
MM-σ	PD	2680.8$^{\parallel}$	2680.5$^{\parallel}$	-	-	734.7‡	302.1‡	380.9‡	-	0.008$^{\parallel}$	4.25$^{\parallel}$	1.01$^{\parallel}$	0.556$^{\parallel}$	1.3$^{\parallel}$
CNRM-3DU	PI	2651.5	2730.2	-78.7	-2.97	1728.7	781.0	220.4	2.49	0.012	13.4	0.63	0.44	1.8
EC-Earth	PI	1145.8	1145.4	0.44	0.04	374.4	511.6	259.4	1.24	0.027	11.6	1.7	1.17	3.7
IPSL	PI	1551.7	1553.2	-1.49	-0.1	330.6	961.0	261.5	0.62	0.027	16.7	0.82	0.82	3.9
NorESM	PI	1407.3	1407.5	-0.21	-0.01	86.8	287.4	1033.2	3.90	0.023	7.4	2.75	1.56	1.9
UKESM	PI	7421.9	7413.6	8.25	0.11	*6475.6*†	938.0	-	6.90	0.01	17.4	0.49	0.29	0.9
MM-mean	PI	2835.6$^{\parallel}$	2850.0$^{\parallel}$	-	-	630.13‡	635.3‡	443.6‡	-	0.02$^{\parallel}$	13.3$^{\parallel}$	1.28$^{\parallel}$	0.87$^{\parallel}$	2.4$^{\parallel}$
MM-σ	PI	2627.4$^{\parallel}$	2622.4$^{\parallel}$	-	-	743.23‡	296.5‡	393.5‡	-	0.008$^{\parallel}$	4.06$^{\parallel}$	0.95$^{\parallel}$	0.52$^{\parallel}$	1.3$^{\parallel}$
CNRM-3DU	PDN	1812.1	1888.7	-77.62	-4.28	1290.6	435.1	164.0	3.34	0.011	11.6	0.63	0.46	2.3
IPSL	PDN	1295.3	1297.1	-1.77	-0.13	268.8	813.1	215.2	0.60	0.024	14.8	0.82	0.82	4.2
NorESM	PDN	1733.6	1733.4	0.12	0.01	115.7	345.5	1272.2	4.02	0.029	9.1	2.87	1.61	1.9
MM-mean	PDN	1613.7$^{\parallel}$	1640.1$^{\parallel}$	-	-	558.4$^{\parallel}$	531.2$^{\parallel}$	550.4$^{\parallel}$	-	0.02$^{\parallel}$	11.8$^{\parallel}$	1.44$^{\parallel}$	0.96$^{\parallel}$	2.8$^{\parallel}$
MM-σ	PDN	278.5$^{\parallel}$	307.1$^{\parallel}$	-	-	638.7$^{\parallel}$	248.2$^{\parallel}$	625.5$^{\parallel}$	-	0.009$^{\parallel}$	2.86$^{\parallel}$	1.24$^{\parallel}$	0.59$^{\parallel}$	1.2$^{\parallel}$
CNRM-6DU	PD	3542.2	4134.7	-592.5	-16.7	1283.9	2108.9	741.9	0.96	0.023	32.6	0.55	0.36	3.4
CNRM-6DU	PI	3887.3	4552.0	-664.7	-17.0	1415.2	2319.1	817.7	0.96	0.025	35.2	0.56	0.36	3.3
CNRM-6DU	PDN	1278.4	1507.3	-228.8	-17.9	499.5	716.8	290.9	1.10	0.011	15.2	0.56	0.38	4.3

† Values including the sedimentation. ‡ Statistic is not including UKESM and CNRM-6DU. $^{\parallel}$ Statistic is not including CNRM-6DU

3.6 MISR aerosol optical depth derived products

The Multi-angle Imaging Spectro-Radiometer (MISR) is a sensor on-board the Terra satellite which takes advantage of its multi-angle ~~measurements~~ measurement capabilities. It is able to ascertain the presence of non-spherical particles on the aerosol products at four different wavelengths. The optical depth at several wavelengths has been used to compute the Ångström exponent between Mar-2000 and Dec-2014 of MISR, and compare with the models' Ångström exponent based ~~in~~ on the same information. This product gives us information on how the models represent the spectral dependence of optical depth. Our computation using the 446 nm and the 672 nm ~~wavelength~~wavelengths, has been compared with the MISR Ångström exponent product to validate our computations, see Figure S.GL.8.

4 Methods

~~Along~~ As part of this study we calculated several diagnostics not directly provided by the different models. Table 4 shows how they ~~has~~ have been estimated together with ~~the unitsused~~their units. Regarding the statistical methods, Table 5 shows the ~~statistics definitions~~ metrics used for the comparison of ~~models with network of instruments~~the CRESCENDO models with the comprehensive suite of observations. The skill of the models to ~~ascertain~~ represent the dust optical depth over dust source regions has been calculated based on the Pearson correlation. Given that this ~~statistics~~ statistic is not robust and ~~it is unable to inform about non-linear~~ only representative of linear relationships, the skill is also estimated based on the Spearman rank correlation to ensure the robustness of the results. For the other comparisons the scatter-plots are informative of the quality of the correlation estimator.

For the comparison against the networks of instrument used: one monitoring surface concentrations, two for total deposition and one that retrieves dust optical ~~depths~~depth, we proceed with the same methodology. For each observation, we chose the model value of the corresponding variable in the grid pixel to which this measuring station belongs. Given the different area covered by the grid cell and the ~~pointed~~ grid point location of the in-situ ~~measurement~~measurements, there is an underlying representation error. However, the observational datasets of total deposition and surface concentrations at point based sites are climatological estimations which can be representative of larger areas. The values for the parameters discussed here are time averaged over the 15-year simulations and hence the produced fields are smooth over ~~subgrid~~ sub-grid scales.

~~Table 5 summarizes the statistical metrics used to evidence differences between models and observations.~~ The surface concentration and total deposition ~~comparison~~ comparisons are presented as scatter-plots together with three associated statistics: the Pearson correlation (evaluated in log-scale), the bias and the RMSE (root mean square error). These last two metrics can be used to ~~characterize~~ characterise quantitative differences between each model and ~~observations.~~ the observations. Additional statistics are summarised in Tables 11, 12 and 13 ~~include in addition, the normalized~~ including the normalised bias and the ~~normalized~~ normalised mean absolute error which help us understand how the models differ when scaled to the observation values.

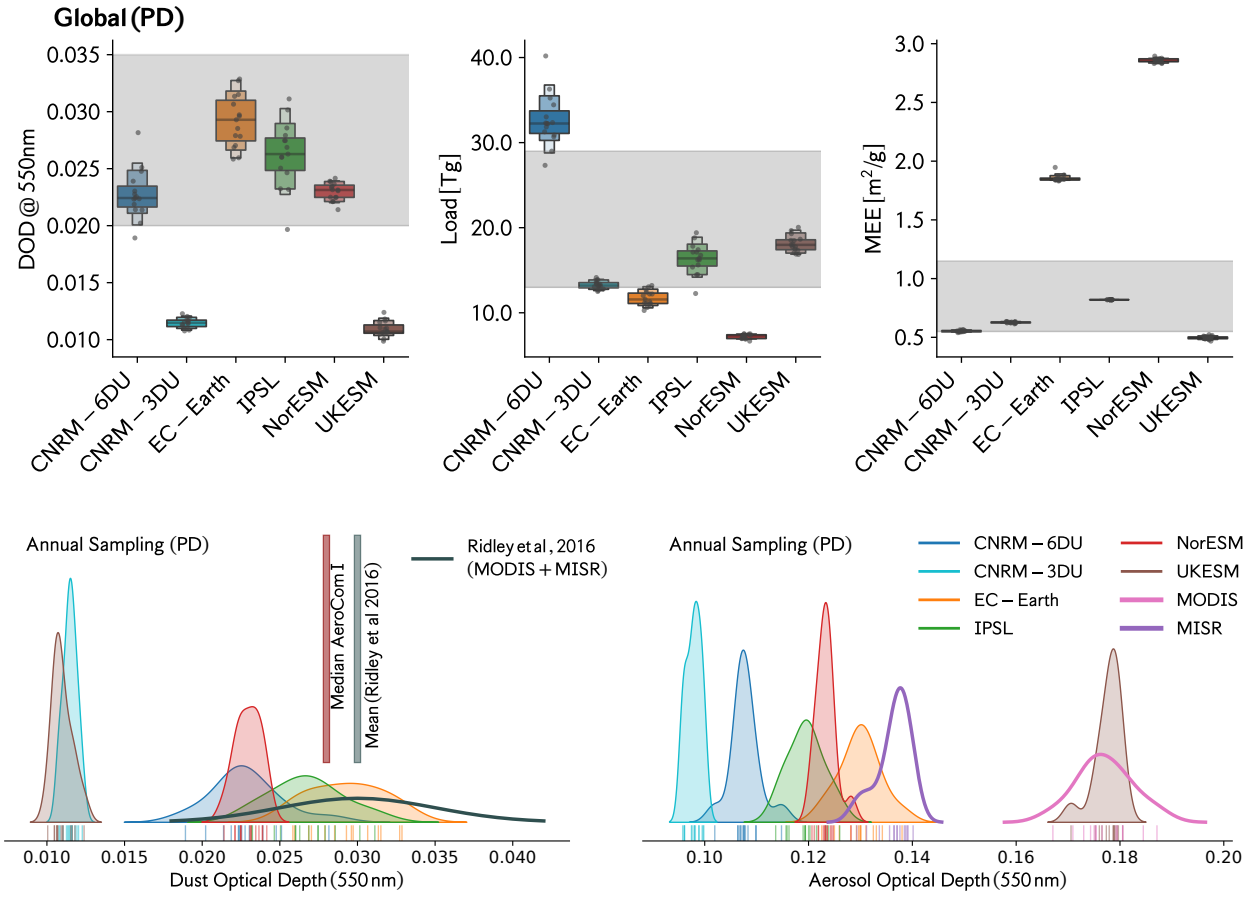

Figure 4. ~~Top panel~~*Top panel*: Global dust cycle values for PD experiment. The gray shaded region represents the expected interval range based on ~~(Kok et al., 2017)~~ Kok et al. (2017) for dust particles with diameter up to 20 μm for Dust Optical Depth (DOD), ~~Loadings~~ Load and mass extinction efficiency (MEE). ~~Bottom left panel~~ The grey dots over the box-plot represent each of the annual values. *Bottom left panel* represents the estimated distribution of global dust optical depth annual values (~~samples~~ our sample values per model are represented by the coloured vertical marks ~~on~~ just above the x-axis). The ~~bottom right panel~~ *bottom right panel* is the analogous for all aerosols optical depth. Both distributions are normalized and vertical axis represents a probability. For both the models and the observations (MISR and MODIS) the estimates are for time-period 2000-2014. Additional analysis analogous to top panel but constrained over different regions are in ~~supplement~~ Supplementary material (~~figures~~ Figures S.GL.1 and S.GL.2).

5 Results

The results are divided ~~in~~ into six different subsections. First a comparison at the global scale summarises the main properties of the global dust cycle in the models ~~analyzed~~analysed, which is complemented with an overview of the spatial pattern of the temporal mean of the 15 years of simulation (based on monthly values) for each of the climate models of the study. The next four sections are detailed analysis of the dust properties: emission, deposition, optical depth and surface concentrations. Each one is described at the regional scale and compared against a network of instruments and/or satellite retrievals when available. In all the cases, the PD experiment simulations ~~has~~ have been taken as the baseline of the inter-comparison and shown in the main paper. The results for the other experiments (PDN and PI), if not present in the main paper, are shown in the supplementary material. The case of nudged wind simulations (PDN) is used to ascertain the role of modelled surface winds on inter-model differences, whereas the ~~other based on PI simulations~~ simulation with PI emissions help us to evaluate ~~a~~ the possible role of prescribed emissions.

5.1 Global dust properties

The global dust cycle ~~have~~ has been analysed in terms of global climatological values and complemented by ~~an~~ a study of the role of the particle size distribution on the direct radiative effects (based ~~in~~ on the IPSL model with 4 dust modes).

The dust particle size distribution is physically constrained by emission, transport and deposition (wet and dry), whereas, other aerosol processes like aerosol nucleation, condensation and coagulation have a minor role on the evolution of ~~this~~ the size distribution (Mahowald et al., 2014). Therefore, the first step to describe the global atmospheric dust cycle in climate models consists of a ~~characterization~~ characterisation of the emission and deposition fluxes at the surface. This analysis is complemented by the analysis of two size-integrated properties: the dust optical depths and loadings. Other phenomena present in the Earth System dust cycle ~~on long timescale~~ more relevant for paleoclimate studies, like those derived from the ~~stabilization~~ stabilisation of dust deposition ~~over~~ on the surface on long time-scales, are not considered in this work~~as they are relevant for paleoclimate studies of dust cycle~~.

The global dust budget is analysed for the whole time period of the simulations over the three different simulations considered: PD, PDN and PI. Table 6 presents the mean global values of each model. It describes the dust mass balance in terms of emission, dry and wet deposition~~, and the parameter~~ . A parameter $\mathcal{R}_{dep}$ is defined to represent the ratio of total dry to total wet deposition. In addition, Δ ~~ascertains~~ represents the fraction (%) of the emissions not deposited relative to the total emission. ~~$\mathcal{R}_{dep}$ represents the ratio of total dry to total wet deposition~~ This last parameter is used to ascertain if the dust cycle from emission to deposition is consistent in terms of global mass conservation, or, to the contrary, whether the model transport introduces any inconsistency in the modelled dust cycle. In particular, the parameter Δ is used to decide those models and experiments that will be included in the multi-model ensemble mean to ensure internal consistency in the ensemble.

~~For global emissions,~~ In this regard, the mass budget of the CNRM-3DU model is closed to within $\Delta \simeq 3\%$ as its dynamical core is based on a semi-Lagrangian method (Voldoire et al., 2012, 2019) which is not fully mass conservative in terms of its tracers. In the case of the PDN experiment there is an increase to $\Delta \simeq 4.3\%$, because the excess of mass in the deposition

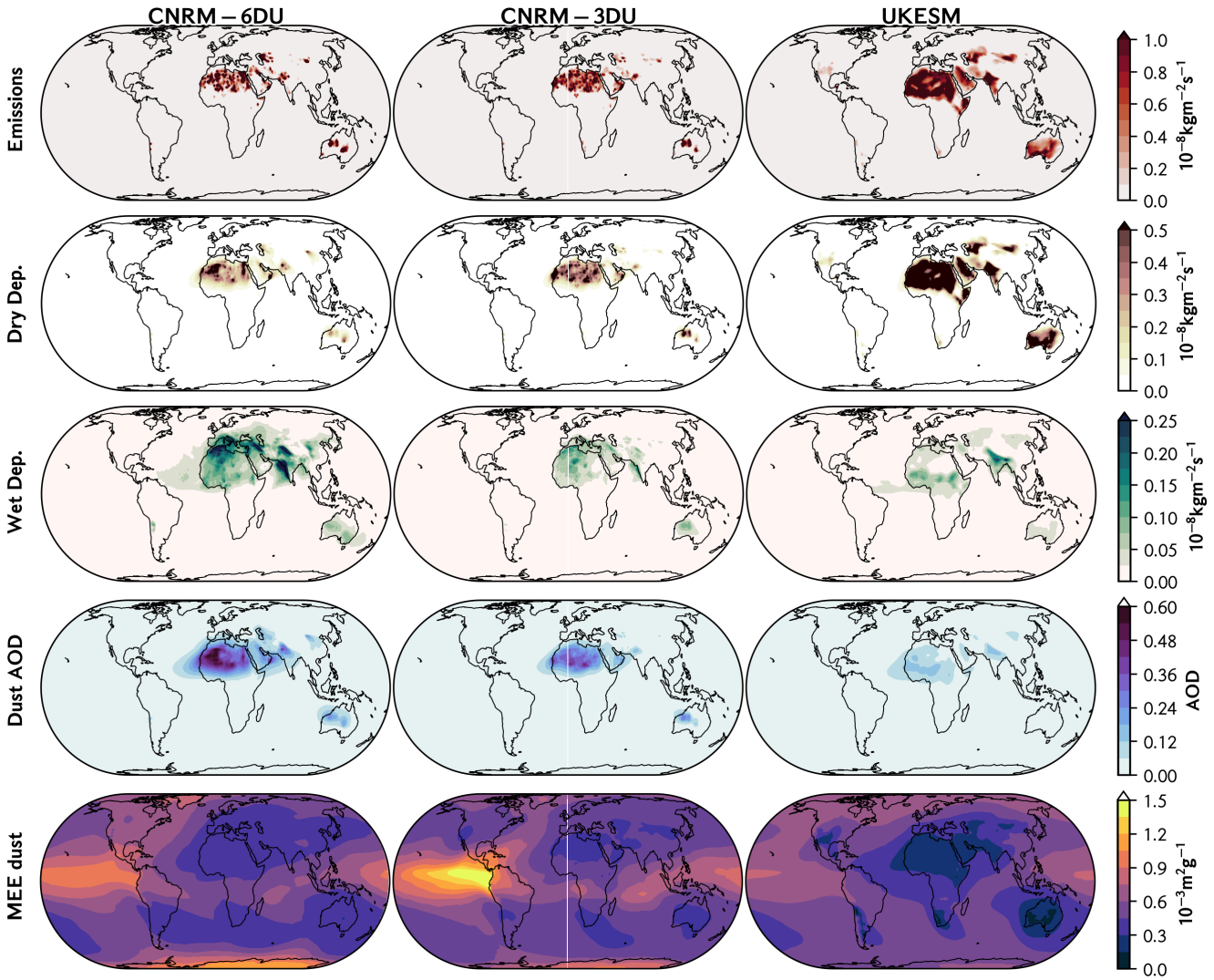

Figure 5. CRESCENDO-ESMs global maps describing dust properties (averaged over the 15 years): emission tendency, ~~depositions~~ deposition tendencies, dust optical ~~depths~~ depth and mass extinction efficiency. The models included have a bin-based dust ~~parametrization~~parametrisation, these models are: CNRM-6DU, CNRM-3DU and UKESM models. The equivalent figures for PI and PDN experiments are shown in ~~supplement material~~Supplementary Material: ~~figure~~ Figure S.GL.3 and ~~figure~~ Figure S.GL.4 respectively.

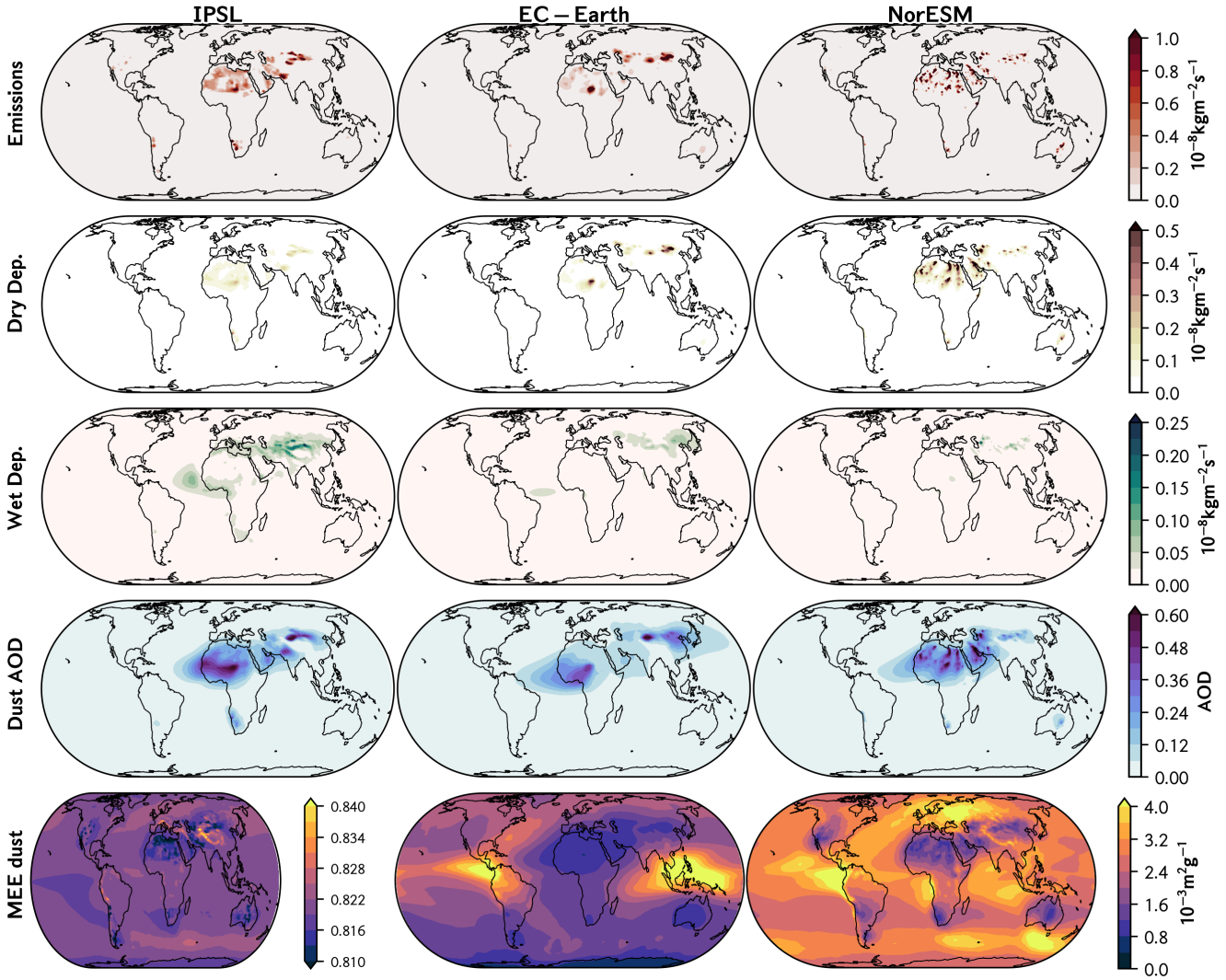

Figure 6. CRESCENDO-ESMs global maps of dust properties (averaged over the 15 years): emission tendency, deposition tendency, dust optical depth and mass extinction efficiency. The models included have a modal based dust parametrisation, these models are: IPSL-INCA, NorESM and EC-Earth. The equivalent figures for PI and PDN experiments are shown in Supplement Material: Figure S.GL.5 and Figure S.GL.6 respectively.

Table 7. Direct Radiative Effects (DRE) at the top of the atmosphere (TOA) and surface (SRF) without clouds in long-wave (LW) and short-wave (SW) for the IPSL model with 4 dust modes as described by Albani and et al (2021). For each mode the value from each method *in* and *out* and their mean value (of both methods) is indicated (the mean value in italics). Both methods are described in the Appendix A, the *method in* adds each specific mode to a case without any mode of dust, the *method out* removes that specific mode to a case with all the modes of dust. Values in italics represent those derived from other values of the table. The value of the sum of the 4 modes is not equal to the value of the multi-modal DRE of dust for each method in/out individually. But the mean of both methods in and out is consistent with the multi-modal DRE.

Dust DRE	TOA LW [W m^{-2}]			TOA SW [W m^{-2}]		
	in	*out*	*Mean*	*in*	*out*	*Mean*
Mode m_1	0.0074	0.0063	*0.0069*	-0.1360	-0.0932	*-0.1146*
Mode $m_{2.5}$	0.0399	0.0349	*0.0375*	-0.2737	-0.2300	*-0.2518*
Mode m_7	0.0913	0.0848	*0.0881*	-0.0779	-0.0440	*-0.0609*
Mode m_{22}	0.0110	0.0087	*0.0099*	0.0188	0.0139	*0.0163*
$\sum$ modes	*0.1497*	*0.1348*	*0.1422*	*-0.4689*	*-0.3533*	*-0.41*
Multimodal			0.142			-0.41

Dust DRE	SRF LW [W m^{-2}]			SRF SW [W m^{-2}]		
	in	*out*	*Mean*	*in*	*out*	*Mean*
Mode m_1	0.0194	0.0142	*0.0168*	-0.2367	-0.1854	*-0.2110*
Mode $m_{2.5}$	0.1180	0.0910	*0.1045*	-0.6413	-0.5378	*-0.5895*
Mode m_7	0.3217	0.2831	*0.3024*	-0.6615	-0.5548	*-0.6082*
Mode m_{22}	0.0540	0.0371	*0.0455*	-0.0653	-0.0442	*-0.0547*
$\sum$ modes	*0.5131*	*0.4253*	*0.4692*	*-1.6047*	*-1.3223*	*-1.4635*
Multimodal			0.467			-1.45

with respect to the emissions is similar for all the experiments, but the emissions of CNRM-3DU decrease with nudged winds by 30%. The deposition value therefore is biased by an approximately constant amount of 75 $\mathrm{Tg\,yr^{-1}}$ independently of the wind field. Given that in any case the value of $\Delta < 5\%$, then we have included the CNRM-3DU model in the ensemble means. In the case of the CNRM-6DU model the consequences of its dynamical core properties are the same, hence there is also a bias. However, it is close to 600 $\mathrm{Tg\,yr^{-1}}$ in total deposition, producing a value of Δ larger than 15%. Therefore, this model is not included in the ensemble means. In both cases, the CNRM-3DU and the CNRM-6DU models the bias in total deposition implies an excess of mineral dust in the atmosphere not consistent with the actual modelled emissions. A further complication is that the bias leads to other biases in variables like concentrations, load and optical depths. For this reason the CNRM-6DU model is not used in our analysis to draw conclusions about the dust cycle. But it is kept in the other analyses to be compared with future developments of the model that improve/fix the mass conservation, and subsequently highlight better

the implications of these kinds of numerical instabilities in dust modelling. For the other models $\Delta < 0.1\%$, with NorESM and EC-Earth presenting values closest to zero.

The multi-model mean global emissions for the PD and PI ~~experiments the multi-model mean 2954~~ simulation experiments are 2836 $\mathrm{Tg\,yr^{-1}}$ and ~~3011~~ 2835 $\mathrm{Tg\,yr^{-1}}$ respectively, with standard deviations of 2680 and 2627 $\mathrm{Tg\,yr^{-1}}$. The PDN experiment shows an ensemble mean value of ~~1530~~ 1614 $\mathrm{Tg\,yr^{-1}}$ which is significantly smaller ~~as UKESM is not present~~ because of the models included (see Table 1), but also because of an important decrease ~~on~~ in the CNRM-3DU ~~and CNRM-6DU~~ total emissions. ~~This value~~ Indeed, the decrease in emissions with nudged winds is even higher in the CNRM-6DU. As a consequence, our ensemble mean value for the PDN experiments agrees well with recent estimations (Kok et al., 2017) when large particles (diameter $\leq$ 20 µm) are not included~~, and~~ . But it also agrees well with previous estimations of 1500 $\mathrm{Tg\,yr^{-1}}$ based on the DEAD model (Zender et al., 2003) for particles with ~~D<~~diameters smaller than 10µm. ~~Also~~ At the same time, when nudged winds are used (PDN ensemble), the standard deviation of total emissions (~~282~~ 278 Tg $\mathrm{yr^{-1}}$) is significantly smaller than ~~in~~ for the PD or PI cases. For the PD experiment~~the multimodel ensemble total emission~~ , the multi-model ensemble mean total emission, for the same models ~~that those of PDNexperiment~~ as available for PDN, has a mean value of ~~2268~~ 1843 $\mathrm{Tg\,yr^{-1}}$ with a standard deviation of ~~1000~~ 544 $\mathrm{Tg\,yr^{-1}}$ ~~.~~

~~The~~ significantly larger than the standard deviation of the PDN experiment. Therefore, nudged winds decrease model diversity in terms of global emissions. Indeed, the CNRM-6DU and CNRM-3DU models have total emissions with nudged winds similar to the CRESCENDO-ESMs ensemble mean, but they produce higher emissions without nudged ~~wind-field~~winds-field, i.e. 2600 $\mathrm{Tg\,yr^{-1}}$ in CNRM-3DU model (diameters up to 10 µm), and 3500 $\mathrm{Tg\,yr^{-1}}$ for CNRM-6DU (diameters up to ~~50~~ 100 µm, see Table 1). These values are similar to the 3000 $\mathrm{Tg\,yr^{-1}}$ reported by Tegen and Fung (1994) for particle sizes between 0.1 and 50 µm. ~~Due~~ Finally, due to the presence of particles with diameters up to 62 µm, the UKESM model has notably higher emissions (although in this case we can't assess the role of surface winds). ~~These~~

This higher value of total emissions due to large particles is not directly correlated with the modelled dust load in the atmosphere. The reason is that the lifetime of dust particles in the atmosphere depends on the size and these large particles sediment faster~~as shown by the~~ . For instance, the UKESM model has monthly mean global ~~loadings with~~ loading values close to the other models, and the smaller lifetime of dust in the atmosphere (less than 12 hours, a characteristic value of ~~larger~~ largest particles).

~~The mass budget of CNRM-6DU and CNRM-3DU models are only closed within $\Delta \simeq 4.5\%$ as their dynamical cores are based on a semi-Lagrangian method (Voldoire et al., 2012, 2019) which is not fully mass conservative in terms of the tracers. The deposition value therefore represents a lower threshold to actual values since a fraction of the emitted mass is effectively deposited (during long-term transport) but not accounted for in deposition fluxes. For the other models $\Delta < 0.1\%$, with NorESM and EC-Earth presenting values closest to zero. Regarding the~~ In fact, the dry deposition of larger particles for UKESM ~~the dry deposition~~ (which for this model includes sedimentation) is truly dominant, resulting in a wet deposition close to other models, like IPSL, without the largest particles modelled~~like IPSL. In~~ . On the contrary the CNRM-6DU wet deposition is two times larger than ~~those of~~ that of the UKESM or IPSL models ~~at~~ in the PD simulation (being CNRM-6DU the only model for which wet deposition ~~exceed~~ exceeds total dry deposition) but close to IPSL with nudged winds. Because larger particles

are deposited faster by gravitational settling, it is expected that $\mathcal{R}_{dep}$ would be larger for those models including the largest particles, but it is only obvious for the UKESM model. For the CNRM-6DU model that is not the case. EC-Earth ~~doubled~~ has double the value of $\mathcal{R}_{dep}$ of IPSL, and NorESM is 6 times larger. Previously, Shao et al. (2011) reported values for $\mathcal{R}_{dep}$ of between 1.03 and 8.1 also uncorrelated with the size range of the dust ~~particle~~ particles modelled. The ~~multimodel~~ multi-model ensemble mean for total dry deposition~~is 562.7~~ , without gravitational settling is 622 $\mathrm{Tg\,yr^{-1}}$ for the PD experiment and ~~430~~ 558 $\mathrm{Tg\,yr^{-1}}$ for PDN~~, in~~ . In the case of wet deposition~~we estimated 920 and 577~~ , we estimated 623 and 531 $\mathrm{Tg\,yr^{-1}}$ ~~multimodel mean for~~ for the multi-model mean for the PD and PDN experiments respectively.

~~CRESCENDO-ESMs global maps of dust properties (averaged over the 15 years): emission tendency, depositions tendency, dust optical depths and mass extinction efficiency. The models included have a modal based dust parametrisation, these models are: IPSL-INCA, NorESM and EC-Earth. The equivalent figures for PI and PDN experiments are shown in supplement material: figure S.GL.5 and figure S.GL.6 respectively.~~

Despite the similar values of our ensemble mean, the standard deviation of dry deposition is more than two times that from wet deposition. To summarise, each of the processes: sedimentation, wet deposition and dry deposition (without sedimentation) has a similar contribution in the ensemble mean for all the experiments, but this is masking strong differences in these three properties from each of the models.

~~The~~ As explained above, the impact of the largest particles on the global behaviour of loading and dust optical depth ~~and loadings~~ is considered less important than coarse particles (up to 10 μm), so this hypothesis allows us to compare ~~with observational constrains~~ all models with observational constraints that rely on optical depth measurements. Figure 4 (top panel) compares the PD experiment with the Kok et al. (2017) proposed values of dust optical depth and total load, ~~whereas in addition we derived~~ where we also derive the mass extinction efficiency (MEE) field as the ratio of dust optical depth to ~~loadings fields~~loading field, see Table 4. ~~The~~

Figure 4 indicates that, aside from the CNRM-6DU model, all models have dust loadings smaller than 20 Tg with the loading of NorESM half that of the ensemble median value. As already noted above, the load of CNRM-6DU model is subject of a bias due to the artificial mass introduced during the transport. Therefore, the set of models included in our ensemble mean (Table 6) agrees with the AeroCom Phase I models where the fine dust dominates with a total load ensemble mean value of 15 Tg.

Based also on AeroCom Phase I, Huneeus et al. (2011) reported a MEE multi-model median of 0.72 $\mathrm{m^2 g^{-1}}$, similar to the global MEE value of 0.6 $\mathrm{m^2 g^{-1}}$ used by Pu and Ginoux (2018b) to compare DOD and dust loadings of CMIP5 models. Recently, Adebiyi et al. (2020) estimated a mean over 13 observational stations giving a value slightly smaller than 0.6 $\mathrm{m^2 g^{-1}}$. Our estimation of MEE shows that EC-Earth and NorESM depart from that value, whereas the other models remain reasonably close to the Pu and Ginoux (2018b) hypothesis and the AeroCom Phase I median value. Our results also highlight that the MEE depends on the modelled dust particle size distribution (in particular the presence of large particles) but with a significantly smaller inter-annual variability than dust optical ~~depths and loadings~~depth and loading. This fact explains ~~the use of MEE~~ its use for ad-hoc relationships between dust optical depths and loadings with a constant factor (Pu and Ginoux, 2018b).

~~Based on the histogram of the annual global values~~ We note that the global mean values for the models, as shown in Figure 4 (top panel) are partially influenced by ocean or land regions with low dust loadings. To complement this analysis, we present

Table 8. First part of the table: Emissions [Tg yr^{-1}] for Present Day (PD) and their contribution fraction to the total global emissions. Globally, over Land and over coastline pixels. (*) Denotes those models with modelled bin diameters larger than $20\mu m$. Sahara desert emissions and its percentage over total emissions is obtained from the sum of the regions: Western Sahara, Mali, Bodele and North Sahara, so it is not including Sahel. Second part of the table: Emissions [Tg yr^{-1}] for Present Day (PD) simulations. Over 16 different regions, see Figure 3. In brackets the order of the 10 regions with the largest emissions. The multi-model ensemble mean (MM-mean) includes the mean values ± the standard deviation for all the models, and (‡MM-mean) for all the models without UKESM. On the Supplementary Information (Section E), Tables E1 to E4 have the analogous information for the PI and PDN experiments. Ensemble mean of emissions are including CNRM-6DU.

	CNRM-6DU (PD)		CNRM-3DU (PD)		EC-Earth (PD)		IPSL (PD)		NorESM (PD)		UKESM (PD)		MM-mean (PD)		‡MM-mean (PD)	
Global Earth	3542.2	(*)	2605.2		1126.6		1557.5		1368.2		7524.4	(*)	2954	(± 2415)	2040	(± 1012)
Land	3377.4	(*)	2526.1		1111.0		1550.9		1343.6		7506.4	(*)	2903	(± 2410)	1982	(± 948)
Ocean (Coast)	164.8	(*)	79.1		15.6		6.6		24.6		18	(*)	52	(± 61)	58	(± 66.)
Sahara Desert	2071.5	(58%)	1734.2	(66%)	445.2	(39%)	715.4	(46%)	651.8	(48%)	4339.5	(58%)	1660	(± 1466)	1124	(± 728)
North. Hemis.	3135.3	(88%)	2292.7	(88%)	1072.9	(95%)	1377.6	(88%)	1256.1	(92%)	6614.9	(89%)	2625	(± 2104)	1827	(± 870)
South. Hemis.	406.9	(12%)	312.5	(12%)	53.7	(5%)	179.9	(12%)	112.1	(8%)	909.5	(11%)	329	(± 313)	213	(± 145)
South America	17.4		13.3		11.3		36.9		9.0		18.2		18	(± 10)	18	(± 11)
South-Africa	5.8		17.0		2.8		113.8	(5)	31.8		30.3		34	(± 41)	34	(± 46)
Australia	343	(4)	235.4	(5)	35.9	(9)	10.7		59.3	(8)	691.2	(5)	229	(± 261)	137	(± 145)
Western Sahara	242.5	(6)	296.1	(4)	52.1	(6)	87.4	(7)	95.8	(4)	788.8	(4)	260	(± 276)	155	(± 108)
Mali/Niger	382.4	(3)	323.2	(3)	49.5	(7)	83.4	(9)	69.5	(7)	841.2	(3)	292	(± 304)	182	(± 158)
Bodele/Sudan	540.4	(2)	569.4	(1)	259.6	(2)	305.8	(1)	190.6	(3)	1852.2	(1)	620	(± 623)	373	(± 171)
North Sahara	906.2	(1)	545.5	(2)	85.0	(5)	238.8	(2)	295.9	(1)	857.3	(2)	488	(± 339)	414	(± 321)
North-MiddleEast	253.7	(5)	112.8	(9)	17.0		28.1		146.1	(4)	303.7	(8)	144	(± 117)	112	(± 97)
South-MiddleEast	208.0	(8)	195.9	(6)	39.5	(8)	68.1		83.7	(5)	441.1	(6)	173	(± 149)	119	(± 77)
Kyzyl Kum	230.3	(7)	118.7	(7)	118.8	(3)	142.4	(4)	198.7	(2)	377.4	(7)	198	(± 99)	162	(± 50)
Thar	136.3		56.1	(8)	19.1		86.2	(8)	13.9		288.7	(9)	100	(± 103)	62	(± 51)
Taklamakan	15.2		15.7		104.6	(4)	153.0	(3)	35.5	(9)	75.0		67	(± 55)	65	(± 61)
Gobi	140.2	(9)	36.2	(9)	269.8	(1)	113.1	(6)	80.6	(6)	230.3		145	(± 89)	128	(± 88)
North-America	0		1.1		2.3		28.4		6.1		57.1		15.8	(± 23)	7.6	(± 12)
Gulf-of-Guinea	2.5		1.4		0.0		0.0		1.9		69.3		12.5	(± 27.8)	1.2	(± 1.1)

‡ These statistics exclude UKESM.

two additional comparisons in the supplementary material. The first is shown in Figure S.GL.1, for the case when only values over land are considered. The second is shown in Figure S.GL.2 for the case when the annual values are estimated over the dust belt that covers most of the Sahara and the Middle-East. Both Figures still indicate important differences between models.

To further understand the properties of dust optical depth~~we estimated the distribution~~ , we calculated the distribution of values for each model ~~based on~~ with a kernel density estimation based on the histogram of the annual global values of dust optical depth. The results shown in Figure 4 (bottom left panel) indicate the presence of two main groups for our model ensemble~~on the one centered~~ : the first one centred around a value close to 0.01, and the second one around 0.025, a value closer to the proposed constraint. The solid black line shows the distribution of dust optical depth at 550 nm ~~for a annual sampling with a kernel density estimation, and how it compares with the distribution proposed by Ridley et al. (2016) and~~ proposed by Ridley et al. (2016), and the vertical lines indicate the mean of that distribution and the AeroCom Phase I median value. The EC-Earth model agrees actually in both central value and typical inter-annual variability (as represented by the width of the distributions). These results should be also interpreted in the context of the total aerosol optical ~~depths~~depth (AOD), Figure 4 (bottom right panel). We observe that the UKESM has ~~lower~~ the lowest values of dust optical depth but actually the largest values of total aerosol optical depth, with similar global mean values to those obtained by MODIS at 550 nm but with a narrower distribution. The EC-Earth model has AOD values slightly smaller than MISR estimates but with similar inter-annual variations.

~~Aside from the CNRM-6DU model, all models have values of dust loadings smaller than 20 with NorESM at about half of the ensemble median value. This agrees with the AeroCom Phase I models where the fine dust dominates the total loads with ensemble value of 15 . The MEE multi-model median reported by Huneeus et al. (2011) is 0.72 , similar to the global MEE value of 0.6 used by Pu and Ginoux (2018b) to compared DOD and dust loadings of CMIP5 models. Recently, Adebiyi et al. (2020) estimated a mean over 13 observational stations giving a values slightly smaller than 0.6 . Our estimation of MEE shows that EC-Earth and NorESM depart from that value, whereas the other models remained close reasonably to (Pu and Ginoux, 2018b) hypothesis and AeroCom median value.~~

~~We note that the global mean values for the models, as shown in Figure 4 (top panel) are partially conditioned by ocean or land regions with low dust loadings. To complement this analysis, we present two additional comparisons in the supplementary material. The first is shown in Figure GL1, for the case when only values over land are considered. The second is shown in~~ The bottom right panel of Figure ~~GL2 for the case when the annual values are estimated over the dust belt that covers most of the Sahara and the Middle-East. Both Figures still indicate important differences between models. Recently, Adebiyi and Kok (2020) proposed that the total load of dust in the atmosphere is higher than typical estimation and give a mean value close to 30 , where the contribution of coarse mode is more important than the fine mode. In this case the estimation of CNRM-6DU model would be the most accurate of the CRESCENDO-ESM in terms of total mass of mineral dust in the atmosphere~~4 indicates model discrepancies in the magnitude of the inter-annual variability (as measured by the width of the distribution) and an overall underestimation of AOD at 550 nm with respect to these satellite platforms.

A specific PDN experiment with the IPSL model was run for 5 years (2010 to 2014) to ~~analyze~~ analyse how the representation of the dust size distribution influences the dust cycle. In this simulation, named IPSL-4DU, the dust scheme is based on 4 dust insoluble modes (m_1,$m_{2.5}$,m_7 and m_{22}, where the number indicates the MMD (mass median diameter) value of that log-normal mode) covering the whole range of sizes from 0.1 to 100 µm and nudged winds were used. The results shown in the ~~Table~~ Supplement Table S.GL.7 are consistent with the impact of larger particles on dust emissions and loadings in UKESM, and allow us to discuss the role of each mode independently. The total emissions for IPSL-4DU are dominated by ~~larger particles~~the largest particles, those of mode m_{22}, but are promptly removed from the atmosphere through their sedimentation which is very rapid compared with the typical lifetime of mineral dust, as shown in Table 6. When comparing the total load for each mode, actually the coarse size mode $m_{2.5}$ is more abundant than m_{22}. Amongst all the modes, mode m_7 has the largest contribution, with 2/3 of the total, which is comparable to the large particles represented in the CNRM-6DU model, consistent with Adebiyi and Kok (2020). Note that the dust loads in CNRM-6DU model are larger than in CNRM-3DU, ~~albeit similar emissions . The~~ to a degree that cannot be explained solely by the larger emissions of CNRM-6DU. An explanation for this difference is that the bin that includes particle sizes from ~~1.25 to 10~~ 2.5 to 20 µm in CNRM-3DU is split into different bins in the CNRM-6DU model, which have different life times in the atmosphere, and that non-conservative transport could create larger aerosol mass in the CNRM-6DU configuration. In contrast to emissions, optical properties are dominated by the contributions of accumulation to coarse size particles compared to the largest particles of mode m_{22} that does not play a large role in its contribution to aerosol extinction. Those values are then used for assessments about modal contributions to direct radiative effects.

Mineral dust aerosol interaction with solar and terrestrial radiation results in both absorption and scattering of light. These interactions are strongly dependent on dust mineralogical composition and particle size distribution, hence they differ regionally (Ginoux, 2017; Kok et al., 2017). We estimated the respective roles of the different modes (that represent different particle ~~sizes~~ size ranges), ~~we remind~~ and note that in the case of multi-modal distributions the estimations of direct radiative effects (DRE) by each mode is, somewhat, non-linear (Di Biagio et al., 2020). This is illustrated ~~when~~ by the sum of the contribution of the DRE from each mode which is not exactly equal to the multi-modal dust contribution. ~~The Appendix A show~~ Appendix A shows how, with an estimation of DRE per mode based on the combination of two different methods, we ~~ascertained~~ determined modal values of DRE that~~combine~~ , when combined, come close to the multi-modal DRE estimation. This is summarised in Table 7 where the ~~estimations~~ estimates per-mode DRE for each method are shown together ~~the~~ with their mean. The sum of these mean values per mode is now consistent with the multi-modal DRE. It is remarkable how the estimations of DRE at TOA-SW (top of the atmosphere in the short-wave) for m_7 ~~by~~ for each method differ by a factor of 2. The non-linear effects ~~in the surface at~~ at the surface in the SW are also important with differences in the sum of the 4 modes between methods of 0.3 Wm^{-2}.

The analysis of direct radiative effects (DRE) by mode, shown in Table 7, indicates that the largest particles (mode m_{22}) have a minor impact on the DRE in both LW and SW according to IPSL-4DU model. In contrast, the inclusion of the mode with the smallest particles contributes to ~~the~~ SW cooling although it is the coarse size mode ~~the one~~ that dominates the net

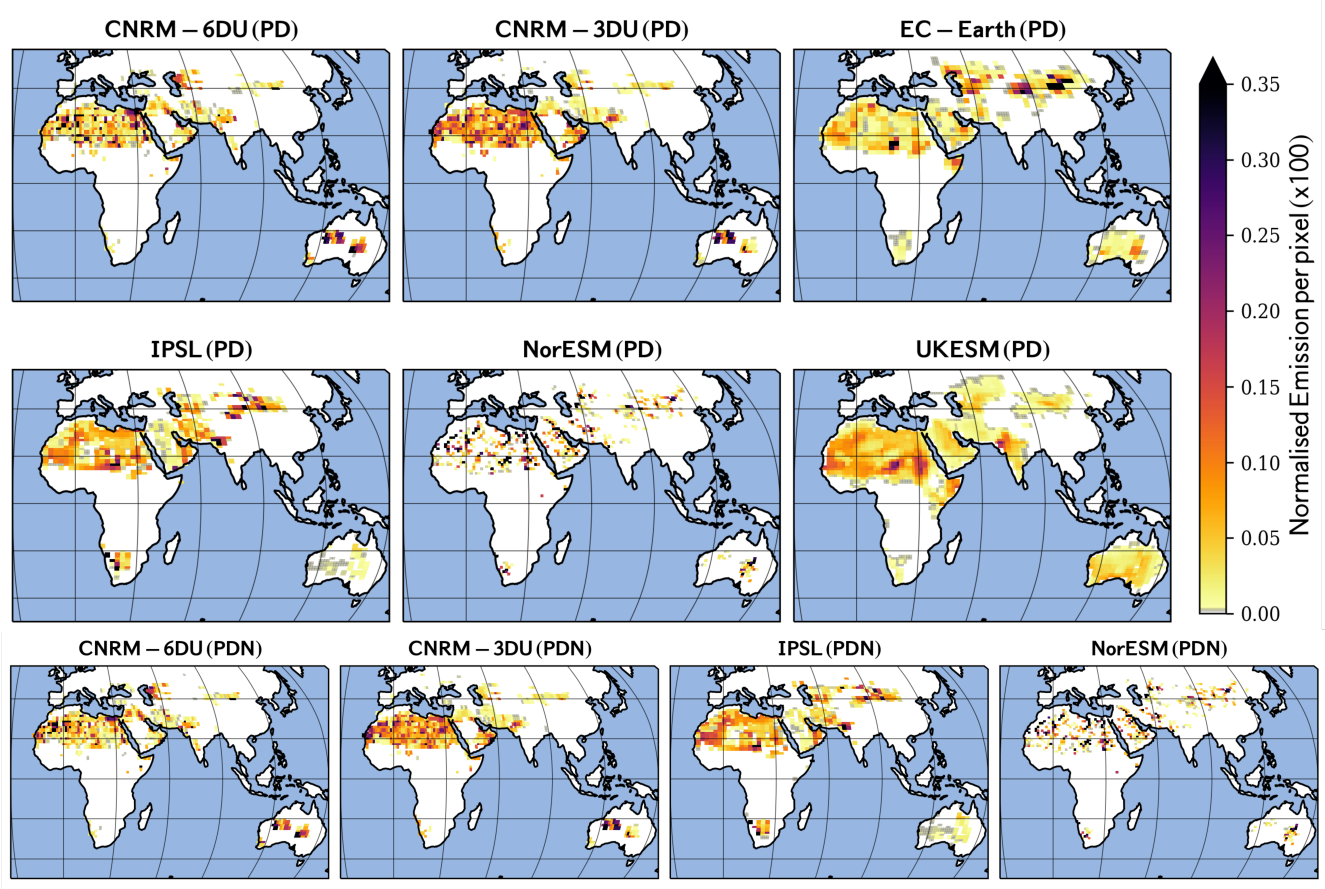

Figure 7. Normalized map of emissions (x100) over NorESM grid resolution. On the top: experiment with present day aerosol and chemistry forcings (PD), on the bottom the PDN experiment. We used a conservative near-neighbour interpolation to create emission maps that preserve global values on higher resolutions, then the maps were normalized to have a common comparison scale. The color-bar represents the normalized emission tendencies per grid with range [0,100]. The figure S.E5 is the ~~analogous~~ correspondent of this figure for PI experiment.

direct radiative effects at the top of the atmosphere. At the surface however, the mode m_7 has the largest effect on both SW and LW but its net contribution (LW+SW) is smaller than the coarse mode $m_{2.5}$.

It is important to note that the DRE shown in Table 7 is estimated without scattering in the LW (only absorption). To neglect the LW scattering in the case of mineral dust implies an underestimation of TOA-DRE-LW (Dufresne et al., 2002), mostly in cloud conditions.

5.2 Dust global spatial patterns

A global picture of the dust cycle is shown in Figures 5 and 6, which describe temporal mean properties of dust in CRESCENDO ESMs (PD simulations) over the 15 years. ~~Models~~ The spatial resolution and vertical levels of the models are introduced in Table 1.

First, those models that have a sectional representation of the DPSD (CNRM-6DU, CNRM-3DU and UKESM) are shown in Figure 5. For all these models, emission and dry deposition show strong spatial correlations because gravitational settling of large particles ~~is happening~~ occurs close to dust sources, whereas wet scavenging dominates the deposition process over the oceans. The extension of regional emissions over the Sahel and Somalia is more pronounced for UKESM than for the CNRM models. Although the Chalbi Desert in Kenya is also a location for emission in the CNRM models, the extent over which emissions occur in the UKESM is significantly larger. The figure also suggests differences in deposition for the CNRM models: the CNRM-3DU model has higher values of dry deposition than CNRM-6DU but the opposite is true for wet deposition. These differences in wet deposition are pronounced over the North Atlantic and the Indian Ocean. In contrast, wet deposition is more intense over the Sahel and the Indian sub-continent in the UKESM model which indicates the strong role of the monsoon at scavenging dust. It is also noticeable that the CNRM-3DU annual mean wet deposition decreases from West to East over the Indian Ocean while the inverse is true for UKESM. Despite systematic smaller values for UKESM optical depth compared to CNRM-3DU, they have rather similar spatial distributions, except in Australia. Analogous of figures 5 for PI and PDN are shown in Figures S.GL.3 and S.GL.5, respectively. The figures of the PI experiment demonstrate no differences with the PD experiment, but the PDN experiment for CNRM models show smaller values of deposition and optical depth but with similar spatial patterns, due to the decrease of their dust emissions with nudged winds.

~~Models~~ Second, the models with a modal description of the DPSD (IPSL, EC-Earth3-AerChem and NorESM) are shown in Figure 6. Dust emissions from EC-Earth are more intense in Asia than ~~other for~~ for the other models whereas EC-Earth has the smallest emissions from the Northern Sahara. This causes the trans-Pacific transport of dust to peak in this model compared to others, and the transport across the Atlantic to be smaller. Northern Sahara emissions from NorESM are more ~~localized~~ localised but with larger peak values. Like for sectional models, dry ~~depositions~~ deposition correlates well spatially with emissions whereas wet deposition dominates over oceanic regions. EC-Earth shows both larger wet deposition and optical depth over East Asia extending into the Sea of Japan. For all models with a modal scheme, wet deposition over the Indian ocean is mostly occurring over its Western part. Analogous of ~~Figures 5 and 6 but~~ figures 6 for the PI and PDN experiments are shown in Figures S.GL~~.3 and S.GL~~.4 ~~for PI and Figures S.GL.5~~ and S.GL.6~~for PDN~~ , respectively. Here, the results of PI and PDN draw a picture with similar global properties of dust cycle to the PD experiment.

5.3 Dust emissions

The dust emission rate is defined as the surface mass flux of mineral dust in the vertical direction F_d. This flux is derived in climate models as a function of surface winds but there are different schemes depending on the complexity of the description. Shao and Dong (2006) classify all dust emission schemes in three different categories named α, β and γ schemes. The α-schemes are those where F_d is directly described in terms of the wind speed (with a non-linear function including a friction velocity threshold) with an imposed empirical size distribution at emission. IPSL-INCA uses this approach. The β-schemes instead estimate the vertical flux from the dust horizontal mass-flux which itself can be ~~parameterized~~ parameterised depending on a geographical erodibility factor and the surface wind. Although this erodibility factor depends on soil properties and moisture, sub-daily global patterns of dust emission are tightly correlated with wind fields, and therefore with the atmospheric general circulation (Shao et al., 2011). Examples of β-schemes are those described by ~~(Zender et al., 2003) and (Woodward, 2001b)~~ Zender et al. (2003) and Woodward (2001b) that are used respectively by NorESM and UKESM models. ~~But also~~ It is also used in the EC-Earth model whose horizontal flux is estimated with the scheme described by Marticorena and Bergametti (1995) which distributes particles in four bins with values up to 8 µm. Those values are mapped in the modes described in the Table S.MD.9. In the case of UKESM the horizontal flux is also calculated based on Marticorena and Bergametti (1995) into 9 bins of diameters between 0.064 to 2000 µm but mapped for transport into 6 bins described in Table S.MD.9. Similarly the CNRM models have a drag partition according to Marticorena and Bergametti (1995) but the size distribution at emission follows that defined ~~at~~ by (Kok, 2011). The γ-schemes aim to describe the physical process driving the size resolved vertical flux but they require additional information of the underlying soil properties and are not used by CRESCENDO-ESM.

Despite the different schemes all of them agree that the regions where most dust is uplifted are subtropical arid and semi-arid regions. Such regions are ~~characterized~~ characterised by atmospheric stability and scarce rainfall. This global pattern is however modulated by the Inter-Tropical Convergence Zone (ITCZ) oscillations, monsoons, and orography, as visible in Figures 5 and 6. Because the Himalayan mountains filter the ~~water-vapor transport from then~~ water-vapour transport from the Indian Ocean all the models have important dust sources in Northern Asia (such as the Taklamakan and Gobi deserts) but the specific location of Asian sources, and their relative contribution to global emissions differs significantly between models.

Nowadays, we understand how regional climate influences the dust emissions and ~~its~~ their variability, together with the atmospheric systems linked to dust emission episodes. But dust emission modelling still constitutes an active research field (Shao, 2008). In particular, the dust particle size distribution (DPSD) at emission is critical for a better description of the global dust cycle (Mahowald et al., 2014) but its modelling ~~need~~ needs to be improved for three main reasons: ~~first~~ (1) because there is not an unified approach; ~~second~~ (2) because there are discrepancies in the role of wind speed at emission for larger dust particles (Alfaro et al., 1998, 1997); and ~~third~~(3), because the quantitative link between soil properties and dust emission fluxes still ~~need~~ needs additional research.

~~Despite the several set of parametrizations~~ Regardless of the several sets of parametrisations of DPSD at emission (Kok, 2011; Alfaro and Gomes, 2001; Shao, 2001, 2004)~~the modeling~~ , the actual modelling of dust in global climate models is highly influenced by a balance of the different elements involved (vertical flux at small scale, soil erodibility, wind fields),

Table 9. Total wet deposition [Tg yr^{-1}] for Present Day (PD) simulations. Over oceanic regions, see Figure 2. The numbers in brackets show the fraction of global deposition over the ocean. The numbers in parentheses indicate the ranking order of contribution to the global total wet deposition by region from the highest to the lowest. The equivalent Tables for the PI and PDN experiments are in Supplementary Information: Tables S.DD.1 and S.DD.2, respectively.

	CNRM-3DU (PD)		EC-Earth (PD)		IPSL (PD)		NorESM (PD)		UKESM (PD)		MM-$\mu \pm \sigma^{\dagger}$		CNRM-6DU (PD)	
Global Earth	753.8		493.2		968.3		275.7		949.8		688±300		2108.9	
Land	541.3		272.9		575.7		203.9		673.6		453±200		1397.1	
Ocean	212.5	[28%]	220.3	[45%]	392.6	[40%]	71.8	[26%]	276.1	[29%]	235±120		711.8	[33%]
North Atlantic	65.4	(1)	61.7	(2)	156.1	(1)	23.7	(1)	103.4	(1)	82±50	(1)	207.4	(1)
South Atlantic	5.1	(5)	14.6	(5)	47.0	(2)	2.5	(4)	11.3	(4)	16±18	(4)	9.1	(6)
North-Indian Ocean	47.8	(2)	16.6	(4)	36.5	(4)	16.2	(2)	33.1	(3)	30±14	(3)	187.2	(2)
South-Indian Ocean	13.9	(4)	4.1	(6)	18.5	(5)	2.4	(5)	11.1	(5)	10±7	(5)	39.3	(4)
Pacific West	21.1	(3)	70.5	(1)	39.1	(3)	7.3	(3)	41.5	(2)	36±24	(2)	93.6	(3)
Pacific North-East	0.2	(8)	21.0	(3)	12.2	(6)	1.0	(6)	10.2	(6)	8.9±8	(6)	2.9	(7)
Pacific South-East	2.5	(6)	3.0	(7)	3.8	(8)	0.9	(7)	5.9	(7)	3.2±2	(8)	9.9	(5)
Antarctic Ocean	2.2	(7)	2.5	(8)	7.3	(7)	0.6	(8)	4.3	(8)	3.4±3	(7)	5.4	(8)
Ocean. North. Hemis.	162.9		188.5		287.4		59.2		218		183±80		569.1	
Ocean. South. Hemis.	49.5		31.8		104.2		12.5		58.1		51±30		142.1	

† Statistic is not including CNRM-6DU.

Table 10. Total dry deposition [Tg yr^{-1}] for Present Day (PD) simulations. Over oceanic-regions, see Figure 2. The numbers in brackets show the fraction of global deposition over the ocean. The numbers in parentheses indicate the ranking order of contribution to the global total dry deposition by region from the highest to the lowest. The ensemble mean (and standard deviation) includes all the models except CNRM-6DU and UKESM. The equivalent Tables for the PI and PDN experiments are in Supplementary Information: Tables S.DD.3 and S.DD.4, respectively. The ensemble statistics for Global Earth and Land is not including UKESM due to their large values of gravitational settling would drive the estimate. Over ocean regions

	CNRM-3DU (PD)		EC-Earth (PD)		IPSL (PD)		NorESM (PD)		UKESM (PD)		MM-$\mu \pm \sigma$		CNRM-6DU (PD)	
Global Earth	1925.8		633.5		590.6		1092.5		6566.3		1061±620‡		2025.9	
Land	1678.1		555.8		523.1		986.6		6366.1		936±540‡		1681.1	
Ocean	247.7	[7.7%]	77.7	[12%]	67.5	[11%]	105.9	[10%]	199.4	[3%]	140±80†		344.8	[17%]
North Atlantic	99.5	(1)	31.7	(1)	31.6	(1)	28.4	(2)	81.9	(1)	54±34†	(1)	120.3	(1)
South Atlantic	5.5	(5)	2.3	(4)	5.3	(3)	2.5	(4)	1.9	(5)	3.5±1.8†	(5)	2.3	(6)
North-Indian Ocean	63.6	(2)	14.3	(2)	13.8	(2)	49.5	(1)	51.3	(2)	38±23†	(2)	106.7	(2)
South-Indian Ocean	18.8	(3)	1.4	(7)	0.9	(6)	0.8	(6)	9.1	(4)	6.2±8†	(4)	26.2	(3)
Pacific West	11.0	(4)	13.3	(3)	2.3	(5)	3.9	(3)	12.5	(3)	8.6±5.1†	(3)	24.5	(4)
Pacific North-East	0.3	(8)	2.2	(5)	2.7	(4)	0.9	(5)	1.5	(6)	1.5±1.0†	(6)	0.4	(7)
Pacific South-East	3.0	(6)	0.4	(7)	0.5	(7)	0.6	(7)	0.6	(7)	1.0±1.1†	(7)	4.9	(5)
Antarctic Ocean	0.1	(8)	0.2	(8)	0.3	(8)	0.1	(8)	0.4	(8)	0.2±0.1†	(8)	0.2	(8)
Ocean. North. Hemis.	199.5		71.3		58.3		98.6		172.4		120±63†		280.9	
Ocean. South. Hemis.	48.1		6.4		9.2		7.3		26.9		20±18†		63.8	

‡ Statistic is not including CNRM-6DU and UKESM. † Statistic is not including CNRM-6DU.

which explains that during last decade the estimation of dust emissions when online coupled with meteorological fields have improved their results significantly. On ~~one side~~ the one hand the modelled wind surface friction velocity and speed agree better with actual meteorological conditions, and on the other ~~side~~ hand, the description of the soil surface properties has become more accurate ~~.~~

due to both, improvements in the soil texture databases, and the use of satellite retrievals to better describe the roughness length, e.g Prigent et al. (2005); Menut et al. (2013).

All those facts explain why the comparison (Table 8) of the emissions (PD experiment) over large regions is fairly consistent among models: they agree on the main source of mineral dust being located in the ~~Sahara~~ Saharan desert but representing ~~,~~ from 39% of total global emissions in the EC-Earth model to 66% in CNRM-3DU. Previous studies (Shao et al., 2011) estimated the contribution of Africa to dust emissions ~~on a~~ in the range from 50% to 68% but also including Namibia Desert emissions. The consistency is larger when we ~~considered~~ consider larger regions like hemispherical contributions where all the models show ~~emissions beyond~~ more than 85% ~~in~~ global dust emissions from the Northern Hemisphere. When smaller regions are considered, the differences in relative contributions between models increase, which is also expected when turbulence at small scale and/or convection (Allen et al., 2015) plays a role in dust events. If we evaluate total values rather than relative contributions, the driving factor ~~to explain~~ that explains differences between modelled emissions ~~relies in~~ is the upper threshold of particle sizes at emission.

Dust emissions by ~~regions~~ region (which are shown in Figure 3) and their intensities (in $\mathrm{Tg\,yr^{-1}}$) are listed in Table 8 for the PD experiment. The most intense source of dust for the EC-Earth model is located over the Gobi Desert, while North Sahara, a key emitting region in all other models, constitutes only the 4th most intense region in emissions (after the Taklamakan and the Kyzyl-Kum). The ~~Bodele~~ Bodélé is remarkably an important dust source across all CRESCENDO ESMs. As expected from the analysis of dust optical depth over Asian regions~~:~~ , the Taklamakan, Kyzyl Kum and Thar deserts exhibit substantial differences. Regarding UKESM, it has an additional and extended dust source over the Somalia Desert (see Fig. 5) which is only a relatively small source in other models. ~~The analogous Tables of 8 can be found for PDN and PI experiments~~ Analogues of Tables 8 for the PDN and the PI experiments can be found in Tables S.DE.1 to S.DE.4, respectively, showing similar model differences.

If we want to compare realistically global climate model emissions over smaller regions, we need to account for the different model resolutions. We opted to display ~~normalized emissions~~ normalised emission estimations over a common grid for all the models. Our method interpolates the emission flux from each model grid to that with the highest spatial resolution (NorESM). We use a near-neighbour interpolation method which conserves the flux in each model when compared to the flux integrated over the original model resolution. This method is not introducing any ad-hoc information on how the emission tendency is distributed within the original grid-pixel. A monthly time-series of ~~normalized~~ normalised emitted dust mass per grid-pixel, with respect to global monthly emissions, is produced using this method. These ~~normalized~~ normalised emissions over a common grid allow us to pick up differences over ~~spots~~ locations that are caused either by the formulation of the source function or by the dust particle size distribution imposed during the emission process.

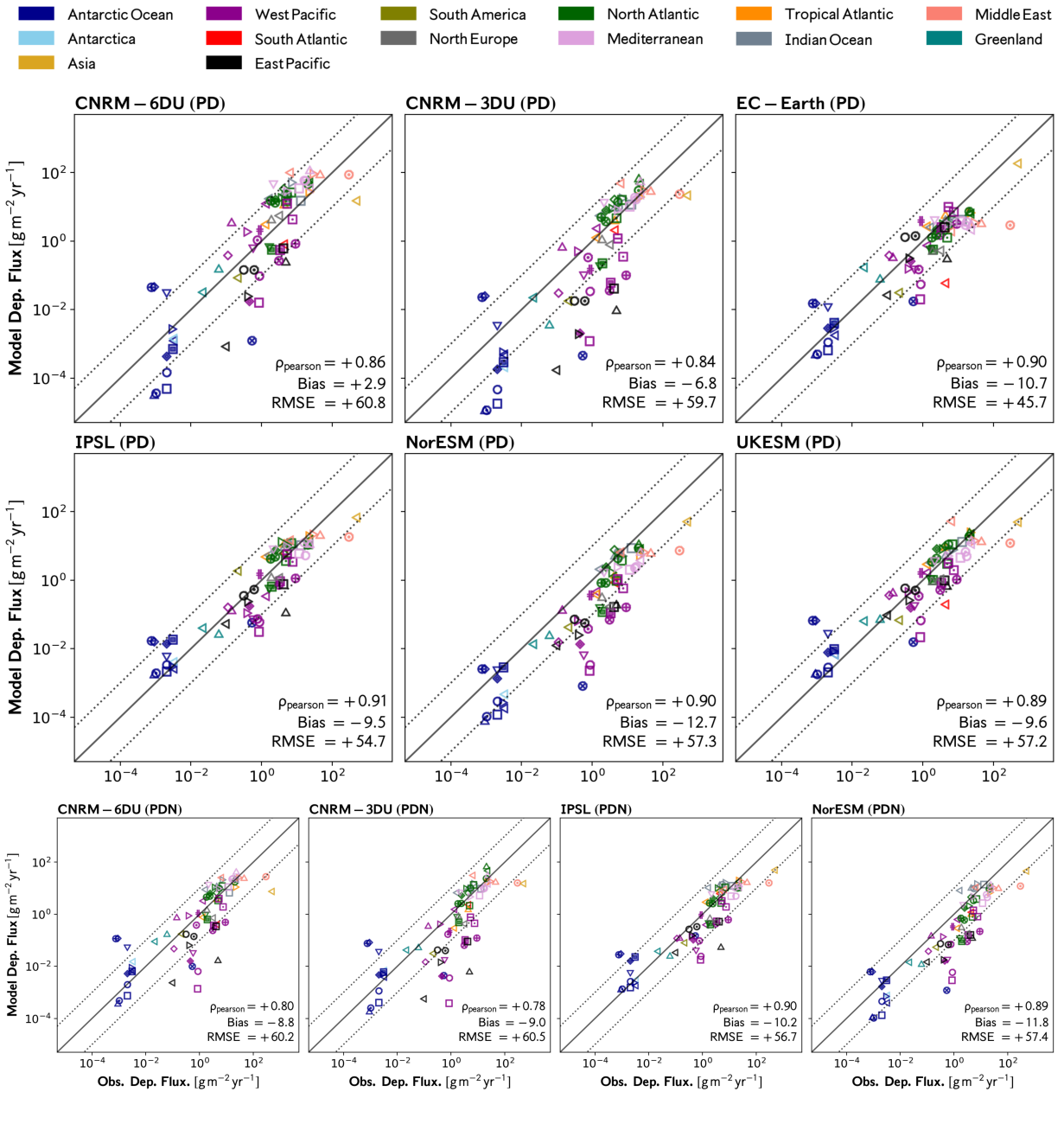

Figure 8. Comparison of estimated total annual deposition flux with CRESCENDO ESMs with the dataset presented ~~at (Huneeus et al., 2011)~~by Huneeus et al. (2011), whose stations are mapped in Figure 1 (left panel). The model values taken are those from the PD experiment (top part) and the PDN experiment for bottom row. Figure S.D11 is the analogous of this figure but for the PI experiment.

A direct comparison of dust emission maps with observations is challenging because it would require ~~to translate~~ the translation of the observed frequency of dust events into a dust emission flux rate (Evan et al., 2015). Assuming the hypothesis of Evan et al. (2015) for this mapping, the hot spots of their ~~SEVIRI emission normalized~~ Spinning Enhanced Visible and InfraRed Imager (SEVIRI) emission normalised product can be compared with our ~~normalized~~ normalised maps (in terms of relative contribution of different pixels over North Africa). In particular they suggest that beyond ~~Bodele Depresion~~ Bodélé Depression an important source is at Hoggar Mountains (west of ~~Bodele~~ Bodélé Depression). This feature is only captured by ~~CNRM model~~the CNRM models.

The annual average of these monthly maps is presented in Figure 7 for PD and PDN experiments. The models CNRM-6DU and CNRM-3DU show similar values per grid-cell, which indicates the use of the same information on soil properties, but the ~~normalized~~ normalised emissions although similar are not identical, reflecting the differences in dust size distribution at emission. In these models, the ~~normalized~~ normalised emissions over Australia are higher than for the other models, and this difference is also appearing in the optical depths simulated at the AERONET station of Birdville. ~~The~~ Their description of semi-desert areas in Northern India has many similarities to the IPSL model. Emission tendencies from the UKESM model extend to areas where other models do not simulate emissions, and the pattern of emissions is more smooth. In particular, significant emissions occur over the Sahel, Ethiopia, Somalia, and over India. For these regions, higher dust emissions in UKESM could have a stronger impact on African and Asian monsoons. The ~~more~~ most granulated pattern is found for the NorESM model ~~, which is because of~~ due to the higher resolution of the source functions implemented. The last row in Figure 7 corresponds to the ~~normalized~~ normalised emission maps for the PDN experiment, ~~they indicate~~ and it indicates that although there are important differences between the PD and PDN experiments in terms of total emissions, the spatial ~~pattern~~ patterns of emissions are similar once they are ~~normalized~~normalised. We can ascertain this fact by comparing the CNRM-6DU ~~normalized~~ normalised emission maps for ~~PD and~~ the PD and the PDN experiment. The ~~study~~ analysis for the PI experiment is in the ~~supplementary information: figure~~ Supplementary Information: Figure S.DE.5.

5.4 Dust deposition

Previous studies (Huneeus et al., 2011; Albani et al., 2014) show that total deposition of dust, when compared with in-situ measurements, ~~agree globally only~~ agrees globally only to within a factor ~~ten.~~ of 10. Part of the reason is that dry and wet deposition ~~depend~~ are dependent on the dust particle size distribution, whose representation is challenging for current global climate models.

~~Processes~~ Indeed, processes driving dry deposition such as turbulent motions of particles and gravitational settling are both particle size dependent, as the aerodynamic resistance and the terminal velocity due to friction depend on the effective dust particle diameter. Wet deposition ~~on~~ during precipitation events also depends on the size of the particle (Seinfeld and Pandis, 1998) but measurements of aerosol lifetimes below clouds are scarce. Furthermore, other aerosol processes inside clouds modify the aerosol size distribution, as well as, their optical properties essentially due to potential aggregation of water-coated aerosols (Mahowald et al., 2014). Thereby, the first step of the analysis is a comparison of dry and wet deposition at a regional scale.

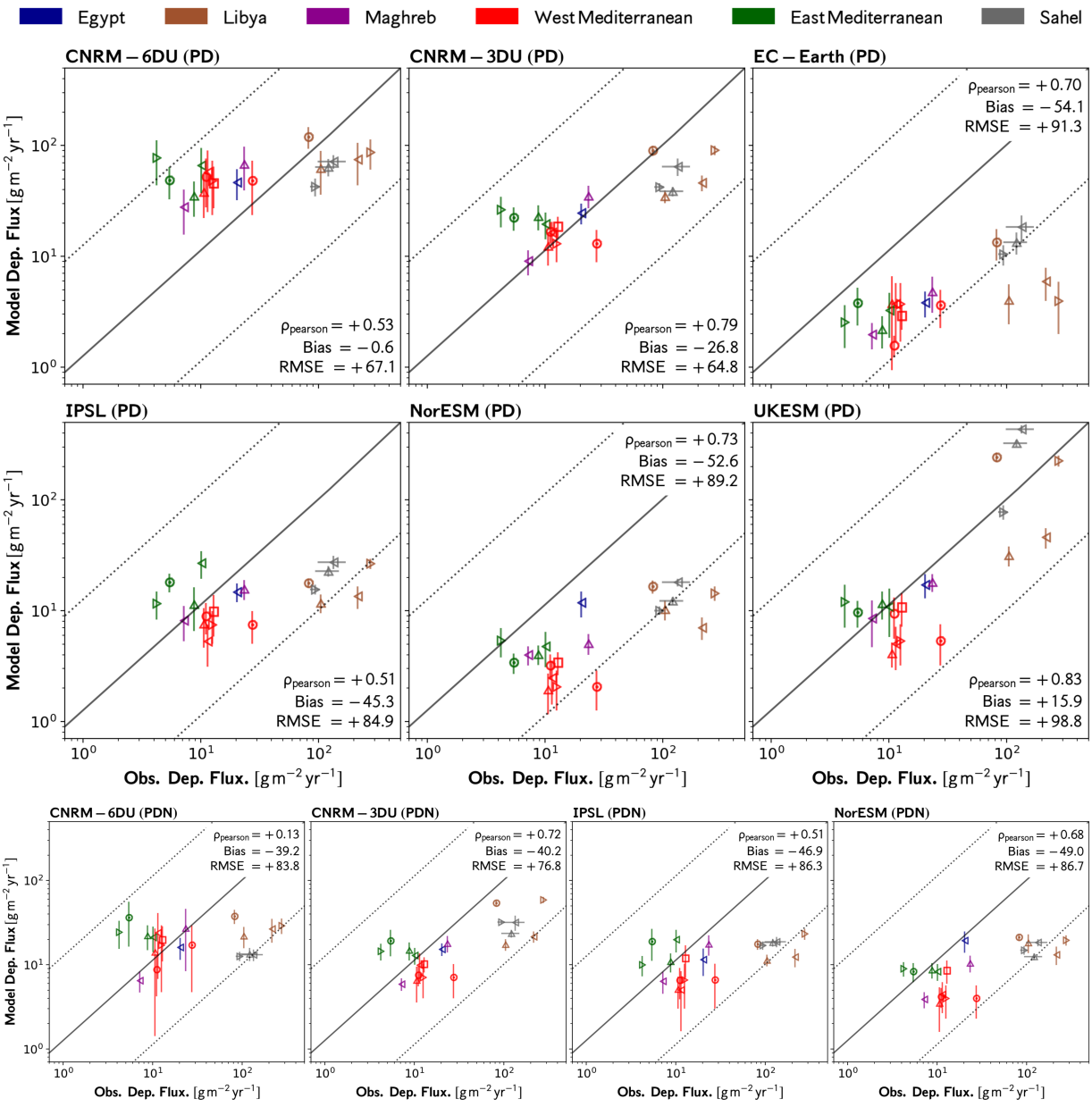

Figure 9. Comparison of estimated total annual deposition flux with CRESCENDO ESMs with the dataset stations shown ~~at~~ in Figure 1 (right panel). The model values taken are those from the PD experiment (top part) and PDN experiment for bottom row. Figure S.D.11 of the ~~supplement~~ Supplement is the analogous ~~of this~~ figure ~~but~~ for the PI experiment. Vertical bars on the bottom panel represent the year to year internal variability captured by each model. The grey horizontal bars displayed for the Sahel stations represent the year to year variations in the observations.

Table 11. Statistical properties of the comparision of the CRESCENDO-ESMs total deposition against the network-SET-M (see Figure 1 panel b). Statistic metrics used in this table are described on Table 5. Pearson Correlation Coefficient (ρ), bias (δ) [$\mathrm{gm^{-2}yr^{-1}}$], normalised bias (δ_N), Ratio standard deviations (Σ), Normalised mean absolute error (θ_N) and Root mean square error (RMSE=η).

Model	Exp.	Deposition Network-SET-M					
		ρ	δ	δ_N	Σ	θ_N	η
CNRM-6DU	PD	+0.53	-0.58	-0.01	+0.27	+0.90	+67.14
CNRM-3DU	PD	+0.79	-26.83	-0.45	+0.31	+0.63	+64.79
EC-Earth	PD	+0.70	-54.12	-0.91	+0.06	+0.91	+91.26
IPSL	PD	+0.51	-45.25	-0.76	+0.09	+0.83	+84.90
NorESM	PD	+0.68	-52.10	-0.87	+0.07	+0.88	+89.01
UKESM	PD	+0.83	+15.91	+0.27	+1.63	+0.88	+98.75
CNRM-6DU	PDN	+0.13	-39.22	-0.66	+0.11	+0.84	+83.81
CNRM-3DU	PDN	+0.72	-40.25	-0.67	+0.19	+0.73	+76.79
IPSL	PDN	+0.51	-46.90	-0.79	+0.07	+0.84	+86.30
NorESM	PDN	+0.62	-48.49	-0.81	+0.07	+0.83	+86.73
CNRM-6DU	PI	+0.47	+5.22	+0.09	+0.29	+0.93	+67.54
CNRM-3DU	PI	+0.74	-23.23	-0.39	+0.31	+0.66	+63.31
EC-Earth	PI	+0.66	-54.17	-0.91	+0.06	+0.91	+91.39
IPSL	PI	+0.36	-45.81	-0.77	+0.10	+0.84	+85.98
NorESM	PI	+0.76	-52.35	-0.88	+0.07	+0.88	+88.98
UKESM	PI	+0.84	+16.05	+0.27	+1.65	+0.88	+100.8

~~As~~ In fact, as the gravitational settling of large particles is dominant close to dust sources, regions remote from the main emission sources are well suited to compare models with different emission schemes, and evaluate their respective total dry and wet deposition. Close to dust sources the upper threshold ~~on~~ of the emitted dust particle sizes plays a role in the comparison with measurements. In particular, wet deposition over oceanic regions is enhanced relative to dry deposition which motivates targeting these specific regions for comparison. Tables 9 and 10 show the regional analysis of wet and dry deposition (including the sedimentation/gravitational settling) over oceans. These results are globally consistent with those shown by Shao et al. (2011). The two main oceanic regions where dust deposition occurs are the North Atlantic and the Indian Ocean even though the EC-Earth model simulated the largest dust wet deposition over the ~~East~~ West Pacific Ocean. For all models, the fraction of dry and wet deposition over ~~ocean~~ the oceans is smaller than over land. Wet deposition over oceans represents 40% and 45% ~~respectively~~ of the total wet deposition for IPSL and EC-Earth, respectively. But for NorESM it represents 26% of the global wet ~~depositions~~deposition. Dry deposition over oceans ranges from 3% to ~~16~~12% of global dry depositions. For the UKESM model, the dry deposition over land is 97% of the total dry deposition, due to the gravitational settling of large particles close to emission regions. Tables 9 and 10 also show ~~higher~~ slightly better consistency in the total dry deposition over oceans in the model ensemble (from 67 to ~~215~~ 250 in $\mathrm{Tg\,yr^{-1}}$) ~~that~~ than in the wet deposition (72 to ~~712~~ 392 in $\mathrm{Tg\,yr^{-1}}$), as we are excluding CNRM-6DU from the model ensemble. Results for ~~PDN and~~ the PDN and the PI experiments are included in Tables S.DD.1 to S.DD.4.

Table 12. Statistical properties of the comparision of the CRESCENDO-ESMs total deposition against the network-H2011 (see Figure 1 panel a). Statistic metrics used in this table are described on Table 5. Pearson Correlation Coefficient (ρ), bias (δ) [$\mathrm{gm}^{-2}\mathrm{yr}^{-1}$], normalised bias ($\delta_N$), Ratio standard deviations (Σ), Normalised mean absolute error (θ_N) and Root mean square error (RMSE=η).

Model	Exp.	Deposition Network-H2011					
		ρ	δ	δ_N	Σ	θ_N	η
CNRM-6DU	PD	+0.86	+2.88	+0.19	+0.46	+1.38	+60.82
CNRM-3DU	PD	+0.84	-6.82	-0.44	+0.24	+0.91	+59.66
EC-Earth	PD	+0.90	-10.71	-0.70	+0.36	+0.73	+45.74
IPSL	PD	+0.91	-9.54	-0.62	+0.16	+0.78	+54.69
NorESM	PD	+0.90	-12.68	-0.83	+0.11	+0.84	+57.26
UKESM	PD	+0.89	-9.58	-0.62	+0.16	+0.81	+57.21
CNRM-6DU	PDN	+0.80	-8.78	-0.57	+0.16	+0.83	+60.16
CNRM-3DU	PDN	+0.78	-9.00	-0.59	+0.19	+0.90	+60.53
IPSL	PDN	+0.90	-10.23	-0.67	+0.13	+0.79	+56.67
NorESM	PDN	+0.89	-11.80	-0.77	+0.11	+0.83	+57.42
CNRM-6DU	PI	+0.86	+4.04	+0.26	+0.46	+1.43	+60.58
CNRM-3DU	PI	+0.84	-6.18	-0.40	+0.25	+0.94	+59.67
EC-Earth	PI	+0.90	-10.28	-0.67	+0.42	+0.70	+43.04
IPSL	PI	+0.92	-9.56	-0.62	+0.16	+0.78	+54.66
NorESM	PI	+0.91	-12.58	-0.82	+0.11	+0.84	+57.12
UKESM	PI	+0.89	-9.37	-0.61	+0.17	+0.82	+57.04

5.4.1 Network of Dust deposition observations

Figure 8 shows the total annual deposition for the PD and PDN experiments for the locations shown ~~in~~ on panel (a) of Figure 1, and Figure 9 shows the total annual deposition for PD and PDN experiments for the locations shown on panel (b) of Figure 1. Figures ~~Dep~~S.DD.11 and ~~Dep~~S.DD.12 show the ~~analogous~~ analogues for the PI experiment. Qualitatively the global results are similar to Huneeus et al. (2011) where at most of the stations the modelled deposition is within a factor of 10 of the observed deposition flux (in the figures, the region between the dotted lines). As a consequence the estimated Pearson correlation of deposition flux calculated over log-values for the full network shows a reasonable value for all models.

All the models agree that Antarctica and ~~Southern Ocean has the lower~~ the Southern Ocean have the lowest values of total deposition. ~~However,~~ While UKESM and IPSL tend to slightly overestimate the total flux ~~whereas~~ in these remote regions, the CNRM models tend to underestimate the flux~~(with also a~~. However, their most prominent property Antarctic regions is a much larger range of ~~total deposition~~ values than the range reported by the observations~~). This is consistent with the~~. Additional research is need to evaluate if this is a consequence of their semi-Lagrangian model implemented in their dynamical core which ~~is expected to underestimate deposition fluxes mainly at distant regions for dust sources.~~ add a non-uniform bias, or instead it is just a combination of the dust source locations in the Southern Hemisphere and wind fields modelled.

Regarding the Pacific region closer to North America (named ~~West~~ East Pacific) NorESM, CNRM-6DU and CNRM-3DU tend to underestimate the deposition. In the case of ~~East~~ West Pacific region NorESM systematically ~~underestimate~~

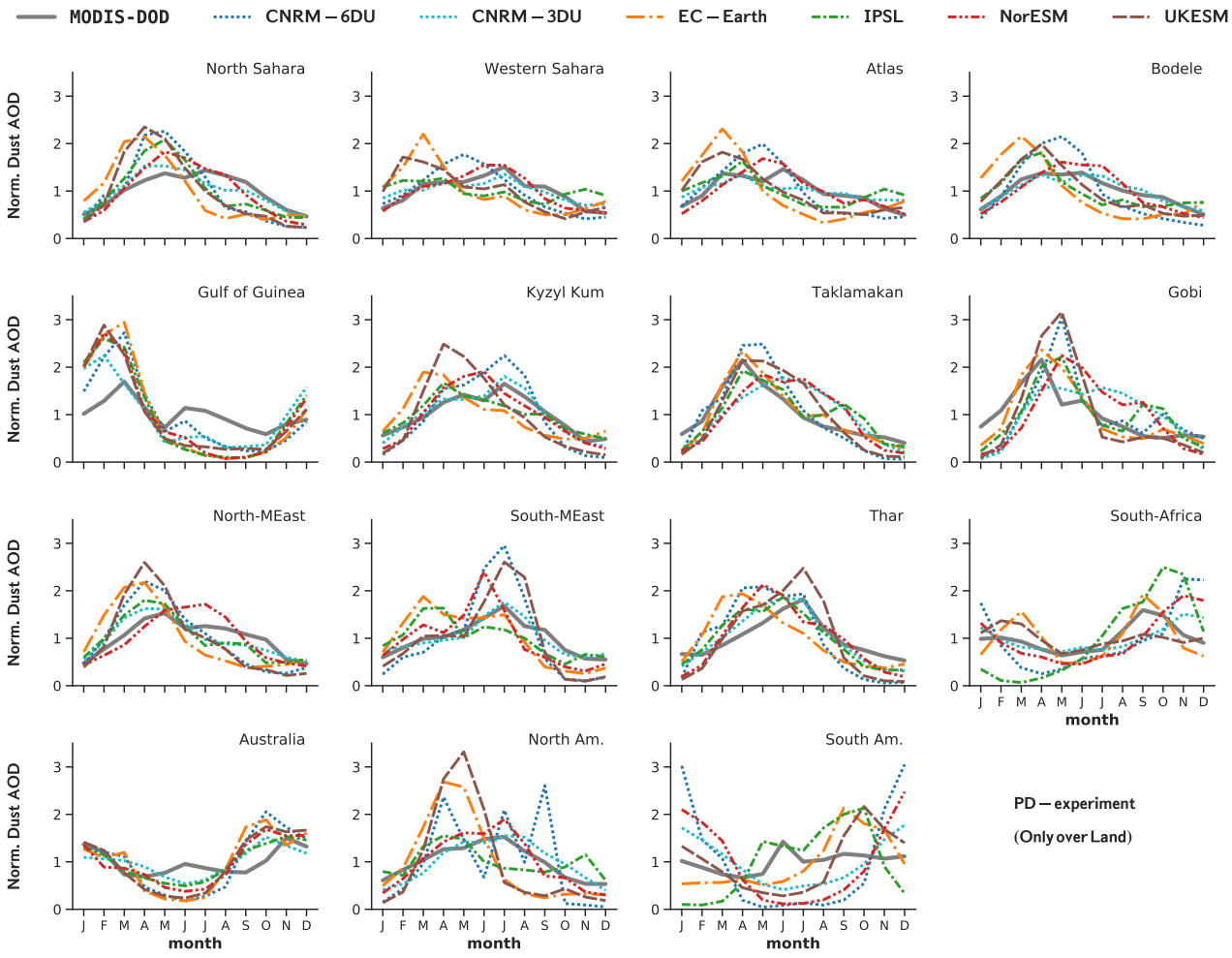

Figure 10. Seasonal cycle relative to the annual mean value of Dust Optical Depth as modelled by CRESCENDO ESMs over 15 regions. These seasonal cycles are compared against the DOD product of derived dust optical depth over land based on MODIS deep-blue retrievals (Pu and Ginoux, 2018b), see supplementary information for the description of how these products are derived and the analogous of this figure for PDN and PI experiments.

underestimates the deposition flux. Regarding CNRM models ~~the~~ they underestimate the total deposition over the ~~north~~ northern hemisphere part of ~~East~~ West Pacific but not in the southern part of ~~East Pacific due~~ West Pacific due probably to the enhanced emissions of these models over ~~Australia~~ Australian deserts. All the models ~~but~~ except the EC-Earth model underestimate the deposition over the single Asia station, ~~also the~~ and EC-Earth model report good values of total deposition over the northern ~~East~~ West Pacific as it has the largest relative contributions over Gobi desert between all the models.

All the models show a good agreement ~~on~~ in the Atlantic region (both North and Tropical regions) and the Middle East although the UKESM and EC-Earth ~~model~~ models underestimate the values ~~in the~~ at the single station in the South Atlantic. The deposition fluxes over the Indian ~~ocean~~ Ocean are fairly well described by all models.

If we compare the observations against the ~~model total depositions~~ modelled total deposition obtained from the experiment with nudged winds (last row in Figure 8) the correlation coefficients are similar, but differences between models are reduced, specially for the CNRM models. This is illustrated in Table 12 with a negative bias for all models (from ~~-9.4~~ -8.8 to -11.8 $\mathrm{gm^{-2}yr^{-1}}$), and the ratio of standard deviations Σ range between 0.11 and ~~0.18~~ 0.19 (for PD experiment between ~~0.1 and 0.41)~~ 0.11 and 0.46). The CNRM-6DU model is the only one with a positive bias (δ in Table 12) against the Network-H2011.

In Figure 9 we ~~analyze~~ analyse the ability of the ESMs to reproduce deposition fluxes regionally and closer to sources (for the PD and PDN experiments). We focus on the Mediterranean Sea~~and~~ , but we include three additional stations over the Sahel where observational annual differences can be compared. The analysis reveals that only the UKESM model reproduces the full range of observed deposition fluxes. All the other models underestimate total depositions fluxes over stations where fluxes exceed 100 $\mathrm{g\,m^{-2}yr^{-1}}$, and only the CNRM-3DU model estimates well the observed dust deposition in the northern Mediterranean Sea. Over the Sahel region, the CNRM models and UKESM provide reasonable values of total deposition flux, but UKESM overestimates the inland ~~depositions~~deposition, whereas the other models ~~provide~~ show a more consistent bias over the whole region.

The Sahel stations ~~are including~~ include horizontal bars describing the inter-annual variability over the mean values, which can be compared with vertical bars describing the variability in the models. In this case EC-Earth is the model that captures best the year-to-year ~~over~~ differences on mean values of dust deposition flux over the inland Sahel stations. For West ~~Mediterranean~~ Mediterranean the CNRM-3DU has the smallest bias, whereas in the full Mediterranean region UKESM and IPSL perform well in terms of global bias.

EC-Earth and NorESM underestimate total depositions close to source ~~total depositions~~ regions consistent with the ~~cutoff in size larger than~~ applied size cutoff around 8 µm ~~the~~ of emitted particles, and CNRM-6DU overestimates the ~~depositions~~ deposition on the whole Mediterranean region. For the experiment with nudged winds, we observe a better consistency between models ~~showing~~ with all of them showing similar values of total deposition ~~of the different sub-regions. However~~in the different subregions. However, this implies an ~~understimation over Sahel for~~ underestimation over the Sahel for the CNRM-6DU model that also has the largest ~~interannual~~ inter-annual variability over the ~~West-Mediterranean~~West-Mediterranean. The statistics metrics are shown in Table 11.

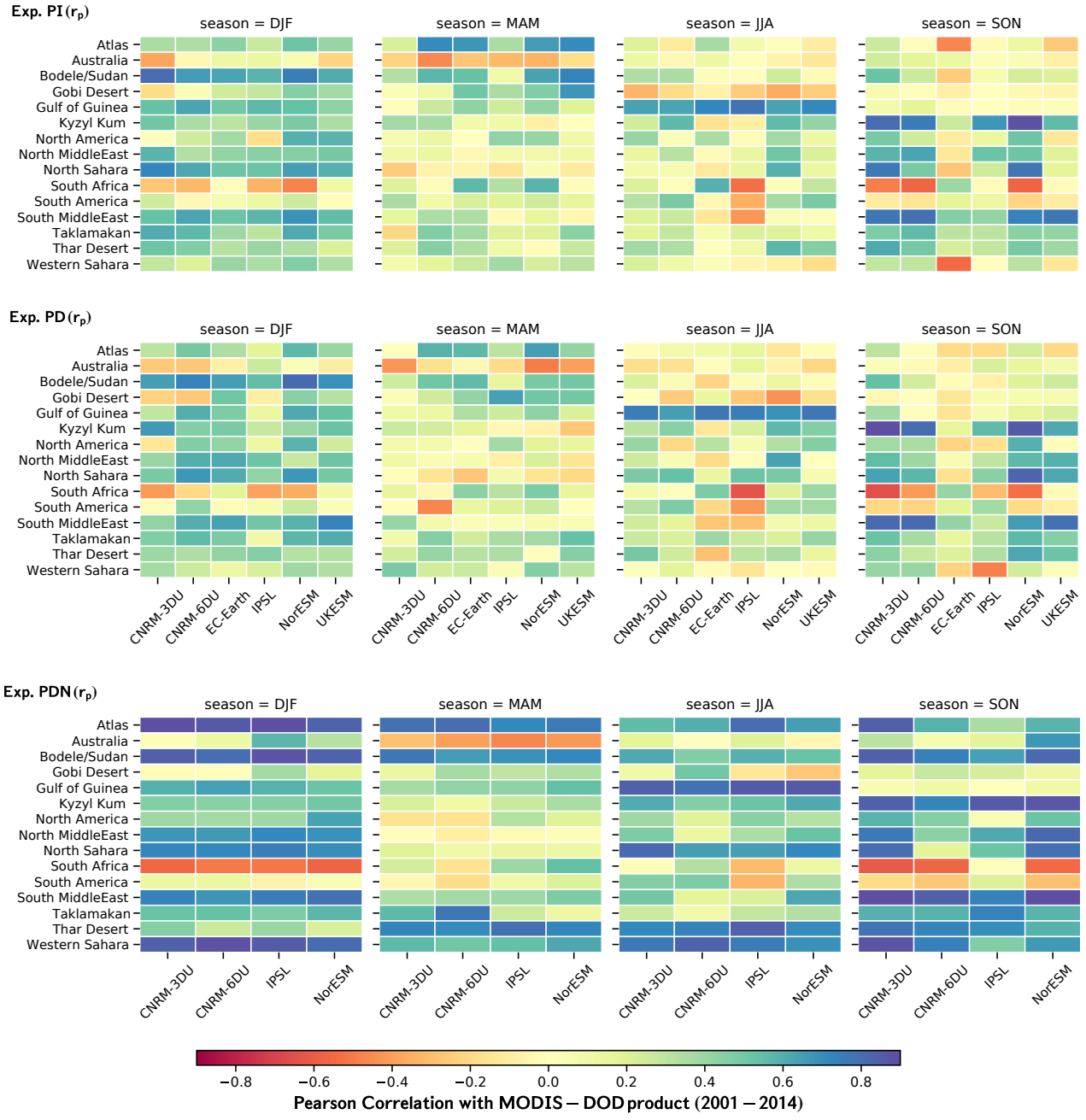

Figure 11. Skill of CRESCENDO-ESMs by regions calculated as the Pearson correlations between the ESM time-series of dust optical depth for each season and that from MODIS-DOD. The time interval spans from 2001 to 2014. It assess the performance of the different models to reproduce the inter-annual variability of each season against observations over dust source regions.

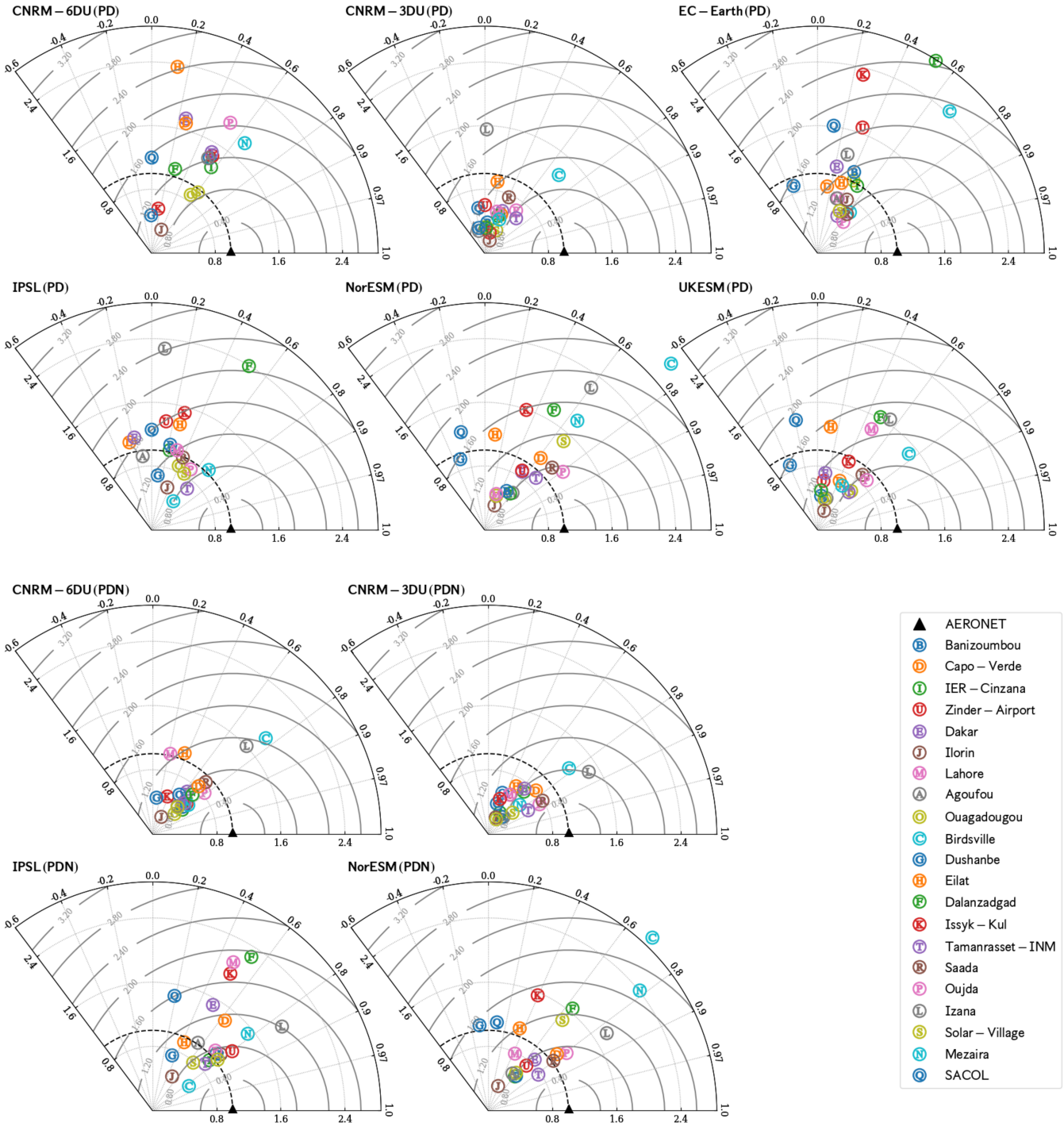

Figure 12. ~~Normalized~~ Normalised Taylor diagrams based ~~for~~ on time series of total aerosol optical depths at 440nm. These diagrams are representing PD and PDN experiments and restricted to ~~aeronet~~ AERONET dusty stations shown in Figure 3 (with color green and blue).

5.5 Dust optical depth

The simulated dust optical depth (~~DAOD~~DOD) by climate models has been compared previously with those retrieved through a network of ground-based sun-photometers (Huneeus et al., 2011) but also with products derived from satellite retrievals (Pu and Ginoux, 2018b; Peyridieu et al., 2013). There are also inter-comparisons between global climate models (Shindell et al., 2013). The overall agreement reported by these studies between retrieved and simulated dust aerosol optical depth is within a factor of two. Those results support the reliability of global estimations of the radiative effect from mineral dust. However, given that it is a vertically integrated parameter, it masks larger differences present in partial ~~columns estimations~~column estimates.

Our study focuses first on the comparison in regions defined in ~~Fig.~~ Figure 3. We ~~compared~~ compare the DOD of the CRESCENDO ESMs with ~~satellite~~satellites, as well as inter-compare simulated dust optical depth. Figure 10 shows the seasonal cycle (relative to the annual mean value of each model) and the MODIS DOD product during the period 2001-2014, for the PD experiment (the PDN and PI experiment are shown in Figures S.DOD.1 and S.DOD.2). We can hence analyse the seasonal amplitude relative to the annual background signal per region for each model. The supplementary Figure S.~~DOD3~~ DOD.3 shows the direct comparison of the seasonal cycle without relative values.

Over the most prominent preferential dust source regions (first row of Figure 10), the amplitude of the seasonal variability is systematically larger in all the models (with respect to the MODIS-DOD product) with a slight offset on the maximum value of the seasonal cycle towards spring time, particularly over Northern Sahara. It is remarkable that in these regions CNRM-3DU and NorESM show consistency in the seasonality with respect to MODIS-DOD, whereas EC-Earth and UKESM show more discrepancies ~~on~~ in the seasonal cycle ~~on~~ in both the amplitude and the phase. The CNRM-6DU model and IPSL have slight discrepancies ~~on~~ in these 4 regions. Over the Asian deserts of Taklamakan and Gobi the seasonal maximum is reasonably represented in the spring with a relative good agreement for EC-Earth, although the seasonality is not well represented for the Thar Desert. The UKESM, NorESM and CNRM-3DU models overestimate summer dust optical depth over the Taklamakan desert. A common feature between all the models is that over the Asian Desert the winter values are smaller than those of MODIS-DOD. Previous studies (Laurent et al., 2006) concluded that the seasonal cycle of Taklamakan desert is controlled by latter spring and summer emissions which most models capture, whereas Gobi, and the associated northern China deserts, have maximum emissions during late winter and early spring. CRESCENDO ESMs reproduce the maximum values of DOD in Spring for the Gobi deserts, and UKESM and EC-Earth models capture that seasonality over Taklamakan as well. Given the structural differences in the soil properties of these Asian regions (more stony at Gobi, mostly sandy at Taklamakan) and the additional role of snow cover over the Gobi desert, further model studies of Asian dust emissions are needed to better constrain the way dust scheme ~~parametrizations~~ parametrisations capture emissions in these regions. Ideally, these studies should be backed up by in-situ surface concentration measurements. Regarding the Middle-East, the combined region of North and South Middle East is in agreement with the Pu and Ginoux (2018b) study based on CMIP5 models.

We quantified the performance skill of the CRESCENDO ESMs by estimating the Pearson's correlation between the time-series of dust optical depth provided by each model for each of the seasons, and the same time-series of dates given by the MODIS-DOD product for the period between January 2001 and December 2014.

Figure 11 displays the values for this Pearson's ~~test~~correlation. The overall assessment indicates marked differences between models for the same season and over the same region. In the case of the PD experiment (middle panel), the correlation between MODIS-DOD and CRESCENDO-ESM is positive over winter except in Australia and South Africa regions which are regions particularly challenging for the ESMs analysed as we reported negative correlations, whereas South America is one of the regions with correlation closer to zero across all the seasons (and models). The overall correlation decreases in Spring (with respect to winter)~~where~~ , as we notice multiple regions where the Pearson correlations are close to zero. In summer, except in the Gulf of Guinea the correlation is also smaller than in the winter season. Finally, in Autumn the performance over Middle East and the Kyzyl Kum region is improved.The better behaviour of all the models is given over ~~Bodele~~ Bodélé in winter season, and the Arabian region (North and South Middle-East) that shows a reasonable agreement over all year for almost all models. Most of the features remain similar with pre-industrial aerosol-chemistry forcings (PI experiment) and the CNRM-6DU and CNMR-3DU behaves identical ~~on~~ in the PI experiment.

The agreement with satellite platforms is significantly improved for the PDN simulations and the consistency between models is enhanced. In particular, the ~~Sahara~~ Saharan region shows a marked improvement in the simulated dust optical depth. Australia and South Africa are still the regions where ~~the most discrepancy~~ most discrepancies are found, and South America ~~has systematically the overall values of the correlation closer~~ systematically has the correlation closest to zero.

We extended the analysis based on the Pearson correlation by using the Spearman coefficient which allows ~~to detect~~ detecting non-linear correlations. The ~~figure in terms of~~ results for the Spearman rank coefficient, can be found in ~~the~~ supplementary information Figure S.DOD.7., yield to similar conclusions, and both methods are consistent.

5.5.1 Network of Aerosol Optical Depth

The comparison relies on the dusty dominant AERONET stations described in ~~section~~ Section 3.4. For each station the monthly time-series of total aerosol optical depth at 440 nm are compared with the climate model value ~~of grid pixel to which the station belongs~~at the grid cell where the the station is located. As we are considering dusty stations, the correlation of the time-series represents how well the seasonal cycle is captured or not, while the representation of the amplitude of the cycle is measured by the standard deviation. Therefore the ratio of standard deviations is an indication of the agreement in seasonal amplitude between ~~model~~ the models and observations. Those statistics are compared using the ~~normalized~~ normalised Taylor diagram (Taylor, 2001). These diagrams are shown in Figure 12 for the PD and PDN simulations. The ~~behavior~~ behaviour of each model with respect to the observations at a station is indicated by both its radial and angle values: the radial value indicates the ~~normalized~~ normalised standard deviation with respect to observations, the angle measures the correlation between time-series.

A common result across all models comparing the PD and PDN experiments is the higher correlation for simulations with nudged-winds, but similar ~~normalized~~ normalised standard deviation for the cloud of points. With nudged winds the correlation is always positive except at one station for NorESM, a model that has a correlation larger than 0.6 for 13 stations in PDN (nine stations for PD). The PD experiment has only one case with correlation values around 0.8 (NorESM at Oujda), but all the models ~~with PDN~~ in PDN experiment have stations with correlations larger than 0.8 indicating that the seasonal cycle of optical depth is clearly improved with wind fields from reanalysis. The CNRM-6DU model has a strong change in the

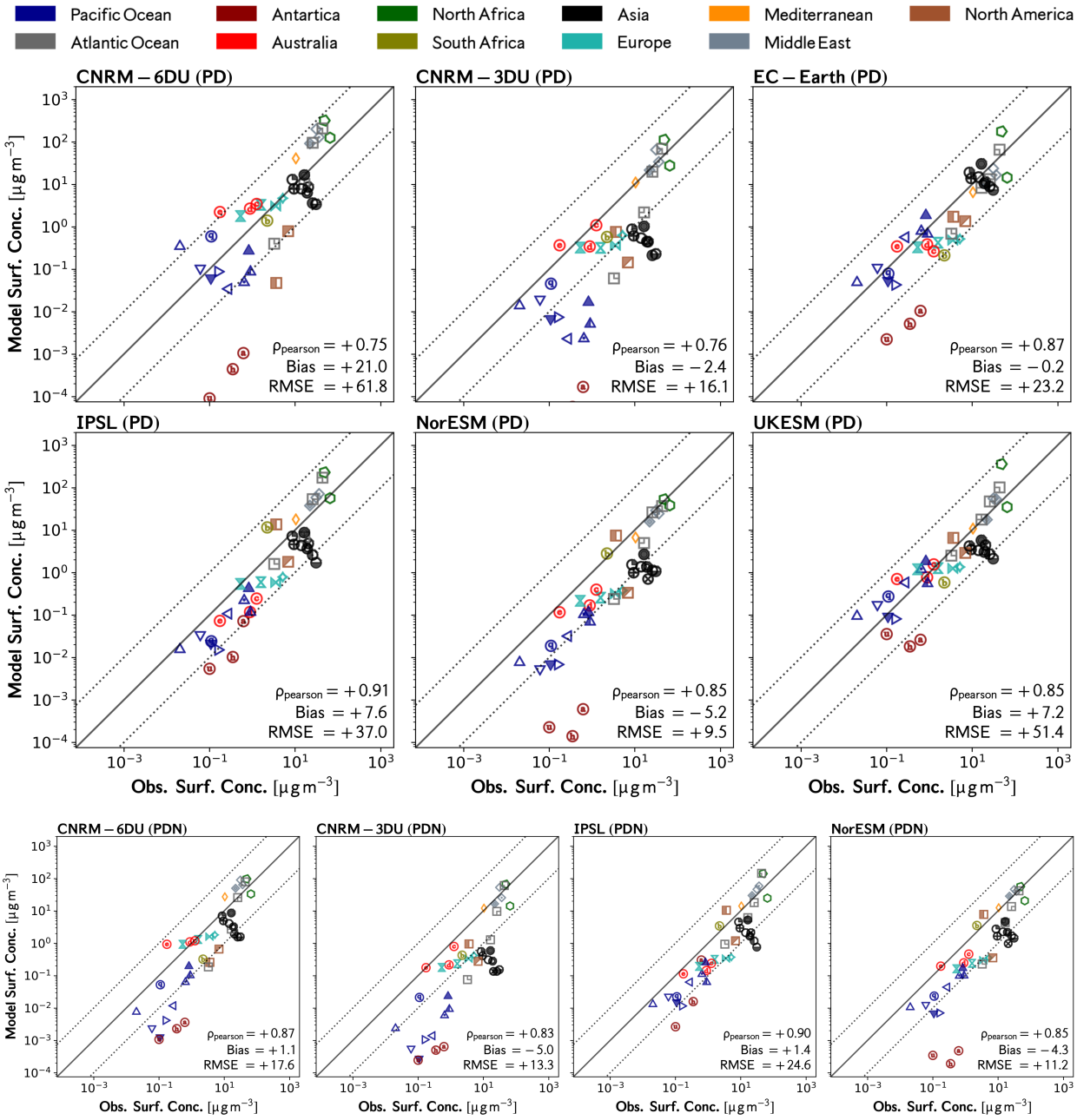

Figure 13. Comparison of dust surface concentrations in the models with the climatological dataset of ~~(Prospero and Nees, 1986; Prospero and Savoie, 1989)~~Prospero and Nees (1986) and Prospero and Savoie (1989) for the PD and PDN experiments. The colors of the points indicate the region to which the measurement station belongs. Climatological datasets were obtained from observations over the period from 1991 to 1994. For the PI experiment see Figure S.SDC.10.

Table 13. Statistical properties of the comparision of the CRESCENDO-ESMs dust surface concentration with respect to the global network shown in Figure 2. Statistic metrics used in this table are described on Table 5. Pearson Correlation Coefficient (ρ), bias (δ) [$\mu g m^{-3}$], normalised bias (δ_N), Ratio standard deviations (Σ), Normalised mean absolute error (θ_N) and Root mean square error (RMSE=η).

Model	Exp.	Surface Concentration Network					
		ρ	δ	δ_N	Σ	θ_N	η
CNRM-6DU	PD	+0.76	+23.19	+1.82	+4.59	+2.26	+65.14
CNRM-3DU	PD	+0.76	-2.46	-0.19	+1.52	+0.74	+16.92
EC-Earth	PD	+0.88	-0.48	-0.04	+1.92	+0.79	+24.36
IPSL	PD	+0.91	+8.53	+0.67	+3.03	+1.26	+38.95
NorESM	PD	+0.87	-5.62	-0.44	+0.84	+0.48	+9.95
UKESM	PD	+0.84	+8.08	+0.63	+3.88	+1.30	+54.14
CNRM-6DU	PDN	+0.87	+1.33	+0.10	+1.70	+0.86	+18.59
CNRM-3DU	PDN	+0.82	-5.36	-0.42	+1.08	+0.68	+13.98
IPSL	PDN	+0.89	+1.69	+0.13	+2.15	+0.98	+25.91
NorESM	PDN	+0.86	-4.58	-0.36	+0.95	+0.55	+11.72

~~normalized~~ normalised standard deviation from PD (for which most of the stations have values larger than 1) to PDN (with most of the stations with values smaller than 1). In terms of the amplitude of the seasonal cycle, the most challenging stations for all models are in Australia (Birdsville station), Gobi Desert (Dalanzadgad and Sacol) and Izaña (close to Sahara but ~~in~~ on an island and ~~in altitude~~at high elevation). In terms of correlation Dushanbe in Thar region, and Sacol (China) are challenging. On the other ~~side~~ hand stations like Sadaa (West-Sahara), Eilat (North-Middle-East) or Dakar are reasonably well captured by models.

5.6 Surface Concentrations

The stations were chosen to cover a range of dust values from low to moderate dust concentrations, mainly located at a distance from the main dust emission regions. According to the instrument location, Sahel and the West coast of North Africa (green and grey squared) together with ~~middle east~~ Middle East stations (grey diamonds) report the highest values of surface concentrations, see Figure 13. The group represented by black circles represents moderate values indicating transport of dust from arid and semi-arid regions of East Asia. The lowest values correspond ~~at~~ to Antarctica and the Pacific Ocean (blue triangles). The values of the dataset are shown in Table S.MD.4 of the Supplementary information.

The comparison between the CRESCENDO models and a network of stations that measure dust surface concentrations is shown in Figure ~~?? for PD~~ 13 for the PD and PDN experiment and in Figure S.~~DD.1 of the supplement for the nudged-wind simulations (Figure S.DD.2 shows the PI results)~~DSC.10 for the PI experiment. The agreement falls into the same range ~~than~~ as previous comparisons with ~~CAM model~~ Community Atmospheric Model (CAM) (Albani et al., 2014) where the full range for the expected differences in annual mean values is close to 10. This range of differences between models compares well with the previous study from Huneeus et al. (2011).

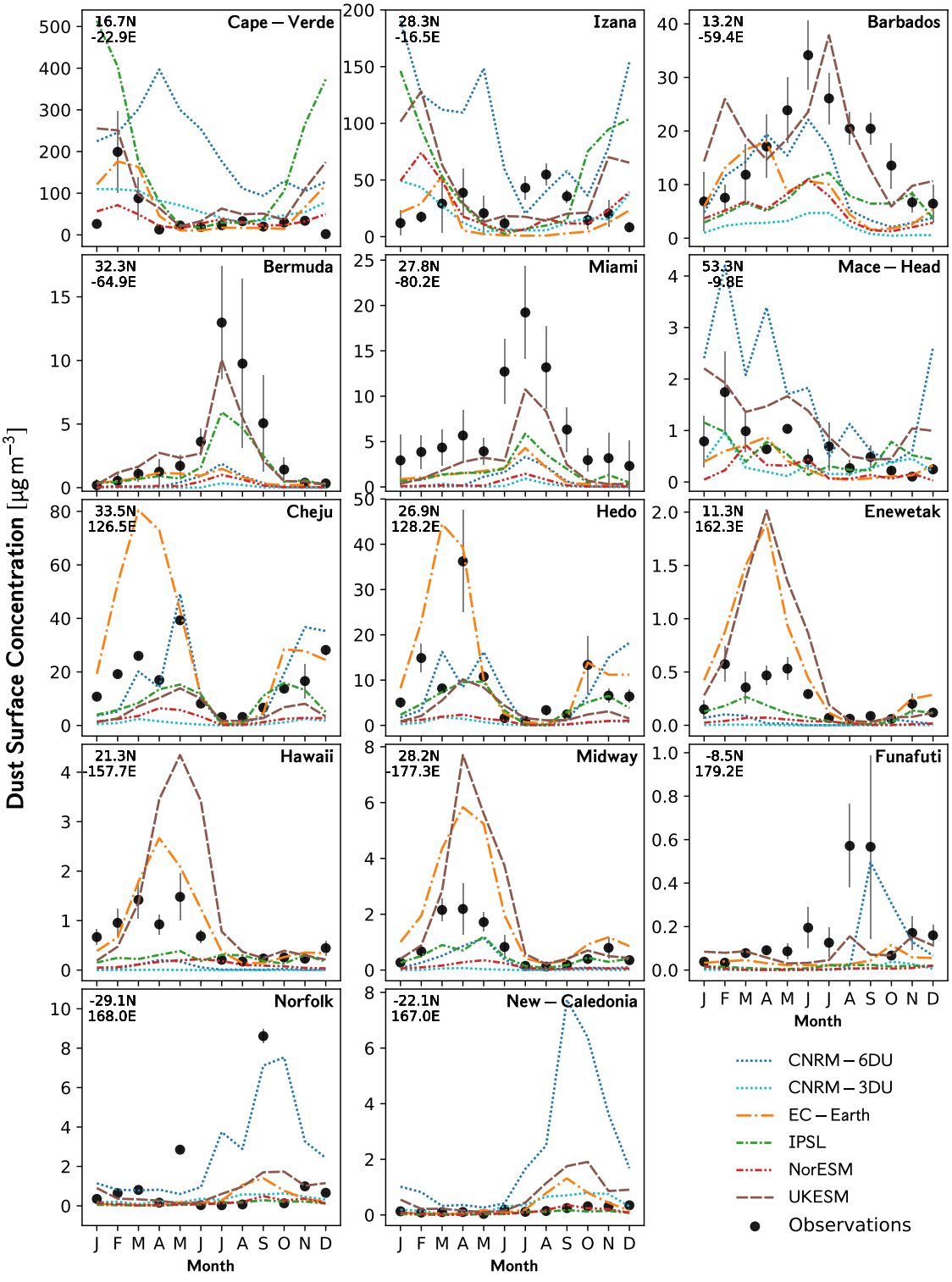

Figure 14. Comparison of ESM models (PD) of dust surface concentration with a station based climatological dataset. For PI and PDN experiment see the supplement figures S.DSC.7 and S.DSC.8.

CNRM-3DU underestimates dust concentrations over the Pacific Ocean. This ~~behavior~~ behaviour over regions remote from dust sources could be partly due to the non-conservative semi-Lagrangian transport scheme that accentuates the differences with the distance of transport (a fact also consistent with their values of the Pearson correlation, mainly in nudged-simulations). All models except IPSL underestimate the concentrations in the Antarctica station. This could be due to the larger emissions from Patagonia that cause the increase in correlation coefficient for this model. Over Northern Europe all models, except CNRM, tend to underestimate dust concentrations and do not reproduce the range of variability found in the observations. When comparing PD and PDN simulations, IPSL and NorESM models show slightly better agreement in PDN conditions, whereas the two CNRM models show higher correlations when using nudged-winds but similar differences over the Pacific Ocean.

The correlation between ~~model~~ the models and observations is significant for all models. The RMSE values are influenced by the stations with the highest concentrations and hence are more representative of the concentrations near the Sahara desert and the Middle East. In this regard, the NorESM and CNRM-3DU models show the best agreement over these regions. The EC-Earth model shows however the smallest bias because it better captures dust concentrations over Japan and East China, where ~~all~~ the other models underestimate concentrations. Values of ~~normalized bias and normalized~~ normalised bias and normalised mean absolute error complement the previous metrics and give us a ~~characterization~~ characterisation of global differences accounting equally for the stations with the lowest concentrations (see Table 13)~~, the normalized~~ . The normalised statistics indicate that the nudged-wind simulations generally show a better agreement with observations.

Although the 36 stations are covering many regions, a complete assessment of the model performance at the surface is not possible due to the absence of stations in South America and Asia, and only one station inland over North America and Africa. Therefore, the global observational ~~constrains~~ constraints, in terms of ~~surface concentrations is~~ the surface concentrations, are only partial.

The comparison of the seasonal cycle of surface concentrations against 14 stations is shown in Figure 14 for the PD experiment. The stations Cape-Verde and Barbados are in the same latitude at opposite sides of the Atlantic, therefore they have a signature of the transatlantic transport of mineral dust from the Sahel region. The IPSL, CNRM-6DU and UKESM models overestimate the early winter contributions to the seasonal cycle in Cape-Verde. The models reproduce the concentrations within a factor ~~two~~ of 2 from May to September (except CNRM-6DU model) ~~in general with~~ with, in general, an overestimation except for EC-Earth. However in the case of Barbados UKESM after April and CNRM-6DU before May reproduce very well the surface concentrations. All the other models, although with a similar seasonal cycle, underestimate the total surface concentrations by a factor from 2 to 4. The stations Izaña, Bermudas ~~,~~ and Miami have also similar latitudes and represent the Atlantic transport from West-Sahara. Izaña Observatory is not ~~a~~ at sea level and all the models have difficulties to reproduce the seasonal cycle. The seasonal cycles of Bermuda and Miami are well reproduced with ~~withj a general understimation~~ a general underestimation of the surface ~~cocentrations~~ concentrations values, where only UKESM and IPSL show a consistency within a factor of 2. Cheju and Hedo are stations on the ~~Eastern~~ Western Pacific Coast and their measurements ~~are representing~~ represent the dust transport from China. The EC-Earth model reproduces well the seasonal cycle but with an overestimation of spring concentrations by a factor of 3. The seasonal cycle and values are well represented by the CNRM-6DU and IPSL ~~model~~models.

Enewetak is located between ~~Filipinas and Hawai~~ Philippines and Hawaii in the middle of the Pacific Ocean, and EC-Earth and UKESM overestimate the spring concentrations whereas all the other models ~~understimate~~ underestimate them. A similar ~~sitation~~ situation is found in ~~Hawai~~ Hawaii and Midway. The rest of the stations are in the Southern Hemisphere where the dust concentrations are smaller and the seasonal cycle is only partially reproduced. The results for the PDN experiment (see supplement DSC) are similar with a slight improvement in the seasonal cycle but with a general underestimation of surface concentrations. All the models with nudged winds exhibit problems in reproducing the observations in Izaña.

6 Discussion and conclusions

The analysis of the results provides insight ~~on how both modelling and measuring~~ into how the combination of modelling and measurements of dust can be used to improve our understanding of the dust cycle. ~~More specifically, through comparison of emission and total deposition fluxeswe are able to propose specific areas for which improvements are needed. Annual~~

A first approach to the evaluation of the dust cycle relies on in the total dust loads and emissions. In this regard, we have shown that the model ensemble values of total emissions with nudged winds has less dispersion. We stress, however, that dust column loads are a better quantity when comparing models with different size distributions at emission than comparing total emission fluxes, since gravitational settling gets rid of the very large particles over a short time span. For dust loads, all models in PDN experiments are in a range between 9.1 and 15.2 Tg which can serve as a baseline to study model improvements. Because new studies support the important role of the coarse mode of dust (Huang et al., 2020), it is recommended to compare the contributions to dust load for fine and coarse modes separately. The range of dust loadings that we obtained is smaller than recent estimations (Kok et al., 2021) that propose values $\geq$ 20 Tg with a multi-model comparison with models with geometric diameters up to 20µm but based on a new methodology where the dust diagnostics are including observational constraints (Kok et al., 2020). Actually, Adebiyi and Kok (2020) propose that the total load of dust in the atmosphere is higher than what is estimated typically, and give a mean value close to 30 Tg, where the contribution of the coarse mode is more important than the fine mode.

Therefore, annual global dust emissions from climate models are dependent on the dust particle size distribution (DPSD) representation~~and~~ . The first result we observe is that those models that account for particles with diameters larger than 10 ~~µm~~ µm produce higher total fluxes. However, although an important diversity in the total emissions depends on the upper threshold, also the specific boundaries of the bin for largest particles used in a sectional scheme seems critical. We observed large differences in total emissions between UKESM1 and CNRM-6DU where an important difference is the lower-boundary of the last bin diameter: 20 µm and 10 µm, respectively. For this reason we have proposed two classifiers for further model analysis, but still we need a reasonable metric to compare the emissions at grid-cell scale.

To overcome the challenge of comparing models with different DPSD at emission, we introduced ~~normalized~~ normalised emission maps, showing first (by a comparison between PD and PDN simulations) that wind fields do not ~~affect substantially these normalized emission estimates~~ substantially affect these normalised emission estimates in terms of spatial patterns when we analyse the 15 year emissions means of the PD and PDN simulations. This led us to interpret differences in regions where

dust was emitted as reflecting differences in ~~underlying~~ the underlying dust *effective* soil erodibility information ~~among models (including soil moisture effects)~~ (DESEI) among models. However, the DESEI is also including a sort of meteorological factors because the role of soil moisture in the emission process, together with specific properties of the dust scheme like the threshold in friction velocity or how the soil texture is translated into a dust size distribution. Note that the simulations compared in our study share the same sea-surface temperatures which reduces the model diversity in terms of precipitation. Nonetheless, the consistency we report between PD and PDN normalised emission maps needs further investigation at smaller spatial and temporal scales, in particular at daily and sub-daily scales.

~~With the aim to reproduce~~ Beyond the interpretation of the re-gridded normalised emission maps, they allow us to compare the relative intensity contribution to dust emissions on the same spatial scale. It is a useful tool, as a direct balance of the several source functions is complex. For example, with the aim of reproducing dust observations at different model resolutions, models have introduced correction factors to ~~those~~ their dust soil erodibility (see for example ~~(Albani et al., 2014; Knippertz and Todd, 2012)). But our normalized emissions~~ Albani et al. (2014) and Knippertz and Todd (2012)). In contrast, our normalised emissions can indicate effective model differences, both in intensity and location, on preferential dust sources. ~~Those~~ We found that these differences are the largest over Asia and are also significant over Australia. Hence, we identified these regions as two source regions that would benefit from further comparison of dust emission observations with actual model occurrences in emission fluxes. ~~Additional~~ Moreover, the diversity in Asia emissions is investigated by Kok et al. (2021) obtaining also important differences with Aerocom Phase I models, and suggesting an underestimation of dust emission from East Asian deserts. Finally, additional research is also needed to ascertain seasonality disagreements in dust sources~~.~~, which our 15 year mean normalised emission maps are not showing, but where seasonal normalised emission maps would be an useful tool.

~~The model ensemble values of total emissions with nudged winds has less dispersion. We stress however that dust column loads are a better quantity when comparing models with different size distribution at emission than compare to total emission fluxes, since gravitational settling gets rid of the very large particles over a short time span. For dust loads, all models are in a range between 9.1 and 15.2 Tg/yrwhich can serve as a baseline to study model improvements. Another~~ Regarding dust deposition, another important point of discrepancy between models is the ratio between wet and dry deposition over similar particle size ~~range~~ranges, indicating that specific sensitivity studies should focus on the treatment of deposition. ~~We also evidenced significant differences~~ Interestingly, we have found that there is not a correlation between the modelling of largest particles and the value of this ratio. Finally, evidence of significant differences is also found in deposition over the oceans, in particular over the Indian Ocean and over the Pacific ~~East~~West, both of which are affected by dust source distributions over Asia.

~~Regarding the direct radiative effects~~To properly evaluate the impact of the dust in the climate system, it is important to ~~ascertain~~ determine an uncertainty range of the direct radiative effects for each model. Based on a calculation with 4 modes over a range from 0.1 to 100 μm, we observe that those models without the smallest particles (without mode m_1) will underestimate the short-wave contribution at the TOA by up to 20%. Models without the largest particles (those represented by the $m_{~~ww,~~ ~~ie~~22}$, i.e. for bins with ~~radius~~ diameter larger than 40μm) are expected however to not be significantly affected in their estimations of DRE in the SW. Nevertheless, we need additional studies to conclude whether these estimates are consistent with other models

with the same range of modelled dust size particles. In particular, it is recommended to attribute diversity in the context of the several refractive indices.

Because The dust optical depth is a key diagnostic in comparative studies. It appears to be logical to try to constrain the dust cycle by relying on dust optical depth (DOD) estimated from satellite observations. This is because the dust emissions depend on mineralogy, on land surface properties and on regional meteorology,. Therefore a few in-situ measurements are not sufficient to constrain the dust cycle at any scale. It appeared logical to try to constrain the dust cycle by relying on dust optical depth (DOD) estimated from the satellite observations. (Ridley et al., 2016) possible scale. Indeed, Ridley et al. (2016) used retrievals from instruments on-board MODIS and MISR to estimate global values for DOD between 0.020 and 0.035 which place two models (CNRM-C6 CNRM-3DU and UKESM) outside this observational range. Although Note, however, that there are difficulties to estimate DOD from satellite retrievals with the method of (Ridley et al., 2016) because it still relies on model simulations to ascertain the fraction of non-dust optical depth. As shown by our results in the supplement material (Section DOD), the non-dust fraction of optical depth can have large inter-model differences. Furthermore, an important result is that, although DOD should be proportional to the mineral dust total column, models with the lowest dust loadings are not those with smaller the smallest DOD. This is illustrated in the differences on in mass extinction efficiency (MEE) between the different models. The magnitude of this property MEE is a good indicator of intrinsic model properties due to its relatively small seasonal cycle. Mass , an aspect in which all the CRESCENDO-ESMs match. But also, because mass extinction efficiency is affected by the DPSD and optical properties of mineral dust modelled. Note however that there are a sensible difficulty in estimate DAOD from satellite retrievals with the method of (Ridley et al., 2016) because it still lies on model simulations to ascertain the fraction of non-dust optical depths. As shown by our results in supplement material (section DOD), the non-dust fraction of optical depths can have large inter-model differences.

, it is also a useful property to compare with observations.

Therefore, based on MODIS satellite estimations Our analysis of dust optical depth include a study at regional scale. Specifically, the regional dust optical depth over dust source regions relies on a comparison with MODIS satellite estimates of DOD based upon on the algorithm described in (Pu and Ginoux, 2018b), we compared the regional dust optical depth over dust source regions. This comparison allowed us to evaluate the skill of each model by evaluating the correlation between the regional time series of observations versus each model. A significant increase in the skill was revealed for the simulations using nudged winds, indicating that a consistent reproduction of the seasonal cycle depends critically on how the strong surface winds are represented . This part of the wind distribution being more consistent when using winds from the ERA-Interim (with a improvement with the use of re-analysis . The correlation is not informing on wind data sets). However, the correlation (skill) is not useful in determining differences in the scale of the signal, and Figure S.DOD.3 shows that there are regions where the seasonal cycle is well reproduced but the mean annual signal is actually underestimated, see also (Pu and Ginoux, 2018b).

This paper analyses the representation of the mineral dust cycle in five ESMs through diagnostics used for the evaluation of their performance with regards to observations. Although the agreement in terms of aerosol optical depth is better than surface fluxes or concentrations, we separate the models into two groups based on the simulated global mean dust optical depth. Those models with values closer to 0.025 (CNRM, EC-Earth, IPSL and UKESM) are more consistent with the proposed satellite

~~estimations (Ridley et al., 2016). Given that the optical depths depends on column loadings rather than dust emission fluxes, the inter-model convergence can be achieved even for those models that are not implementing particles with radius larger than 10. Also, to achieve an inter-model convergence in terms of optical depths is important to better constrain the dust radiative forcings and direct radiative effects (DRE). Note that according to (Di Biagio et al., 2020) and to our results of Table 7 the DRE at the top of the atmosphere and at the surface have an important contribution from particles with diameters larger than 10altough the contribution of the fraction of particles larger than 40is marginal. The DOD seasonal cycle asserted by MODIS satellite estimates (see (Pu and Ginoux, 2018b)) gives us a key reference to understand the sources of the model discrepancies as illustrated by figure 11. The second diagnostic that we find useful is the mass extintion efficency (MEE) coefficient has a smaller inter-annual variability are reflects modelling properties such as assumptions on the size distribution modelled.~~

~~The models exhibit important differences in preferential dust sources, in particular a better agreement of preferential sources found over Asia and Australia would give us more consistency on global dust transport over the Indian and the Pacific Oceans. Although there is an scarcity of measurement campaigns~~ Pu and Ginoux (2018b). A further example of the difficulties in specific regions is given in the newly incorporated stations over Asia compared ~~to the Sahara and Sahel, studies based on empirical relationships between visibility and dust surface concentrations give us an additional insight on dust sources over these regions (Shao and Dong, 2006). Compared to (Huneeus et al., 2011) we added AERONET stations over Asia, which resulted~~ with Huneeus et al. (2011), because these stations has been proven to be challenging for the CRESCENDO-ESMs in terms of the comparison provided by Taylor diagrams (see figure 12).

7 Future research directions

Currently, the dust source disagreements/differences between models make it difficult to quantify the fraction of the uncertainties of dust emission due to those small-scale atmospheric phenomena that are not well represented by global models. The use of wind fields from reanalysis ~~datasets~~ data sets reduces the differences between models, but a benchmark reference dataset regarding dust sources is needed to establish a range for those uncertainties. In particular, specific model comparisons based on a common soil erodibility information would illuminate on specific model improvements to decrease diversity. Indeed, these studies should use a similar prescribed seasonal vegetation fraction and bare soil distribution to improve the seasonal consistency.

~~Note also that~~ The dust particle size distribution is a key point of research for current ESM. Specifically, the global description of the dust cycle in terms of the amount of aerosol mass ~~mobilized~~ mobilised needs to be extended to larger particles as they can significantly increase the total emissions~~, and~~. At the same time according to recent studies the fraction of dust mass in the atmosphere due to the coarser particles would be dominant with respect to fine mode (Adebiyi and Kok, 2020). ~~However, still the method in which they~~ A further complication, we found in our analysis is that the method by which the largest particles are incorporated in the models can drive strong differences in total emissions with ranges from 3500 $\mathrm{Tg\,yr^{-1}}$ ~~of~~ in CNRM-6DU to about 7000 $\mathrm{Tg\,yr^{-1}}$ ~~of~~ in UKESM model. ~~Even more~~ In particular, the specific bins used to model the contribution of

largest particles are critical to understand model diversity. Additionally, a better discrimination of particles larger than 10μm but smaller than about 20 to 30 μm will conclude if the results in the Table 7 are consistent between different models.

However, these differences in total emissions are not directly translated ~~in~~ into proportional loadings because of the differences in deposition between models, and therefore in the lifetime.

~~Regarding~~ In particular, regarding total deposition one priority should be given to ~~analyze~~ analysing the large differences in the ratio between dry and wet deposition between models ~~and observations~~ which is only partially explained by the modelled size distribution. From the aerosol micro-physical point of view differences in the dominance of wet scavenging over ocean regions could account for part of these differences. ~~Whereas~~However, as indicated by ~~(Shao et al., 2011)~~ Shao et al. (2011) observations of dry deposition velocities in wind tunnels are not reproduced by current dry deposition schemes. ~~At present, all models have difficulties to estimate local values wet /dry depositions, which can exceed a factor of 10.~~ In this scenario it becomes necessary to compare with measurements of wet and dry deposition separately (Marticorena et al., 2017). In fact, although our ensemble mean global contributions of gravitational settling, wet deposition and dry deposition without sedimentation are similar, there is a large model diversity. To explain better the model diversity in sedimentation a first step is to ensure that gravitational settling is estimated for all atmospheric levels before a comparison of sedimentation for each size range. Because, wet deposition involve the modelling dust-cloud and dust-rainfall interactions the model diversity is partially conditioned by other parts of climate models (Croft et al., 2010). However, sensitivity studies for each model based on the plausible range of values of their dust scavenging coefficients (in-cloud and below-cloud) can provide valuable information on the actual range of uncertainties expected for each model.

The models exhibit important differences in preferential dust sources, in particular a better agreement of preferential sources found over Asia and Australia would give us more consistency in global dust transport over the Indian and the Pacific Oceans. Although there is a scarcity of measurement campaigns over Asia compared to the Sahara and Sahel, studies based on empirical relationships between visibility and dust surface concentrations give us an additional insight into dust sources over these regions (Shao and Dong, 2006). This information, supported by new regional studies is needed to suggest best lines of model improvements in these regions.

Given that the optical depth depends on column load rather than dust emission fluxes, the inter-model convergence can be reasonably achieved even for those models that are not implementing particles with radius larger than 10μm. Also, an inter-model convergence in terms of optical depth is important to better constrain the dust radiative forcings and direct radiative effects (DRE). However, as said earlier, the link between dust loads and dust optical depth, i.e. the MEE, shows important model differences. Additional MEE observations to better constrain the expected values would definitively help modellers to improve the dust load description by comparing with satellite dust optical depth estimates. Finally, given the different role of each mode: fine, coarse, super-coarse and giant in the dust-radiation interaction, further studies, not only on the mineral composition but also in possible dependence of the composition with size of dust particles would improve our estimates of dust radiative forcings and direct radiative effects.

Appendix A: ~~Methods~~ Method to estimate Direct Radiative Effects in multi-modal size distributions

In section 5.1 ~~it was shown~~ the direct radiative effects for a dust scheme with several dust modes were shown. Here we present the methods used to obtain the results of Table 7. The *direct radiative effect* of a species is defined by the *earth's instantaneous imbalance* at the top of the atmosphere due to ~~a specific atmospheric specie~~that specific atmospheric species/component~~introduced at (Boucher and Tanré, 2000)~~ . It has been introduced at Boucher and Tanré (2000) and discussed by ~~Bellouin et al. (2013); Heald et al. (20~~ Heald et al. (2014). This imbalance is conceptually different from the radiative forcing (either defined as ~~an~~ a stratospherically adjusted instantaneous radiative forcing or by an effective radiative forcing) which is a comparison between ~~a~~ two different time periods, usually between pre-industrial ~~and a~~ time and present day. In our case the estimations of direct radiative effects are estimated during a single simulation with present day conditions but with multiple calls to the radiative transfer model implemented in the climate model. The aerosols in the climate model have actually direct, indirect and semi-direct effects ~~along~~ in the simulation but the method only estimated the direct radiative effects due to scattering and absorption of specific aerosol species. Therefore there are observational based estimations of the direct radiative effects of the aerosols (Yu et al., 2006). However, from the point of view of aerosol ~~modeling~~ modelling based on multi-modal approaches~~it has been reported a non-linearity properties for the estimation~~ , differences have been reported (Di Biagio et al., 2020) between (a) the calculation by the sum of each mode contribution ~~(Di Biagio et al., 2020) here the~~ estimated individually, and (b) the estimation for the joint multi-modal directly.

In this appendix two different approaches and a joint new method with four calls to the radiative scheme are described to decrease these differences.

In general, in the calculation done by current radiative transfer schemes it is considered a state of the atmosphere with several aerosols species $\mathcal{X}, \mathcal{Y}, \ldots$ where each ~~specie~~ species is possibly described by a multi-modal distribution with modes $X_1, \ldots, X_n$. The state with all the aerosol species is named hereafter $\mathcal{A}$, therefore $\mathcal{A} = \mathcal{X} \cup \mathcal{Y} \cup \mathcal{Z} \cup \ldots$. We define another state named $\widetilde{\mathcal{A}}$ that includes all the modes of every aerosol specie except those modes corresponding ~~of the specie~~ to the species $\mathcal{X}$. Therefore, $\mathcal{A} = \widetilde{\mathcal{A}} \cup \mathcal{X}$. The radiative effect of the aerosol $\mathcal{X}$ described by several modes $X_1, ..., X_n$, ~~would be~~is defined by,

$$\widehat{\mathcal{F}_X} = \mathcal{R}(\mathcal{A}, \delta) - \mathcal{R}(\widetilde{\mathcal{A}}, \delta)$$

where $\mathcal{R}$ represents the radiance obtained in our radiative transfer scheme which is intrinsically a non-linear forward model. δ represents all others elements considered by our radiative scheme beyond the aerosol species which are invariant for both ~~estimation~~ estimations of the radiance.

However, in order to disentangle the contribution of each mode X_i of the specie $\mathcal{X}$, ~~there results differs~~ results differ depending on the methodology used due to the ~~non linearity~~ non-linearity of $\mathcal{R}$. We define here two methods: the first approach considers each X_i mode added individually to $\widetilde{\mathcal{A}}$ with respect to the experiment given by $\widetilde{\mathcal{A}}$, hereafter we name this as *method in*. The second approach compares ~~a~~ an experiment $\mathcal{A}$ with a scenario $\widetilde{\mathcal{A}}$ where all the modes X_j with $j \neq i$ are included, named hereafter *method out*. Visually, the *method in* would compare a base state without any mode of the target component

with a state where the specific mode is added (therefore, *in*). The *method out* compares a state with all the modes of a target component with a state in which the specific mode is removed (therefore named *out*).

The ~~method A would be~~ *method in* is written for the radiative effects of X_i as,

$$\widehat{\mathcal{F}_{X_i}} = \mathcal{R}(\widetilde{\mathcal{A}} \cup X_i, \delta) - \mathcal{R}(\widetilde{\mathcal{A}}, \delta)$$

whereas the ~~method B~~ *method out* is written as,

$$\mathcal{F}_{X_i} = \mathcal{R}(\mathcal{A}, \delta) - \mathcal{R}(\mathcal{A} \cup X_i^*, \delta) \quad \text{with} \quad X_i^* = \cup_{i \neq j} X_j$$

and we note that $\mathcal{F}_X = \widehat{\mathcal{F}_X}$ but $\mathcal{F}_{X_i} \neq \widehat{\mathcal{F}_{X_i}}$. In particular, we have both, $\sum_i \mathcal{F}_{X_i} \neq \mathcal{F}_X$ and $\sum_i \widehat{\mathcal{F}_{X_i}} \neq \widehat{\mathcal{F}_X}$.

However, the results for 4 modes of mineral dust of ~~IPSL showed~~ IPSL-4DU, shown at Table 7, indicate that $\frac{1}{2}\sum_i(\widehat{\mathcal{F}_{X_i}} + \mathcal{F}_{X_i}) \approx \widehat{\mathcal{F}_X} = \mathcal{F}_X$.

Therefore the joint method described based on four calls to the radiative transfer scheme to calculate the direct radiative effect is providing ~~estimations~~ estimates per mode that combine linearly to reproduce the ~~multimodal~~ multi-modal direct radiative effect.

Code availability. The core functions of the software used for data-analysis are available on the reference (Checa-Garcia, 2020) and its related open-source code repository

Author contributions. RC-G and YB designed the research. RC-G analysed the data and wrote the manuscript with input from YB, SA, PN, DO, FMO'C and TvN. Data from climate model simulations were provided by: TB, PLS and TvN for EC-Earth, MS and DO for NorESM, FMO'C and CD for the UKESM, MM and PN for the CNRM, RC-G for IPSL and IPSL-4DU. SA, YB and AC developed the IPSL-4DU dust scheme. BM and JMP provided observational data sets used in the analysis.

Competing interests. The authors declare that they have no conflict of interest.

Acknowledgements. This work has been supported by the European Union's Horizon 2020 research and innovation programme under grant agreement No 641816 (CRESCENDO). ~~S.A.~~ SA acknowledges funding from the European Union's Horizon 2020 research and innovation program under the Marie Sklodowska-Curie grant agreement 708119, for the project DUS3C. The French National Observatory Service INDAAF is supported by the INSU/CNRS, the IRD (Institut de Recherche pour le Développement) and the Observatoires des Sciences de l'Univers EFLUVE and Observatoire Midi-Pyrénées. The authors would like to thank the French and African PIs and operators for

maintaining the stations and providing the PM10 concentrations. The INDAAF data are distributed on the web site : https://indaaf.obs-mip.fr/. ~~We thank to Mohit Dalvi for their support with UKESM, and Jane Mulcahy for implement the AMIP in the UKESM~~The authors would like to acknowledge the contribution of Mohit Dalvi, Jane Mulcahy and Stephanie Woodward from the UK Met Office Hadley Centre in developing and/or running the UKESM1 simulations. RC-G and YB gratefully acknowledge the hospitality of the Institut Pascal during the Paris-Saclay Indices Program 2019, supported by ANR-11-IDEX-0003-01. We also thank comments of the three anonymous reviewers.

References

Adebiyi, A. A. and Kok, J. F.: Climate models miss most of the coarse dust in the atmosphere, Science Advances, 6, eaaz9507, https://doi.org/10.1126/sciadv.aaz9507, 2020.

Adebiyi, A. A., Kok, J. F., Wang, Y., Ito, A., Ridley, D. A., Nabat, P., and Zhao, C.: Dust Constraints from joint Observational-Modelling-experiMental analysis (DustCOMM): comparison with measurements and model simulations, Atmospheric Chemistry and Physics, 20, 829–863, https://doi.org/10.5194/acp-20-829-2020, 2020.

Albani, S. and et al: The global dust cycle in the IPSL climate model revisited: particle size distributions and dependence of emissions on land surface properties, in preparation, 2021.

Albani, S., Mahowald, N. M., Perry, A. T., Scanza, R. A., Zender, C. S., Heavens, N. G., Maggi, V., Kok, J. F., and Otto-Bliesner, B. L.: Improved dust representation in the Community Atmosphere Model, Journal of Advances in Modeling Earth Systems, 6, 541–570, https://doi.org/https://doi.org/10.1002/2013MS000279, 2014.

Alfaro, S. C. and Gomes, L.: Modeling mineral aerosol production by wind erosion: Emission intensities and aerosol size distributions in source areas, Journal of Geophysical Research: Atmospheres, 106, 18 075–18 084, https://doi.org/10.1029/2000JD900339, 2001.

Alfaro, S. C., Gaudichet, A., Gomes, L., and Maillé, M.: Modeling the size distribution of a soil aerosol produced by sandblasting, Journal of Geophysical Research: Atmospheres, 102, 11 239–11 249, https://doi.org/10.1029/97JD00403, 1997.

Alfaro, S. C., Gaudichet, A., Gomes, L., and Maillé, M.: Mineral aerosol production by wind erosion: Aerosol particle sizes and binding energies, Geophysical Research Letters, 25, 991–994, https://doi.org/10.1029/98GL00502, 1998.

Allen, C. J. T., Washington, R., and Saci, A.: Dust detection from ground-based observations in the summer global dust maximum: Results from Fennec 2011 and 2012 and implications for modeling and field observations, Journal of Geophysical Research: Atmospheres, 120, 897–916, https://doi.org/10.1002/2014jd022655, 2015.

Astitha, M., Lelieveld, J., Abdel Kader, M., Pozzer, A., and de Meij, A.: New parameterization of dust emissions in the global atmospheric chemistry-climate model EMAC, Atmospheric Chemistry & Physics Discussions, 12, 13 237–13 298, https://doi.org/https://doi.org/10.5194/acpd-12-13237-2012, 2012.

Atkinson, J., Murray, B., Woodhouse, M., Whale, T., Baustian, K., Carslaw, K., Dobbie, S., O'Sullivan, D., and Malkin, T.: The importance of feldspar for ice nucleation by mineral dust in mixed-phase clouds, Nature, 498, https://doi.org/10.1038/nature12278, 2013.

Balkanski, Y., Schulz, M., Claquin, T., and Guibert, S.: Reevaluation of Mineral aerosol radiative forcings suggests a better agreement with satellite and AERONET data, Atmospheric Chemistry and Physics, 7, 81–95, https://doi.org/10.5194/acp-7-81-2007, 2007.

Balkanski, Y., Bonnet, R., Boucher, O., Checa-Garcia, R., and Servonnat, J.: Dust Induced Atmospheric Absorption Improves Tropical Precipitations In Climate Models, Atmospheric Chemistry and Physics Discussions, 2021, 1–24, https://doi.org/10.5194/acp-2021-12, 2021.

Bauer, S. E.: Global modeling of heterogeneous chemistry on mineral aerosol surfaces: Influence on tropospheric ozone chemistry and comparison to observations, Journal of Geophysical Research, 109, https://doi.org/10.1029/2003jd003868, 2004.

Bègue, N., Tulet, P., Pelon, J., Aouizerats, B., Berger, A., and Schwarzenboeck, A.: Aerosol processing and CCN formation of an intense Saharan dust plume during the EUCAARI 2008 campaign, Atmospheric Chemistry and Physics, 15, 3497–3516, https://doi.org/10.5194/acp-15-3497-2015, 2015.

Bellouin, N., Boucher, O., Haywood, J., and Reddy, M. S.: Global estimate of aerosol direct radiative forcing from satellite measurements, Nature, 438, 1138–1141, https://doi.org/10.1038/nature04348, 2005.

Bellouin, N., Quaas, J., Morcrette, J.-J., and Boucher, O.: Estimates of aerosol radiative forcing from the MACC re-analysis, Atmospheric Chemistry and Physics, 13, 2045–2062, https://doi.org/10.5194/acp-13-2045-2013, 2013.

Biasutti, M.: Rainfall trends in the African Sahel: Characteristics, processes, and causes, Wiley Interdisciplinary Reviews: Climate Change, 10, e591, https://doi.org/10.1002/wcc.591, 2019.

Boucher, O. and Tanré, D.: Estimation of the aerosol perturbation to the Earth's Radiative Budget over oceans using POLDER satellite aerosol retrievals, Geophysical Research Letters, 27, 1103–1106, https://doi.org/10.1029/1999GL010963, 2000.

Boucher, O., Servonnat, J., Albright, A. L., Aumont, O., Balkanski, Y., Bastrikov, V., Bekki, S., Bonnet, R., Bony, S., Bopp, L., Braconnot, P., Brockmann, P., Cadule, P., Caubel, A., Cheruy, F., Codron, F., Cozic, A., Cugnet, D., D'Andrea, F., Davini, P., de Lavergne, C., Denvil, S., Deshayes, J., Devilliers, M., Ducharne, A., Dufresne, J.-L., Dupont, E., Éthé, C., Fairhead, L., Falletti, L., Flavoni, S., Foujols, M.-A., Gardoll, S., Gastineau, G., Ghattas, J., Grandpeix, J.-Y., Guenet, B., Guez, Lionel, E., Guilyardi, E., Guimberteau, M., Hauglustaine, D., Hourdin, F., Idelkadi, A., Joussaume, S., Kageyama, M., Khodri, M., Krinner, G., Lebas, N., Levavasseur, G., Lévy, C., Li, L., Lott, F., Lurton, T., Luyssaert, S., Madec, G., Madeleine, J.-B., Maignan, F., Marchand, M., Marti, O., Mellul, L., Meurdesoif, Y., Mignot, J., Musat, I., Ottlé, C., Peylin, P., Planton, Y., Polcher, J., Rio, C., Rochetin, N., Rousset, C., Sepulchre, P., Sima, A., Swingedouw, D., Thiéblemont, R., Traore, A. K., Vancoppenolle, M., Vial, J., Vialard, J., Viovy, N., and Vuichard, N.: Presentation and Evaluation of the IPSL-CM6A-LR Climate Model, Journal of Advances in Modeling Earth Systems, 12, e2019MS002 010, https://doi.org/10.1029/2019MS002010, e2019MS002010 10.1029/2019MS002010, 2020.

Checa-Garcia, R.: CMIP6 Ozone forcing dataset: supporting information, https://doi.org/10.5281/zenodo.1135127, 2018.

Checa-Garcia, R.: FunFAN: FUNctions For Aerosol Modelling (v1.0), Zenodo (10.5281/zenodo.3672001), https://doi.org/10.5281/zenodo.3672001, 2020.

Checa-Garcia, R., Hegglin, M. I., Kinnison, D., Plummer, D. A., and Shine, K. P.: Historical Tropospheric and Stratospheric Ozone Radiative Forcing Using the CMIP6 Database, Geophysical Research Letters, 45, 3264–3273, https://doi.org/10.1002/2017GL076770, 2018.

Colarco, P. R., Nowottnick, E. P., Randles, C. A., Yi, B., Yang, P., Kim, K.-M., Smith, J. A., and Bardeen, C. G.: Impact of radiatively interactive dust aerosols in the NASA GEOS-5 climate model: Sensitivity to dust particle shape and refractive index, Journal of Geophysical Research (Atmospheres), 119, 753–786, https://doi.org/https://doi.org/10.1002/2013JD020046, 2014.

Croft, B., Lohmann, U., Martin, R. V., Stier, P., Wurzler, S., Feichter, J., Hoose, C., Heikkilä, U., van Donkelaar, A., and Ferrachat, S.: Influences of in-cloud aerosol scavenging parameterizations on aerosol concentrations and wet deposition in ECHAM5-HAM, Atmospheric Chemistry and Physics, 10, 1511–1543, https://doi.org/10.5194/acp-10-1511-2010, 2010.

Dee, D. P., Uppala, S. M., Simmons, A. J., Berrisford, P., Poli, P., Kobayashi, S., Andrae, U., Balmaseda, M. A., Balsamo, G., Bauer, P., Bechtold, P., Beljaars, A. C. M., van de Berg, L., Bidlot, J., Bormann, N., Delsol, C., Dragani, R., Fuentes, M., Geer, A. J., Haimberger, L., Healy, S. B., Hersbach, H., Hólm, E. V., Isaksen, L., Kållberg, P., Köhler, M., Matricardi, M., McNally, A. P., Monge-Sanz, B. M., Morcrette, J.-J., Park, B.-K., Peubey, C., de Rosnay, P., Tavolato, C., Thépaut, J.-N., and Vitart, F.: The ERA-Interim reanalysis: configuration and performance of the data assimilation system, Quarterly Journal of the Royal Meteorological Society, 137, 553–597, https://doi.org/https://doi.org/10.1002/qj.828, 2011.

Denjean, C., Cassola, F., Mazzino, A., Triquet, S., Chevaillier, S., Grand, N., Bourrianne, T., Momboisse, G., Sellegri, K., Schwarzenbock, A., Freney, E., Mallet, M., and Formenti, P.: Size distribution and optical properties of mineral dust aerosols transported in the western Mediterranean, Atmospheric Chemistry and Physics, 16, 1081–1104, https://doi.org/10.5194/acp-16-1081-2016, 2016.

Dentener, F. J., Carmichael, G. R., Zhang, Y., Lelieveld, J., and Crutzen, P. J.: Role of mineral aerosol as a reactive surface in the global troposphere, Journal of Geophysical Research: Atmospheres, 101, 22 869–22 889, https://doi.org/10.1029/96JD01818, 1996.

Di Biagio, C., Balkanski, Y., Albani, S., Boucher, O., and Formenti, P.: Direct Radiative Effect by Mineral Dust Aerosols Constrained by New Microphysical and Spectral Optical Data, Geophysical Research Letters, 47, https://doi.org/10.1029/2019gl086186, 2020.

Diner, D. J., Beckert, J. C., Bothwell, G. W., and Rodriguez, J. I.: Performance of the MISR instrument during its first 20 months in Earth orbit, IEEE Transactions on Geoscience and Remote Sensing, 40, 1449–1466, https://doi.org/10.1109/tgrs.2002.801584, 2002.

Dufresne, J.-L., Gautier, C., Ricchiazzi, P., and Fouquart, Y.: Longwave Scattering Effects of Mineral Aerosols, Journal of the Atmospheric Sciences, 59, 1959 – 1966, https://doi.org/10.1175/1520-0469(2002)059<1959:LSEOMA>2.0.CO;2, 2002.

Durack, P. J. and Taylor, K. E.: PCMDI AMIP SST and sea-ice boundary conditions version 1.1.4, https://doi.org/10.22033/ESGF/input4MIPs.2204, 2018.

Evan, A. T., Fiedler, S., Zhao, C., Menut, L., Schepanski, K., mant, C. F., and Doherty, O.: Derivation of an observation-based map of North African dust emission, Aeolian Research, 16, 153 – 162, https://doi.org/https://doi.org/10.1016/j.aeolia.2015.01.001, 2015.

Ge, J. M., Liu, H., Huang, J., and Fu, Q.: Taklimakan Desert nocturnal low-level jet: climatology and dust activity, Atmospheric Chemistry and Physics, 16, 7773–7783, https://doi.org/10.5194/acp-16-7773-2016, 2016.

Giles, D. M., Sinyuk, A., Sorokin, M. G., Schafer, J. S., Smirnov, A., Slutsker, I., Eck, T. F., Holben, B. N., Lewis, J. R., Campbell, J. R., Welton, E. J., Korkin, S. V., and Lyapustin, A. I.: Advancements in the Aerosol Robotic Network (AERONET) Version 3 database – automated near-real-time quality control algorithm with improved cloud screening for Sun photometer aerosol optical depth (AOD) measurements, Atmospheric Measurement Techniques, 12, 169–209, https://doi.org/10.5194/amt-12-169-2019, 2019.

Ginoux, P.: Warming or cooling dust?, Nature Geoscience, 10, 246–248, https://doi.org/10.1038/ngeo2923, 2017.

Ginoux, P., Chin, M., Tegen, I., Prospero, J. M., Holben, B., Dubovik, O., and Lin, S.-J.: Sources and distributions of dust aerosols simulated with the GOCART model, Journal of Geophysical Research: Atmospheres, 106, 20 255–20 273, https://doi.org/10.1029/2000JD000053, 2001.

Gläser, G., Kerkweg, A., and Wernli, H.: The Mineral Dust Cycle in EMAC 2.40: sensitivity to the spectral resolution and the dust emission scheme, Atmospheric Chemistry & Physics, 12, 1611–1627, https://doi.org/https://doi.org/10.5194/acp-12-1611-2012, 2012.

Gruber, N., Gloor, M., Mikaloff Fletcher, S. E., Doney, S. C., Dutkiewicz, S., Follows, M. J., Gerber, M., Jacobson, A. R., Joos, F., Lindsay, K., Menemenlis, D., Mouchet, A., Müller, S. A., Sarmiento, J. L., and Takahashi, T.: Oceanic sources, sinks, and transport of atmospheric CO2, Global Biogeochemical Cycles, 23, https://doi.org/10.1029/2008GB003349, 2009.

Heald, C. L., Ridley, D. A., Kroll, J. H., Barrett, S. R. H., Cady-Pereira, K. E., Alvarado, M. J., and Holmes, C. D.: Contrasting the direct radiative effect and direct radiative forcing of aerosols, Atmospheric Chemistry and Physics, 14, 5513–5527, https://doi.org/10.5194/acp-14-5513-2014, 2014.

Hegglin, M., Kinnison, D., Lamarque, J.-F., and Plummer, D.: CCMI ozone in support of CMIP6 - version 1.0, https://doi.org/10.22033/ESGF/input4MIPs.1115, 2016.

Heinold, B., Knippertz, P., Marsham, J. H., Fiedler, S., Dixon, N. S., Schepanski, K., Laurent, B., and Tegen, I.: The role of deep convection and nocturnal low-level jets for dust emission in summertime West Africa: Estimates from convection-permitting simulations, Journal of Geophysical Research: Atmospheres, 118, 4385–4400, https://doi.org/10.1002/jgrd.50402, 2013.

Hoose, C. and Möhler, O.: Heterogeneous ice nucleation on atmospheric aerosols: a review of results from laboratory experiments, Atmospheric Chemistry & Physics, 12, 9817–9854, https://doi.org/10.5194/acp-12-9817-2012, 2012.

Huang, Y., Kok, J. F., Kandler, K., Lindqvist, H., Nousiainen, T., Sakai, T., Adebiyi, A., and Jokinen, O.: Climate Models and Remote Sensing Retrievals Neglect Substantial Desert Dust Asphericity, Geophysical Research Letters, 47, e2019GL086 592, https://doi.org/https://doi.org/10.1029/2019GL086592, e2019GL086592 2019GL086592, 2020.

Huneeus, N., Schulz, M., Balkanski, Y., Griesfeller, J., Prospero, J., Kinne, S., Bauer, S., Boucher, O., Chin, M., Dentener, F., Diehl, T., Easter, R., Fillmore, D., Ghan, S., Ginoux, P., Grini, A., Horowitz, L., Koch, D., Krol, M. C., Landing, W., Liu, X., Mahowald, N., Miller, R., Morcrette, J.-J., Myhre, G., Penner, J., Perlwitz, J., Stier, P., Takemura, T., and Zender, C. S.: Global dust model intercomparison in AeroCom phase I, Atmospheric Chemistry and Physics, 11, 7781–7816, https://doi.org/10.5194/acp-11-7781-2011, 2011.

Jin, Q., Wei, J., Lau, W. K., Pu, B., and Wang, C.: Interactions of Asian mineral dust with Indian summer monsoon: Recent advances and challenges, Earth-Science Reviews, 215, 103 562, https://doi.org/https://doi.org/10.1016/j.earscirev.2021.103562, 2021.

Kaufman, Y. J., Koren, I., Remer, L. A., Tanré, D., Ginoux, P., and Fan, S.: Dust transport and deposition observed from the Terra-Moderate Resolution Imaging Spectroradiometer (MODIS) spacecraft over the Atlantic Ocean, Journal of Geophysical Research: Atmospheres, 110, https://doi.org/10.1029/2003JD004436, 2005.

Kirkevåg, A., Grini, A., Olivié, D., Seland, Ø., Alterskjær, K., Hummel, M., Karset, I. H. H., Lewinschal, A., Liu, X., Makkonen, R., Bethke, I., Griesfeller, J., Schulz, M., and Iversen, T.: A production-tagged aerosol module for Earth system models, OsloAero5.3 – extensions and updates for CAM5.3-Oslo, Geoscientific Model Development, 11, 3945–3982, https://doi.org/10.5194/gmd-11-3945-2018, 2018.

Klingmüller, K., Metzger, S., Abdelkader, M., Karydis, V. A., Stenchikov, G. L., Pozzer, A., and Lelieveld, J.: Revised mineral dust emissions in the atmospheric chemistry–climate model EMAC (MESSy 2.52 DU-Astitha1 KKDU2017 patch), Geoscientific Model Development, 11, 989–1008, https://doi.org/10.5194/gmd-11-989-2018, 2018.

Knippertz, P. and Stuut, J.-B. W., eds.: Mineral Dust - A Key Player in the Earth System, Springer-Verlag, https://doi.org/10.1007/978-94-017-8978-3, 2014.

Knippertz, P. and Todd, M. C.: Mineral dust aerosols over the Sahara: Meteorological controls on emission and transport and implications for modeling, Reviews of Geophysics, 50, https://doi.org/10.1029/2011RG000362, 2012.

Kohfeld, K. and Harrison, S.: DIRTMAP: The geological record of dust, Earth-Science Reviews, 54, 81 – 114, 2001.

Kok, J. F.: A scaling theory for the size distribution of emitted dust aerosols suggests climate models underestimate the size of the global dust cycle, Proceedings of the National Academy of Sciences, 108, 1016–1021, https://doi.org/10.1073/pnas.1014798108, 2011.

Kok, J. F., Ridley, D. A., Zhou, Q., Miller, R. L., Zhao, C., Heald, C. L., Ward, D. S., Albani, S., and Haustein, K.: Smaller desert dust cooling effect estimated from analysis of dust size and abundance, Nature Geoscience, 10, 274–, https://doi.org/10.1038/ngeo2912, 2017.

Kok, J. F., Adebiyi, A. A., Albani, S., Balkanski, Y., Checa-Garcia, R., Chin, M., Colarco, P. R., Hamilton, D. S., Huang, Y., Ito, A., Klose, M., Leung, D. M., Li, L., Mahowald, N. M., Miller, R. L., Obiso, V., Pérez García-Pando, C., Rocha-Lima, A., Wan, J. S., and Whicker, C. A.: Improved representation of the global dust cycle using observational constraints on dust properties and abundance, Atmospheric Chemistry and Physics Discussions, 2020, 1–45, https://doi.org/10.5194/acp-2020-1131, 2020.

Kok, J. F., Adebiyi, A. A., Albani, S., Balkanski, Y., Checa-Garcia, R., Chin, M., Colarco, P. R., Hamilton, D. S., Huang, Y., Ito, A., Klose, M., Li, L., Mahowald, N. M., Miller, R. L., Obiso, V., Pérez García-Pando, C., Rocha-Lima, A., and Wan, J. S.: Contribution of the world's main dust source regions to the global cycle of desert dust, Atmospheric Chemistry and Physics Discussions, 2021, 1–34, https://doi.org/10.5194/acp-2021-4, 2021.

Konare, A., Zakey, A. S., Solmon, F., Giorgi, F., Rauscher, S., Ibrah, S., and Bi, X.: A regional climate modeling study of the effect of desert dust on the West African monsoon, Journal of Geophysical Research: Atmospheres, 113, https://doi.org/10.1029/2007JD009322, 2008.

Laurent, B., Marticorena, B., Bergametti, G., and Mei, F.: Modeling mineral dust emissions from Chinese and Mongolian deserts, Global and Planetary Change, 52, 121 – 141, https://doi.org/https://doi.org/10.1016/j.gloplacha.2006.02.012, monitoring and Modelling of Asian Dust Storms, 2006.

LeGrand, S. L., Polashenski, C., Letcher, T. W., Creighton, G. A., Peckham, S. E., and Cetola, J. D.: The AFWA dust emission scheme for the GOCART aerosol model in WRF-Chem v3.8.1, Geoscientific Model Development, 12, 131–166, https://doi.org/10.5194/gmd-12-131-2019, 2019.

Li, F., Ginoux, P., and Ramaswamy, V.: Distribution, transport, and deposition of mineral dust in the Southern Ocean and Antarctica: Contribution of major sources, Journal of Geophysical Research: Atmospheres, 113, https://doi.org/10.1029/2007JD009190, 2008.

Li, J. and Osada, K.: Preferential settling of elongated mineral dust particles in the atmosphere, Geophysical Research Letters, 34, https://doi.org/10.1029/2007GL030262, 2007.

Longueville, F. D., Hountondji, Y.-C., Henry, S., and Ozer, P.: What do we know about effects of desert dust on air quality and human health in West Africa compared to other regions?, Science of The Total Environment, 409, 1 – 8, https://doi.org/https://doi.org/10.1016/j.scitotenv.2010.09.025, 2010.

Mahowald, N.: Aerosol Indirect Effect on Biogeochemical Cycles and Climate, Science, 334, 794–796, https://doi.org/10.1126/science.1207374, 2011.

Mahowald, N., Albani, S., Kok, J. F., Engelstaeder, S., Scanza, R., Ward, D. S., and Flanner, M. G.: The size distribution of desert dust aerosols and its impact on the Earth system, Aeolian Research, 15, 53 – 71, https://doi.org/https://doi.org/10.1016/j.aeolia.2013.09.002, 2014.

Mahowald, N. M., Baker, A. R., Bergametti, G., Brooks, N., Duce, R. A., Jickells, T. D., Kubilay, N., Prospero, J. M., and Tegen, I.: Atmospheric global dust cycle and iron inputs to the ocean, Global Biogeochemical Cycles, 19, https://doi.org/10.1029/2004GB002402, 2005.

Mahowald, N. M., Ballantine, J. A., Feddema, J., and Ramankutty, N.: Global trends in visibility: implications for dust sources, Atmospheric Chemistry and Physics, 7, 3309–3339, https://doi.org/10.5194/acp-7-3309-2007, 2007.

Mahowald, N. M., Engelstaedter, S., Luo, C., Sealy, A., Artaxo, P., Benitez-Nelson, C., Bonnet, S., Chen, Y., Chuang, P. Y., Cohen, D. D., Dulac, F., Herut, B., Johansen, A. M., Kubilay, N., Losno, R., Maenhaut, W., Paytan, A., Prospero, J. M., Shank, L. M., and Siefert, R. L.: Atmospheric Iron Deposition: Global Distribution, Variability, and Human Perturbations, Annual Review of Marine Science, 1, 245–278, https://doi.org/10.1146/annurev.marine.010908.163727, pMID: 21141037, 2009.

Marticorena, B. and Bergametti, G.: Modeling the atmospheric dust cycle: 1. Design of a soil-derived dust emission scheme, Journal of Geophysical Research: Atmospheres, 100, 16 415–16 430, https://doi.org/10.1029/95JD00690, 1995.

Marticorena, B., Chatenet, B., Rajot, J. L., Traoré, S., Coulibaly, M., Diallo, A., Koné, I., Maman, A., NDiaye, T., and Zakou, A.: Temporal variability of mineral dust concentrations over West Africa: analyses of a pluriannual monitoring from the AMMA Sahelian Dust Transect, Atmospheric Chemistry and Physics, 10, 8899–8915, https://doi.org/10.5194/acp-10-8899-2010, 2010.

Marticorena, B., Chatenet, B., Rajot, J. L., Bergametti, G., Deroubaix, A., Vincent, J., Kouoi, A., Schmechtig, C., Coulibaly, M., Diallo, A., Koné, I., Maman, A., NDiaye, T., and Zakou, A.: Mineral dust over west and central Sahel: Seasonal patterns of dry and wet deposition fluxes from a pluriannual sampling (2006–2012), Journal of Geophysical Research: Atmospheres, 122, 1338–1364, https://doi.org/10.1002/2016JD025995, 2017.

Matthes, K., Funke, B., Kruschke, T., and Wahl, S.: input4MIPs.SOLARIS-HEPPA.solar.CMIP.SOLARIS-HEPPA-3-2, https://doi.org/10.22033/ESGF/input4MIPs.1122, 2017.

Meinshausen, M., Vogel, E., Nauels, A., Lorbacher, K., Meinshausen, N., Etheridge, D. M., Fraser, P. J., Montzka, S. A., Rayner, P. J., Trudinger, C. M., Krummel, P. B., Beyerle, U., Canadell, J. G., Daniel, J. S., Enting, I. G., Law, R. M., Lunder, C. R., O'Doherty, S.,

Prinn, R. G., Reimann, S., Rubino, M., Velders, G. J. M., Vollmer, M. K., Wang, R. H. J., and Weiss, R.: Historical greenhouse gas concentrations for climate modelling (CMIP6), 10, 2057–2116, https://doi.org/10.5194/gmd-10-2057-2017, 2017.

Menut, L., Pérez, C., Haustein, K., Bessagnet, B., Prigent, C., and Alfaro, S.: Impact of surface roughness and soil texture on mineral dust emission fluxes modeling, Journal of Geophysical Research: Atmospheres, 118, 6505–6520, https://doi.org/https://doi.org/10.1002/jgrd.50313, 2013.

Michou, M., Nabat, P., Saint-Martin, D., Bock, J., Decharme, B., Mallet, M., Roehrig, R., Séférian, R., Sénési, S., and Voldoire, A.: Present-Day and Historical Aerosol and Ozone Characteristics in CNRM CMIP6 Simulations, Journal of Advances in Modeling Earth Systems, 12, e2019MS001 816, https://doi.org/10.1029/2019MS001816, e2019MS001816 10.1029/2019MS001816, 2020.

Miller, R. L., Cakmur, R. V., Perlwitz, J., Geogdzhayev, I. V., Ginoux, P., Koch, D., Kohfeld, K. E., Prigent, C., Ruedy, R., Schmidt, G. A., and Tegen, I.: Mineral dust aerosols in the NASA Goddard Institute for Space Sciences ModelE atmospheric general circulation model, Journal of Geophysical Research (Atmospheres), 111, D06 208, https://doi.org/https://doi.org/10.1029/2005JD005796, 2006.

Monks, P. S., Granier, C., Fuzzi, S., Stohl, A., Williams, M. L., Akimoto, H., Amann, M., Baklanov, A., Baltensperger, U., Bey, I., Blake, N., Blake, R. S., Carslaw, K., Cooper, O. R., Dentener, F., Fowler, D., Fragkou, E., Frost, G. J., Generoso, S., Ginoux, P., Grewe, V., Guenther, A., Hansson, H. C., Henne, S., Hjorth, J., Hofzumahaus, A., Huntrieser, H., Isaksen, I. S. A., Jenkin, M. E., Kaiser, J., Kanakidou, M., Klimont, Z., Kulmala, M., Laj, P., Lawrence, M. G., Lee, J. D., Liousse, C., Maione, M., McFiggans, G., Metzger, A., Mieville, A., Moussiopoulos, N., Orlando, J. J., O'Dowd, C. D., Palmer, P. I., Parrish, D. D., Petzold, A., Platt, U., Pöschl, U., Prévôt, A. S. H., Reeves, C. E., Reimann, S., Rudich, Y., Sellegri, K., Steinbrecher, R., Simpson, D., ten Brink, H., Theloke, J., van der Werf, G. R., Vautard, R., Vestreng, V., Vlachokostas, C., and von Glasow, R.: Atmospheric composition change - global and regional air quality, Atmospheric Environment, 43, 5268–5350, https://doi.org/10.1016/j.atmosenv.2009.08.021, 2009.

Mulcahy, J. P., Johnson, C., Jones, C. G., Povey, A. C., Scott, C. E., Sellar, A., Turnock, S. T., Woodhouse, M. T., Abraham, N. L., Andrews, M. B., Bellouin, N., Browse, J., Carslaw, K. S., Dalvi, M., Folberth, G. A., Glover, M., Grosvenor, D. P., Hardacre, C., Hill, R., Johnson, B., Jones, A., Kipling, Z., Mann, G., Mollard, J., O'Connor, F. M., Palmiéri, J., Reddington, C., Rumbold, S. T., Richardson, M., Schutgens, N. A. J., Stier, P., Stringer, M., Tang, Y., Walton, J., Woodward, S., and Yool, A.: Description and evaluation of aerosol in UKESM1 and HadGEM3-GC3.1 CMIP6 historical simulations, Geoscientific Model Development, 13, 6383–6423, https://doi.org/10.5194/gmd-13-6383-2020, 2020.

Nabat, P., Solmon, F., Mallet, M., Kok, J. F., and Somot, S.: Dust emission size distribution impact on aerosol budget and radiative forcing over the Mediterranean region: a regional climate model approach, Atmospheric Chemistry and Physics, 12, 10 545–10 567, https://doi.org/10.5194/acp-12-10545-2012, 2012.

Nousiainen, T.: Optical modeling of mineral dust particles: A review, Journal of Quantitative Spectroscopy and Radiative Transfer, 110, 1261–1279, https://doi.org/10.1016/j.jqsrt.2009.03.002, 2009.

O'Hara, S. L., Clarke, M. L., and Elatrash, M. S.: Field measurements of desert dust deposition in Libya, Atmospheric Environment, 40, 3881 – 3897, https://doi.org/https://doi.org/10.1016/j.atmosenv.2006.02.020, 2006.

Painter, T. H., Barrett, A. P., Landry, C. C., Neff, J. C., Cassidy, M. P., Lawrence, C. R., McBride, K. E., and Farmer, G. L.: Impact of disturbed desert soils on duration of mountain snow cover, Geophysical Research Letters, 34, https://doi.org/10.1029/2007GL030284, 2007.

Perlwitz, J. P., Pérez García-Pando, C., and Miller, R. L.: Predicting the mineral composition of dust aerosols - Part 1: Representing key processes, Atmospheric Chemistry & Physics, 15, 11 593–11 627, https://doi.org/10.5194/acp-15-11593-2015, 2015.

Peyridieu, S., Chédin, A., Capelle, V., Tsamalis, C., Pierangelo, C., Armante, R., Crevoisier, C., Crépeau, L., Siméon, M., Ducos, F., and Scott, N. A.: Characterisation of dust aerosols in the infrared from IASI and comparison with PARASOL, MODIS, MISR, CALIOP, and AERONET observations, Atmospheric Chemistry and Physics, 13, 6065–6082, https://doi.org/10.5194/acp-13-6065-2013, 2013.

Piedra, P. G., Llanza, L. R., and Moosmüller, H.: Optical losses of photovoltaic modules due to mineral dust deposition: Experimental measurements and theoretical modeling, Solar Energy, 164, 160 – 173, https://doi.org/https://doi.org/10.1016/j.solener.2018.02.030, 2018.

Prenni, A. J., Petters, M. D., Kreidenweis, S. M., Heald, C. L., Martin, S. T., Artaxo, P., Garland, R. M., Wollny, A. G., and Pöschl, U.: Relative roles of biogenic emissions and Saharan dust as ice nuclei in the Amazon basin, Nature Geoscience, 2, 402–405, https://doi.org/https://doi.org/10.1038/ngeo517, 2009.

Prigent, C., Tegen, I., Aires, F., Marticorena, B., and Zribi, M.: Estimation of the aerodynamic roughness length in arid and semi-arid regions over the globe with the ERS scatterometer, Journal of Geophysical Research: Atmospheres, 110, https://doi.org/https://doi.org/10.1029/2004JD005370, 2005.

Prospero, J. M. and Nees, R. T.: Impact of the North African drought and El Niño on mineral dust in the Barbados trade winds, Nature, 320, 735–738, https://doi.org/10.1038/320735a0, 1986.

Prospero, J. M. and Savoie, D. L.: Effect of continental sources on nitrate concentrations over the Pacific Ocean, Nature, 339, 687–689, https://doi.org/10.1038/339687a0, 1989.

Prospero, J. M., Barkley, A. E., Gaston, C. J., Gatineau, A., Campos y Sansano, A., and Panechou, K.: Characterizing and Quantifying African Dust Transport and Deposition to South America: Implications for the Phosphorus Budget in the Amazon Basin, Global Biogeochemical Cycles, 34, e2020GB006 536, https://doi.org/https://doi.org/10.1029/2020GB006536, e2020GB006536 2020GB006536, 2020.

Pu, B. and Ginoux, P.: Climatic factors contributing to long-term variations in surface fine dust concentration in the United States, Atmospheric Chemistry & Physics, 18, 4201–4215, https://doi.org/10.5194/acp-18-4201-2018, 2018a.

Pu, B. and Ginoux, P.: How reliable are CMIP5 models in simulating dust optical depth?, Atmospheric Chemistry and Physics, 18, 12 491–12 510, https://doi.org/10.5194/acp-18-12491-2018, 2018b.

Pérez, C., Nickovic, S., Baldasano, J. M., Sicard, M., Rocadenbosch, F., and Cachorro, V. E.: A long Saharan dust event over the western Mediterranean: Lidar, Sun photometer observations, and regional dust modeling, Journal of Geophysical Research: Atmospheres, 111, https://doi.org/10.1029/2005JD006579, 2006.

Pérez, C., Haustein, K., Janjic, Z., Jorba, O., Huneeus, N., Baldasano, J. M., Black, T., Basart, S., Nickovic, S., Miller, R. L., Perlwitz, J. P., Schulz, M., and Thomson, M.: Atmospheric dust modeling from meso to global scales with the online NMMB/BSC-Dust model - Part 1: Model description, annual simulations and evaluation, Atmospheric Chemistry & Physics, 11, 13 001–13 027, https://doi.org/https://doi.org/10.5194/acp-11-13001-2011, 2011.

Ridley, D. A., Heald, C. L., Kok, J. F., and Zhao, C.: An observationally constrained estimate of global dust aerosol optical depth, Atmospheric Chemistry and Physics, 16, 15 097–15 117, https://doi.org/10.5194/acp-16-15097-2016, 2016.

Rocha-Lima, A., Martins, J. V., Remer, L. A., Todd, M., Marsham, J. H., Engelstaedter, S., Ryder, C. L., Cavazos-Guerra, C., Artaxo, P., Colarco, P., and Washington, R.: A detailed characterization of the Saharan dust collected during the Fennec campaign in 2011: in situ ground-based and laboratory measurements, Atmospheric Chemistry and Physics, 18, 1023–1043, https://doi.org/10.5194/acp-18-1023-2018, 2018.

Ryder, C. L., Marenco, F., Brooke, J. K., Estelles, V., Cotton, R., Formenti, P., McQuaid, J. B., Price, H. C., Liu, D., Ausset, P., Rosenberg, P. D., Taylor, J. W., Choularton, T., Bower, K., Coe, H., Gallagher, M., Crosier, J., Lloyd, G., Highwood, E. J., and Murray, B. J.: Coarse-

mode mineral dust size distributions, composition and optical properties from AER-D aircraft measurements over the tropical eastern Atlantic, Atmospheric Chemistry and Physics, 18, 17 225–17 257, https://doi.org/10.5194/acp-18-17225-2018, 2018.

Ryder, C. L., Highwood, E. J., Walser, A., Seibert, P., Philipp, A., and Weinzierl, B.: Coarse and giant particles are ubiquitous in Saharan dust export regions and are radiatively significant over the Sahara, Atmospheric Chemistry and Physics, 19, 15 353–15 376, https://doi.org/10.5194/acp-19-15353-2019, 2019.

Sayer, A. M., Munchak, L. A., Hsu, N. C., Levy, R. C., Bettenhausen, C., and Jeong, M.-J.: MODIS Collection 6 aerosol products: Comparison between Aqua's e-Deep Blue, Dark Target, and "merged" data sets, and usage recommendations, Journal of Geophysical Research: Atmospheres, 119, 13,965–13,989, https://doi.org/10.1002/2014JD022453, 2014.

Scanza, R. A., Mahowald, N., Ghan, S., Zender, C. S., Kok, J. F., Liu, X., Zhang, Y., and Albani, S.: Modeling dust as component minerals in the Community Atmosphere Model: development of framework and impact on radiative forcing, Atmospheric Chemistry & Physics, 15, 537–561, https://doi.org/https://doi.org/10.5194/acp-15-537-2015, 2015.

Schulz, M., Balkanski, Y. J., Guelle, W., and Dulac, F.: Role of aerosol size distribution and source location in a three-dimensional simulation of a Saharan dust episode tested against satellite-derived optical thickness, Journal of Geophysical Research: Atmospheres, 103, 10 579–10 592, https://doi.org/10.1029/97JD02779, 1998.

Schulz, M., Cozic, A., and Szopa, S.: LMDzT-INCA dust forecast model developments and associated validation efforts, IOP Conference Series: Earth and Environmental Science, 7, 012 014, https://doi.org/https://doi.org/10.1088/1755-1307/7/1/012014, 2009.

Schulz, M., Prospero, J. M., Baker, A. R., Dentener, F., Ickes, L., Liss, P. S., Mahowald, N. M., Nickovic, S., García-Pando, C. P., Rodríguez, S., Sarin, M., Tegen, I., and Duce, R. A.: Atmospheric Transport and Deposition of Mineral Dust to the Ocean: Implications for Research Needs, Environmental Science and Technology, 46, 10 390–10 404, https://doi.org/10.1021/es300073u, 2012.

Seinfeld, J. and Pandis, S.: Atmospheric chemistry and physics: from air pollution to climate change, A Wiley interscience publication, Wiley, https://books.google.fr/books?id=lK8PAQAAMAAJ, 1998.

Sellar, A. A., Jones, C. G., Mulcahy, J. P., Tang, Y., Yool, A., Wiltshire, A., O'Connor, F. M., Stringer, M., Hill, R., Palmieri, J., Woodward, S., de Mora, L., Kuhlbrodt, T., Rumbold, S. T., Kelley, D. I., Ellis, R., Johnson, C. E., Walton, J., Abraham, N. L., Andrews, M. B., Andrews, T., Archibald, A. T., Berthou, S., Burke, E., Blockley, E., Carslaw, K., Dalvi, M., Edwards, J., Folberth, G. A., Gedney, N., Griffiths, P. T., Harper, A. B., Hendry, M. A., Hewitt, A. J., Johnson, B., Jones, A., Jones, C. D., Keeble, J., Liddicoat, S., Morgenstern, O., Parker, R. J., Predoi, V., Robertson, E., Siahaan, A., Smith, R. S., Swaminathan, R., Woodhouse, M. T., Zeng, G., and Zerroukat, M.: UKESM1: Description and Evaluation of the U.K. Earth System Model, Journal of Advances in Modeling Earth Systems, 11, 4513–4558, https://doi.org/10.1029/2019MS001739, 2019.

Shaffer, G., Olsen, S. M., and Pedersen, J. O. P.: Long-term ocean oxygen depletion in response to carbon dioxide emissions from fossil fuels, Nature Geoscience, 2, 105, https://doi.org/10.1038/ngeo420, 2009.

Shao, Y.: A model for mineral dust emission, Journal of Geophysical Research: Atmospheres, 106, 20 239–20 254, https://doi.org/10.1029/2001JD900171, 2001.

Shao, Y.: Simplification of a dust emission scheme and comparison with data, Journal of Geophysical Research: Atmospheres, 109, https://doi.org/10.1029/2003JD004372, 2004.

Shao, Y.: Physics and Modelling Wind Erosion, vol. 23, Springer-Werlag, 2008.

Shao, Y. and Dong, C.: A review on East Asian dust storm climate, modelling and monitoring, Global and Planetary Change, 52, 1–22, https://doi.org/10.1016/j.gloplacha.2006.02.011, 2006.

Shao, Y., Wyrwoll, K.-H., Chappell, A., Huang, J., Lin, Z., McTainsh, G. H., Mikami, M., Tanaka, T. Y., Wang, X., and Yoon, S.: Dust cycle: An emerging core theme in Earth system science, Aeolian Research, 2, 181–204, https://doi.org/10.1016/j.aeolia.2011.02.001, 2011.

Sharma, D. and Miller, R. L.: Revisiting the observed correlation between weekly averaged Indian monsoon precipitation and Arabian Sea aerosol optical depth, Geophysical Research Letters, 44, 10,006–10,016, https://doi.org/10.1002/2017GL074373, 2017.

Shindell, D. T., Lamarque, J. F., Schulz, M., Flanner, M., Jiao, C., Chin, M., Young, P. J., Lee, Y. H., Rotstayn, L., Mahowald, N., Milly, G., Faluvegi, G., Balkanski, Y., Collins, W. J., Conley, A. J., Dalsoren, S., Easter, R., Ghan, S., Horowitz, L., Liu, X., Myhre, G., Nagashima, T., Naik, V., Rumbold, S. T., Skeie, R., Sudo, K., Szopa, S., Takemura, T., Voulgarakis, A., Yoon, J. H., and Lo, F.: Radiative forcing in the ACCMIP historical and future climate simulations, Atmospheric Chemistry and Physics, 13, 2939–2974, https://doi.org/10.5194/acp-13-2939-2013, 2013.

Solomos, S., Kallos, G., Kushta, J., Astitha, M., Tremback, C., Nenes, A., and Levin, Z.: An integrated modeling study on the effects of mineral dust and sea salt particles on clouds and precipitation, Atmospheric Chemistry and Physics, 11, 873–892, https://doi.org/10.5194/acp-11-873-2011, 2011.

Strong, J. D. O., Vecchi, G. A., and Ginoux, P.: The Response of the Tropical Atlantic and West African Climate to Saharan Dust in a Fully Coupled GCM, Journal of Climate, 28, 7071–7092, https://doi.org/10.1175/JCLI-D-14-00797.1, 2015.

Séférian, R., Nabat, P., Michou, M., Saint-Martin, D., Voldoire, A., Colin, J., Decharme, B., Delire, C., Berthet, S., Chevallier, M., Sénési, S., Franchisteguy, L., Vial, J., Mallet, M., Joetzjer, E., Geoffroy, O., Guérémy, J.-F., Moine, M.-P., Msadek, R., Ribes, A., Rocher, M., Roehrig, R., Salas-y Mélia, D., Sanchez, E., Terray, L., Valcke, S., Waldman, R., Aumont, O., Bopp, L., Deshayes, J., Éthé, C., and Madec, G.: Evaluation of CNRM Earth-System model, CNRM-ESM 2-1: role of Earth system processes in present-day and future climate, Journal of Advances in Modeling Earth Systems, 11, 4182– 4227, https://doi.org/10.1029/2019MS001791, 2019.

Tang, M., Cziczo, D. J., and Grassian, V. H.: Interactions of Water with Mineral Dust Aerosol: Water Adsorption, Hygroscopicity, Cloud Condensation, and Ice Nucleation, Chemical Reviews, 116, 4205–4259, https://doi.org/10.1021/acs.chemrev.5b00529, pMID: 27015126, 2016.

Tang, M., Huang, X., Lu, K., Ge, M., Li, Y., Cheng, P., Zhu, T., Ding, A., Zhang, Y., Gligorovski, S., Song, W., Ding, X., Bi, X., and Wang, X.: Heterogeneous reactions of mineral dust aerosol: implications for tropospheric oxidation capacity, Atmospheric Chemistry and Physics, 17, 11 727–11 777, https://doi.org/10.5194/acp-17-11727-2017, 2017.

Taylor, K. E.: Summarizing multiple aspects of model performance in a single diagram, Journal of Geophysical Research: Atmospheres, 106, 7183–7192, https://doi.org/10.1029/2000jd900719, 2001.

Tegen, I. and Fung, I.: Modeling of mineral dust in the atmosphere: Sources, transport, and optical thickness, Journal of Geophysical Research, 99, 22 897, https://doi.org/https://doi.org/10.1029/94jd01928, 1994.

Tegen, I., Harrison, S. P., Kohfeld, K., Prentice, I. C., Coe, M., and Heimann, M.: Impact of vegetation and preferential source areas on global dust aerosol: Results from a model study, Journal of Geophysical Research: Atmospheres, 107, AAC 14–1–AAC 14–27, https://doi.org/10.1029/2001JD000963, 2002.

Timmreck, C. and Schulz, M.: Significant dust simulation differences in nudged and climatological operation mode of the AGCM ECHAM, Journal of Geophysical Research: Atmospheres, 109, n/a–n/a, https://doi.org/10.1029/2003jd004381, 2004.

van der Does, M., Knippertz, P., Zschenderlein, P., Harrison, R. G., and Stuut, J.-B. W.: The mysterious long-range transport of giant mineral dust particles, Science Advances, 4, eaau2768, https://doi.org/10.1126/sciadv.aau2768, 2018.

van Noije, T., Bergman, T., Le Sager, P., O'Donnell, D., Makkonen, R., Gonçalves-Ageitos, M., Döscher, R., Fladrich, U., von Hardenberg, J., Keskinen, J., Korhonen, H., Laakso, A., Myriokefalitakis, S., Ollinaho, P., Pérez García-Pando, C., Reerink, T., Schrödner, R., Wyser, K.,

and Yang, S.: EC-Earth3-AerChem, a global climate model with interactive aerosols and atmospheric chemistry participating in CMIP6, Geoscientific Model Development Discussions, 2020, 1–46, https://doi.org/10.5194/gmd-2020-413, 2020.

Vincent, J., Laurent, B., Losno, R., Bon Nguyen, E., Roullet, P., Sauvage, S., Chevaillier, S., Coddeville, P., Ouboulmane, N., di Sarra, A. G., Tovar-Sánchez, A., Sferlazzo, D., Massanet, A., Triquet, S., Morales Baquero, R., Fornier, M., Coursier, C., Desboeufs, K., Dulac, F., and Bergametti, G.: Variability of mineral dust deposition in the western Mediterranean basin and south-east of France, Atmospheric Chemistry and Physics, 16, 8749–8766, https://doi.org/10.5194/acp-16-8749-2016, 2016.

Voldoire, A., Sanchez-Gomez, E., Mélia, D. S. y., Decharme, B., Cassou, C., Sénési, S., Valcke, S., Beau, I., Alias, A., Chevallier, M., Déqué, M., Deshayes, J., Douville, H., Fernandez, E., Madec, G., Maisonnave, E., Moine, M. P., Planton, S., Saint-Martin, D., Szopa, S., Tyteca, S., Alkama, R., Belamari, S., Braun, A., Coquart, L., and Chauvin, F.: The CNRM-CM5.1 global climate model: description and basic evaluation, Climate Dynamics, 40, 2091–2121, https://doi.org/10.1007/s00382-011-1259-y, 2012.

Voldoire, A., Saint-Martin, D., Sénési, S., Decharme, B., Alias, A., Chevallier, M., Colin, J., Guérémy, J.-F., Michou, M., Moine, M.-P., Nabat, P., Roehrig, R., Salas y Mélia, D., Séférian, R., Valcke, S., Beau, I., Belamari, S., Berthet, S., Cassou, C., Cattiaux, J., Deshayes, J., Douville, H., Ethé, C., Franchistéguy, L., Geoffroy, O., Lévy, C., Madec, G., Meurdesoif, Y., Msadek, R., Ribes, A., Sanchez-Gomez, E., Terray, L., and Waldman, R.: Evaluation of CMIP6 DECK Experiments With CNRM-CM6-1, Journal of Advances in Modeling Earth Systems, 11, 2177–2213, https://doi.org/10.1029/2019MS001683, 2019.

Wang, R., Balkanski, Y., Boucher, O., Bopp, L., Chappell, A., Ciais, P., Hauglustaine, D., Peñuelas, J., and Tao, S.: Sources, transport and deposition of iron in the global atmosphere, Atmospheric Chemistry & Physics, 15, 6247–6270, https://doi.org/10.5194/acp-15-6247-2015, 2015.

Wang Rong, Balkanski Yves, Boucher Olivier, Ciais Philippe, Peñuelas Josep, and Tao Shu: Significant contribution of combustion-related emissions to the atmospheric phosphorus budget, Nature Geoscience, 8, 48, https://doi.org/https://doi.org/10.1038/ngeo2324 10.1038/ngeo2324, 2014.

Washington, R. and Todd, M. C.: Atmospheric controls on mineral dust emission from the Bodélé Depression, Chad: The role of the low level jet, Geophysical Research Letters, 32, https://doi.org/10.1029/2005gl023597, 2005.

Woodward, S.: Modeling the atmospheric life cycle and radiative impact of mineral dust in the Hadley Centre climate model, Journal of Geophysical Research: Atmospheres, 106, 18 155–18 166, https://doi.org/10.1029/2000jd900795, 2001a.

Woodward, S.: Modeling the atmospheric life cycle and radiative impact of mineral dust in the Hadley Centre climate model, Journal of Geophysical Research: Atmospheres, 106, 18 155–18 166, https://doi.org/10.1029/2000JD900795, 2001b.

Yu, H., Kaufman, Y. J., Chin, M., Feingold, G., Remer, L. A., Anderson, T. L., Balkanski, Y., Bellouin, N., Boucher, O., Christopher, S., DeCola, P., Kahn, R., Koch, D., Loeb, N., Reddy, M. S., Schulz, M., Takemura, T., and Zhou, M.: A review of measurement-based assessments of the aerosol direct radiative effect and forcing, Atmospheric Chemistry and Physics, 6, 613–666, https://doi.org/10.5194/acp-6-613-2006, 2006.

Yu, Y., Kalashnikova, O. V., Garay, M. J., and Notaro, M.: Climatology of Asian dust activation and transport potential based on MISR satellite observations and trajectory analysis, Atmospheric Chemistry and Physics, 19, 363–378, https://doi.org/10.5194/acp-19-363-2019, 2019.

Zender, C. S., Bian, H., and Newman, D.: Mineral Dust Entrainment and Deposition (DEAD) model: Description and 1990s dust climatology, Journal of Geophysical Research (Atmospheres), 108, 4416, https://doi.org/https://doi.org/10.1029/2002JD002775, 2003.